# UNIVERSITÀ DEGLI STUDI DI MILANO

## FACOLTÀ di MEDICINA e CHIRURGIA

**Dipartimento di Farmacologia, Chemioterapia e Tossicologia Medica**

**Dottorato di ricerca in Farmacologia, Chemioterapia e Tossicologia Mediche**

**(XXIV ciclo)**

***"Analysis of neuromuscular junctions and effects of nandrolone administration in a mouse model for ALS"***

**(Settore disciplinare BIO/14)**

**Tesi di Dottorato di Ricerca**

**Di: Valentina Cappello**

**Matricola: R08238**

**Coordinatore: Chiarissimo Prof. Alberto E. Panerai**

**Docente Guida: Dott.ssa Maura Francolini**

**Anno accademico 2010-2011**

Index:

# 1. ABSTRACT

Several lines of evidence indicate that neuromuscular junction (NMJ) destruction and disassembly is an early phenomenon in the amyotrophic lateral sclerosis (ALS) neurodegenerative disease. Here we analyzed by confocal and electron microscopy the NMJ structure in the diaphragm of Superoxide dismutase (SOD)1 G93A mice at symptom onset and we compared these observation with animals sacrificed at the pathological end stage. In young transgenic mice, which provide a model for familial ALS, the present findings showed marked denervation both in the diaphragm and in the gastrocnemius, which partially spares soleus muscle. At the clinical end stage even the soleus is slight denervated, but less severely than other muscles. In addition, the size of the synaptic vesicle (SV) pool was found reduced and alterations of mitochondria were observed in approximately 40% of the remaining presynaptic terminals. Treatment of SOD1 G93A mice with the anabolic steroid nandrolone during the presymptomatic stage preserved the diaphragm muscle mass and features indicative of synaptic activity, represented by the number of vesicles docked within 200 nm from the presynaptic membrane and area of acetylcholine receptor clusters. Furthermore, structural preservation of mitochondria was documented in presynaptic terminals, but innervation of diaphragm muscle fibers was only slightly increased in nandrolone-treated SOD1-mutant mice. Altogether the results point out and define fine structural alterations of diaphragm NMJs in the murine model of familial ALS at symptom onset, and indicate that nandrolone may prevent or delay structural alterations in NMJ mitochondria and stimulate presynaptic activity but does not prevent muscle denervation in the disease.

# 2. INTRODUCTION

## 2.1 Amyotrophic lateral sclerosis characteristic

Amyotrophic lateral sclerosis (ALS) is the most common degenerative disease involving both upper and lower motoneurons (UMN and LMN) and is characterized by an onset delayed in the adulthood and by the selective and progressive loss of motoneurons (MNs) in the in spinal cord, in brainstem and in motor cortex except for the neurons that control the bladder, and the oculomotoneurons.

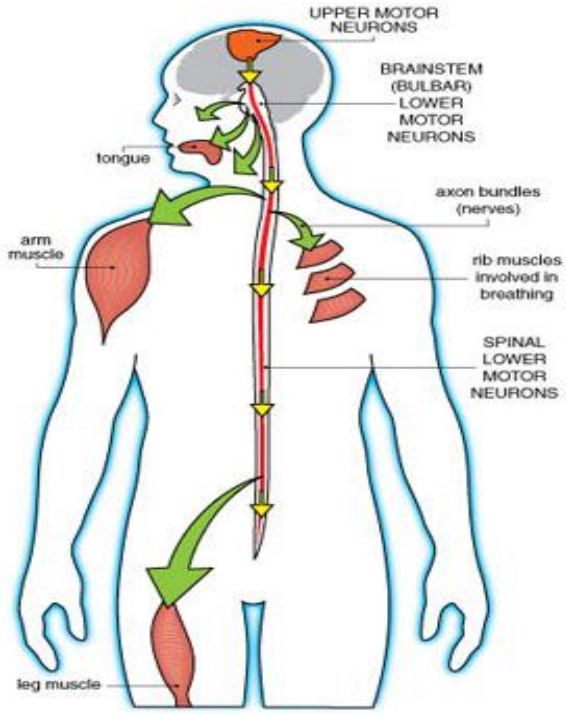


FIG.1 Upper and lower MN and their target muscles

ALS is also known as Charcot's Syndrome name that derived from the French neurobiologist and physician that described for the first time this disease in 1869, while the conventional name is due to the main features of the disease, in particular:

- ✓ Amyotrophic derived from the atrophy that affects skeletal muscle fibers
- ✓ Lateral refers to the network of motor axons that run down both sides of the spinal cord
- ✓ Sclerosis is due to the scar tissue that remains following degeneration of the nerves

Every year are diagnosed 1 to 3 new cases over a population of 100.000 people while the prevalence of individuals with ALS is almost the same of the incidence value because patients generally live only two to five years after the clinical onset/diagnosis.

ALS is often used to define a spectrum of neurodegenerative disorders (MND) that are characterized by progressive degeneration of motoneurons and that include 'progressive muscular atrophy' or PMA, 'primary lateral sclerosis' or PLS, 'flail arm/leg syndromes' and 'ALS with frontotemporal involvement'. Primary symptoms of these disorders, clinical

presentation, rate of progression and prognosis reflect the motoneural subtype which is affect at the onset of the disease, even if it is possible that other subtypes will be involved in later stages.

Thus PMA is a pure LMN disease, that involved speech ability and swallowing, flail arm and leg are prevalently LMN, PLS is a pure UMN disease while the classical 'Charcot ALS' shows both upper and lower signs.

Regarding this point upper motoneurons sings include hyperreflexia, extensor plantar response and increased muscular tone, while lower motoneurons sings include weakness, muscular wasting (atrophy), hyporeflexia, cramps and fasciculations. In the classical (or Charcot's) ALS both the classes of MN are involved.

In some cases also the frontotemporal cortex is affected and patients show in addiction to classical MN signs also an impairment of cognitive functions and behavioural alteration (Neary et al., 1998).

It is possible to distinguish inside the total amount of ALS cases two different forms of the disease: sporadic forms (sALS) that include 90-95% of all cases while the remaining 5-10% are due to genetic forms (fALS) of the disease related with mutations in known sites of the genome (Musarò, 2010). Despite the phenotype of these two forms is quite the same, sporadic forms has their onset 10 years later respect to familial cases (45 in fALS versus 55 in sALS). In both forms is present a slight prevalence in men respect to women.

The early stage of the disease is characterized by a massive skeletal muscle weakness followed by atrophy, accompanied by spasticity phenomena and/or fasciculation, then paralysis that is the main feature till the death of patients that occurs within five years of clinical onset.

### 2.11 Sporadic ALS

The causes of sporadic forms of ALS are still unknown nevertheless it has been hypothesized that ALS is a multifactorial-caused disorder in which several conditions and risk factors could play an additive role in the pathogenesis of the disease.

*Excitotoxicity mediated by excitatory aminoacids*

Several lines of evidence implicate glutamatergic toxicity as one of the most important cofactor in the neuronal injury in ALS. Excessive stimulation of glutamate receptors causes

excitotoxicity. Under physiological conditions, excitotoxicity is prevented by the fast clearance of glutamate by the glial glutamate transporters (GLT1) that play a crucial role in the regulation of extracellular glutamate concentration. Notably, GLT1 is the major glutamate transporter and is widely distributed in the human central nervous system (CNS). The selective localization of GLT1 in glial cells has implications for its excitotoxic mechanisms. In ALS patients as well as in animal model (where is expressed the murine homologous Excitatory AminoAcid Transporter (EAAT-2)) has been demonstrated that the level of expression of the transporter is diminished both in motor cortex and in spinal cords (Van Damme et al., 2005). Alterations in this protein might interfere with the normal clearance, which allows glutamate to remain in the environment and continue to activate the receptors. Once activated, the receptors cause calcium influx that cells are not able to buffer because of an insufficient number of calcium-binding proteins. Altered concentration of calcium activates apoptotic pathways, which leads to motoneuron death and degeneration.

*Oxidative stress and Reactive oxygen species (ROS) production*

Physiological activity of living organism needs an appropriate level of ROS for the balance of redox status in cells, while high concentration of these reactive species can lead to modification and/or inactivation of nucleic acids, proteins and lipids (Zablocka et al., 2008). Thus, to cope with injury from oxidative damage and maintain redox homeostasis, aerobic organisms have developed efficient defence systems of enzymatic and non-enzymatic antioxidants which includes Superoxide dismutase (SOD), Catalase, glutathione system and plasma proteins. SOD in particular is able to scavenge superoxide anions produced by the cellular metabolism and to convert them in hydrogen peroxide and molecular oxygen.

There are several evidences that suggest a primary role of oxidative stress in the pathogenesis of ALS, both in neurons and in muscle where antioxidant enzyme activity is altered.

Mutations in the *SOD1* gene are responsible for 20% of fALS forms but are also highlighted in some sALS where the enzyme was able to form proteic aggregates in cellular cytoplasm. Dysfunction of one of the most important scavenging system of eukaryotic cells can lead to increased oxidative damage, which promotes activation of apoptotic pathways. In SOD1-caused ALS mitochondrial pool is one of the first targets of degeneration because of the presence of ROS induces alteration as membrane depolarization, decreased activity of respiratory complexes and cytochrome C release.

*Mitochondrial pool dysfunction*

As mentioned above, there is a clear involvement of mitochondrial pool in the ALS pathogenesis. Mitochondria represent a primary site of intracellular production of reactive oxygen species, and can activate the apoptosis process through the cytosolic release of cytochrome C. Despite numerous reports demonstrating anatomical and functional mitochondrial abnormalities associated with ALS, the role of mitochondrial dysfunction in disease onset and progression remains unknown. It has been suggested that mutant SOD1 causes dysfunction and structural damage of mitochondria in human patients and mouse models of ALS (Higgins et al., 2003).

A proposed mechanism suggests that mutant SOD1 is imported into mitochondria, where directly causes the damage of the organelle and activation of apoptotic pathway.
In 2010 Zhou and colleagues indicated that mitochondrial dysfunction, which appears early in the course of ALS pathology, does not seem to be restricted to motoneurons, and it is present in other tissues, particularly skeletal muscle (Zhou et al., 2010).
Moreover the damaged mitochondria may contribute to cell death activating the apoptotic pathway trough the release of calcium and cytochrome C.

*Abnormal proteins aggregation both in MN soma and axons*

Common features in neurodegenerative diseases are abnormal protein aggregation and formation of inclusion bodies in cells as happened for Alzheimer's disease, Parkinson and polyglutamine diseases as Huntington's disease. Also in ALS has been observed that misfolded and/or polyubiquitinated proteins tend to holigomerize and to form intracellular aggregates in motoneurons and, in some cases also in the surrounding glial cell (Bruijn et al., 1998). Both in sporadic and in familial forms of ALS are found aggregates positive for SOD1 protein that tends to be misfolded or forms aggregates that in turn trigger a toxic cascade that leads to neuronal degeneration. More recently, it has been demonstrated that TAR DNA binding protein (TDP)-43 spontaneously forms aggregates (Johnson et al., 2009).

The C-terminal domain of TDP-43 is crucial for spontaneous aggregation thus several ALS-linked TDP-43 mutations within this domain increase the number of TDP-43 aggregates and promote toxicity *in vivo*. Normally, cells are able to sequestrate aberrant proteins into inclusions that could be degradated, while, in pathological conditions, such as the increase of physiological or environmental stress, the ubiquitin-proteasome system can become

overloaded and impaired. This results in engulfment of the cells, which become defective in the disposal of altered macromolecules and more prone to damage (Kabashi et al., 2006). Moreover the P56S substitution over the gene encoding for VAPB induces the formation of insoluble aggregates (Nishimura et al., 2004; Kim et al., 2010), and into these aggregates even the WT protein is sequestrated leading to the loss of its Unfolded protein response (UPR)-associated activity (Prosser et al., 2008; Fasana et al., 2010)

On the other hands also in motoneuronal axons protein aggregation could exert its effect by the formation of 'spheroid' (aggregates of neurofilament) in the proximal axons, which slow down the axonal transport both the retrograde and the anterograde or block them (axonal strangulation).

*Inflammation*

A common pathological hallmark in ALS is the strong inflammatory reaction, due to the presence of ubiquitin-immunoreactive cytoplasmatic inclusions/aggregates (McGeer and McGeer, 2002). Both CNS and spinal cords are affected by a diffused gliosis and the accumulation of activated microglia that become hypertrophied in the grey matter, while in the white matter cells engorged with myelin products, lose their processes and become 'fat granule cells'. Even astrocytes are observed throughout these degenerating areas. Moreover in ALS was observed an increased level of expression of cytotoxic species (ROS as mentioned above), mediators of inflammation and proinflammatory cytokines.

*Viral agents*

Over the last years have been reported several cases of ALS or ALS-like disease in association with human immunodeficiency virus type 1 (HIV) infection (Verma and Berger, 2006). Additionally, other forms of motoneuron disease, such as, brachial amyotrophic diplegia, have also been observed in HIV infected patients (Berger et al., 2005).

Higher frequency of ALS syndrome in HIV seropositive population, even if the clinical features of these disorders is partially different in term of age of onset and timing of progression to classical Charcot's forms, have been proposed as evidence for the causal relationship between the HIV infection and ALS.

*Acquired causes*

Heavy metals exposure is referred as a risk factor for the development of ALS. A higher risk related to the report of occupational exposure to lead was observed, while it seems to have no effects in terms of occasional exposure.

In a paper of 2007, it has been shown that although no other assessments were performed (genetic, environmental or biologic), the probable aetiology for ALS in some cases was exposure to lead (Oh et al., 2007).

Similarly, acute and chronic intoxication with mercury may cause ALS syndrome. In 1996 was reported a case of acute intoxication with mercury followed by the appearance, three years later of ALS symptoms (Schwarz et al., 1996) possibly explained by the slow accumulation of mercury in the CNS, since other acquired causes may have favoured retrograde axonal transportation.

Excessive exposure to selenium has also been reported among the possible aetiologies for ALS, with its unknown origin and indicative of severe prognosis. This relation has been based on epidemiological investigations, which demonstrate an increase of ALS risk associated with the residency in a Selenium-impregnated area or with the consumption of water with high inorganic levels of this metal. It has also been shown that selenium, mainly in its inorganic form, presents a selective toxicity to motoneurons, with the compromise of muscular function in animal models (Vinceti et al., 2010).

Occupational exposure to pesticides and insecticides are some of the factors associated with an ALS development increased risk as reported in a 2006 study on the chronic inhalation of pyrethroid insecticides (Doi et al., 2006).

Moreover, increased post-war risk of ALS has been observed in soldiers who were deployed to the Gulf Region during the first Gulf War period, suggesting that the exposure to neurotoxins as an environmental risk factor (Horner et al., 2003).

Several hypotheses have been formulated trying to explain the high incidence of ALS among soccer players, including as possible candidates excessive physical activity, drugs and doping, dietary supplements, pesticides used on the playgrounds, and traumas to the head and to other body parts (Belli and Vanacore, 2005; Chen et al., 2007).

Finally has to be mentioned the possible role of dietary factors in sALS pathogenesis, as indicated by the high incidence of a malignant ALS form associated with Parkinson-dementia complex (PDC), that is reported as a consequence of the exposure and ingestion of *Cycas micronesica* (Steele and McGeer, 2008).

## 2.12 Familial ALS

Table I.- Different subtypes of FALS and their genetic determinants.

| ALS type | Onset | Inheritance | Locus | Gene | Protein |
|---|---|---|---|---|---|
| ALS1 | Adult | AD[1] | 21q22.1 | *SOD1* | Cu/Zn superoxide dismutase |
| ALS2 | Juvenile | AR | 2q33-35 | *ALS2* | Alsin |
| ALS3 | Adult | AD | 18q21 | unknown | |
| ALS4 | Juvenile | AD | 9q34 | *SETX* | Senataxin |
| ALS5 | Juvenile | AR | 15q15-21 | *SPG11* | Spatacsin |
| ALS6 | Adult | AD[2] | 16p11.2 | *FUS* | Fused in sarcoma |
| ALS7 | Adult | AD | 20p13 | unknown | |
| ALS8 | Adult | AD | 20q13.33 | *VAPB* | VAMP-associated protein B |
| ALS9 | Adult | AD | 14q11 | *ANG* | Angiogenin |
| ALS10 | Adult | AD | 1q36 | *TARDBP* | TAR DNA-binding protein |
| ALS11 | Adult | AD | 6q21 | *FIG4* | PI(3,5)P(2)5-phosphatase |
| ALS12 | Adult | AR/AD | 10p15-p14 | *OPTN* | Optineurin |
| ALS-FTD1 | Adult | AD | 9q21-22 | unknown | |
| ALS-FTD2 | Juvenile | AD | 9p13.2-21.3 | unknown | |

TAB1. Familial forms of ALS (Ticozzi et al., 2011)

Cu, Zn Superoxide dismutase 1 (SOD1)

SOD1 is an homodimer, codified by a single gene that localizes in 21q22 position, in which both the monomers are linked with copper and zinc ions (Gurney et al., 1994). This protein is ubiquitously expressed, with a predominant localization in the cytosol but also in mitochondria, peroxisomes and lysosomes (Raimondi et al., 2006; Forsberg et al., 2010) and it catalyzes the dismutation of superoxide anion in atoxic products (molecular oxygen and hydrogen peroxide).

SOD1 mutations are responsible for the 20% of familial forms of ALS; the linkage between the enzyme and the pathology was discovered at the beginning of ‘90s by Siddique and colleagues (Siddique, 1991) while, three years later, has been described the presence of several mutations over this gene able to induce an ALS phenotype (Rosen et al., 1993).

To date over one hundred and forty mutations have been identified in the coding region of this gene associated with an ALS phenotype. Almost all mutation are inherited in a dominant autosomal manner, D90A substitution is a partial exception because it is a recessive in Scandinavian population but it is dominant in others (Robberecht et al., 1996). The enzyme is particularly plentiful in the spinal cord and brain, where it has been estimated to comprise between 0.1% and 2.0% of the detergent-soluble protein (Pardo et al., 1995). This abundance likely reflects the copious superoxide generated by these highly respiring tissues. The

fundamental role of SOD1 as an antioxidant protein, combined with its abundance in neural tissue, suggested an initial hypothesis that the pathogenic SOD1 mutations might result in an enzyme that is unable to detoxify reactive oxygen species.

Over time, this loss of enzymatic function could lead to oxidative damage and death of neural cells. However, mice lacking SOD1 do not develop motoneuron disease (Reaume et al., 1996) and transgenic mice expressing human fALS SOD1 mutants in addition to their own endogenous SOD1 develop paralytic symptoms strikingly similar to those observed in human patients (Bruijn et al., 1997; Gurney et al., 1994). Together, these observations imply that pathogenic SOD1 molecules act through the gain of a cytotoxic property and not a loss of function.

Alsin (ALS2)

ALS type two is a autosomal recessive form of fALS due to mutation in the gene coding for alsin mapping on chromosome 2q33-35.
Also this juvenile-onset form induces atrophy and weakness of distal skeletal muscles, spasticity progressively ascending from the lower limbs to the cervical and bulbar segments. The gene for alsin could generate two different splicing isoforms the long and the short one. At least 13 different ALS2 mutations have been described so far, the majority of which are frame-shift deletions resulting in a prematurely truncated protein, or nonsense mutations. Interestingly, it has been observed that the mutations that affect both the long and short form of the protein result in the juvenile ALS phenotype, while those that alter only the long form are responsible for the milder phenotypes of juvenile primary lateral sclerosis or infantile-onset ascending hereditary spastic paraparesis, both characterized by an isolated involvement of the corticospinal tracts (Kress et al., 2005; Eymard-Pierre et al., 2006; Panzeri et al., 2006). Alsin localizes to the cytosolic face of endosomal membranes and acts as a guanine nucleotide exchange factor for Rab5 and other small GTPases (Otomo et al., 2003). It is thought to be involved in vesicular trafficking, cytoskeletal organization, and endosomal dynamics. The fact that all ALS2 pedigrees are homozygous, and the observation that mutations lead to protein instability suggests that the loss of the physiological functions of alsin leads to ALS (Yamanaka et al., 2003). It must however be noticed that ALS2 knockout mice do not develop motoneuron disease (Cai et al., 2005).

Sentaxin (SETX)

ALS4 is a slow progression motoneuron disease with a autosomal-recessive inheritance and an early onset in the adulthood. Patients usually develop symmetrical weakness and atrophy of the distal muscles of the limbs in their second decade. The phenotype is characterized by the involvement of the corticospinal tracts, while bulbar muscles are consistently spared (Chance et al., 1998). It has been found that ALS4, initially linked to the chromosome 9q34, is caused by mutations in the *SETX* gene (Chen et al., 2004) that encodes for sentaxin.

To date, only four *SETX* mutations have been identified, and all of them are missense substitutions (Chen et al., 2004; Zhao et al., 2009).

Sentaxin is a ubiquitously expressed DNA/RNA helicase, possibly involved in repairing DNA double-strand breaks following oxidative stress (Suraweera et al., 2007). Moreover, it has been shown to bind RNA polymerase II and other proteins involved in mRNA transcription and processing, suggesting that it is involved in transcriptional regulation (Suraweera et al., 2009).

Spatacsin (SPG11)

ALS5 is another recessive form of fALS with an early onset and it is characterized by distal muscle atrophy and weakness associated with pyramidal signs and involvement of bulbar muscles. The disease has been mapped to a locus on chromosome 15q15- 21 (Hentati et al., 1998). Recently, are identified 12 homozygous, or compound heterozygous, mutations in the *SPG11* gene in 10 unrelated pedigrees (Orlacchio et al., 2010). The majority of the identified variants are frame-shift mutations or nonsense substitutions. Homozygous mutations in the same gene have been previously described in patients with autosomal recessive hereditary spastic paraplegia with thin corpus callosum (Stevanin et al., 2007). In a single case, a *post-mortem* examination revealed pathological evidence of neurodegeneration in lower motoneurons, although Bunina bodies and ubiquitinated inclusions seem to be absent. *SPG11* is composed of 40 exons and encodes for the 2443-residue long protein spatacsin. The physiological role of spatacsin is still unknown, although it is reputed to be involved in axonal transport (Salinas et al., 2008).

Fused in sarcoma (FUS)

The ALS type 6 is a dominant classic fALS linked with the genetic locus on chromosome 16p12.1-q21 (Sapp et al., 2003). Recently it has been identified a novel variants in the *FUS* gene (Kwiatkowski et al., 2009; Vance et al., 2009) as the disease-causing mutations in ALS6 families that is responsible of about 4% of familial cases of ALS and about 1% of sporadic ones (Yamamoto-Watanabe et al., 2010; Yan et al., 2010).

To date more than 30 different mutations have been described, the vast majority of which are missense substitutions and the rest are frame-shift or nonsense mutations. Although genotype-phenotype correlations are not possible for the majority of *FUS* mutations, it has been suggested that mutations R521C over this gene may result in an uncommon phenotype characterized by a symmetrical and proximal spinal onset, with early involvement of the axial muscles (Ticozzi et al., 2009). The *FUS* gene encodes for a DNA/RNA binding protein that is involved in several cellular pathways, including transcriptional regulation, maintenance of genomic stability, and splicing, nucleo-cytoplasmic shuttling, transport, and maturation of mRNAs (Law et al., 2006). In the central nervous system, the protein is involved in regulating mRNA transport towards the dendrites and synaptic plasticity upon the activation of glutamate receptors (Fujii et al., 2005).

The majority of the mutations identified so far are clustered in the region containing the nuclear localization signals that could led to a unbalance between nuclear and cytoplasmatic forms of FUS protein and the consequent formation of proteic aggregates (Vance et al., 2009).

It has been hypothesized that *FUS* mutations may contribute to ALS pathogenesis through the formation of cytoplasmic inclusions and/or the loss of the physiological nuclear functions of the protein.

Vesicle-associated membrane protein (VAMP)-associated protein B (VAPB)

ALS8 is linked with a locus on chromosome 20q13.33 and has been initially described as an autosomal-dominant, slow progressive ALS (Nishimura et al., 2004) Characterized by lower motoneuron symptoms, predominantly in the limb muscles. A single patient also presented upper motoneuron signs.

ALS8 is caused by a single mutation, the P56S substitution over the *VAPB* gene, which encodes for the VAMP-associated protein B.

The *VAPB* gene spans 57.7 kb of genomic DNA and it is composed of six exons. Through alternative splicing, it gives rise to two proteins of 243 (VAPB) and 99 residues (VAPC). VAPB/C are ubiquitously expressed, localize to the endoplasmic reticulum and associate with microtubules, suggesting a role in vesicle trafficking (Nishimura et al., 2004; Kanekura et al., 2006).

Since VAPB/C are present as homo or heterodimers it has been hypnotized that the P56S mutation exerts a dominant negative effect on the WT protein, in fact, it has been shown that P56S-VAPB can form insoluble cytoplasmic inclusions in neural and non-neural cell lines, sequestering and co-precipitating WT-VAPB (Suzuki et al., 2009).

Aggregates formation and the loss of the physiological functions of VAPB may lead to motoneuron degeneration. Supporting the latter hypothesis is the observation that the silencing of the *Drosophila melanogaster Dvap33* gene, homologous to *VAPB*, leads to progressive paralysis of the larvae, formation of cytoplasmic inclusions and neurodegeneration. The phenotype is rescued by overexpressing the human *VAPB* gene (Chai et al., 2008).

In cellular culture the overexpression of VAPB has a dominant negative effect on the WT protein, the P56S mutation has the tendency to holigomerize and to form aggregates in the perinuclear zone (Prosser et al., 2008).

Previous work in our department indicate that in HeLa cells, transfected transiently with VAPB P56S, is possible to observe the formation of aggregates positive for this mutated protein (FIG.2), to better clarify the mutation role in the aggregates formation *in vivo* experiment of microinjection were performed and indicate that the clusterization of protein is a very fast event (Fasana et al., 2010).

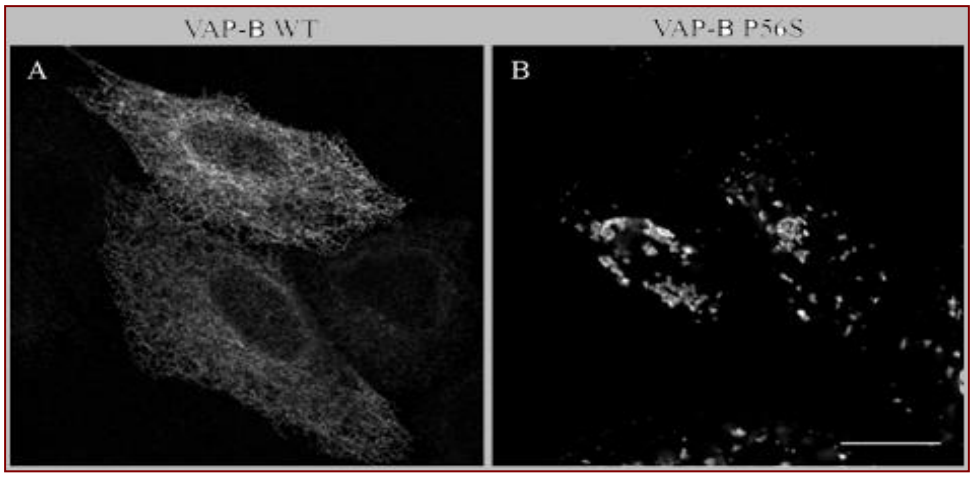


FIG.2 HeLa cells transiently transfected with VAPB P56S

(Modified from Fasana et al., 2010)

Ultastructural analysis of these aggregates indicates a close relationship with the surrounding endoplasmic reticulum and that *cisternae* in transfected cells (both in HeLa and in NSC34) are stacked in structure with a peculiar electron density of the cytosol among a pair of *cisternae*.

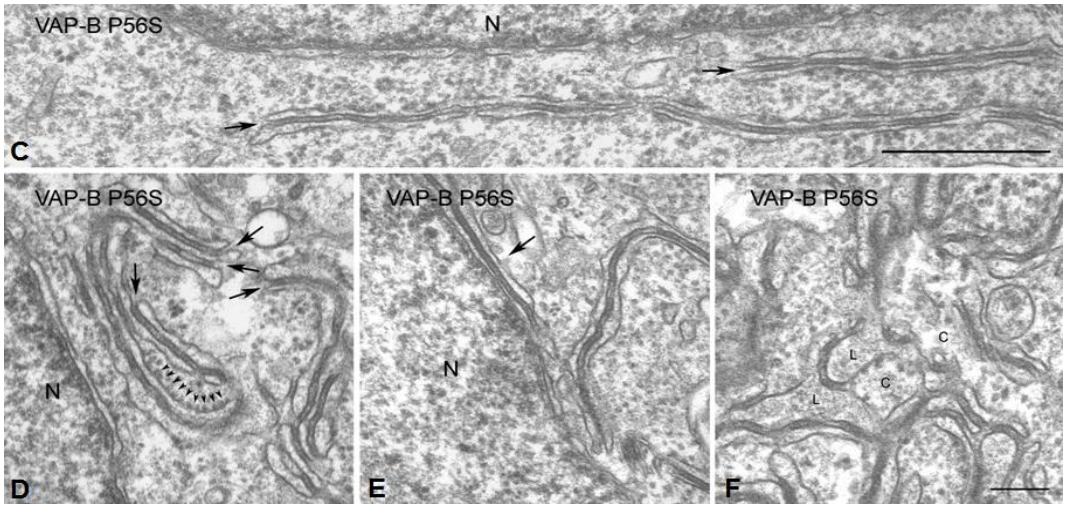


FIG.3 Ultrastructural characterization of VAPB positive aggregates in HeLa cell line. (modified from Fasana et al., 2010)

Through an EM tomography approach the architecture of these structures has been solved, indicating that those structure show continuity both to the nuclear envelope and to conventional ER.

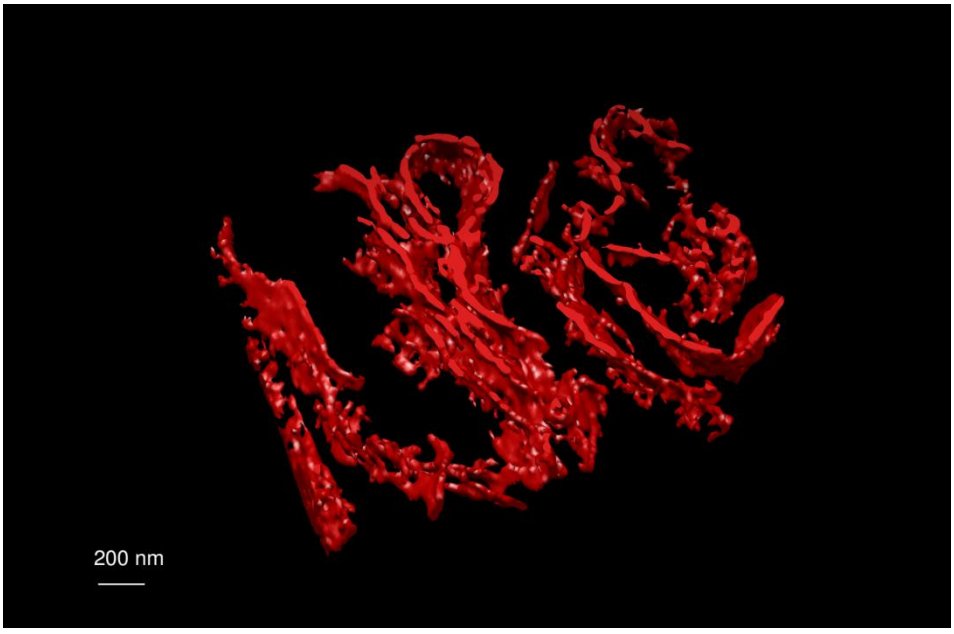


FIG.4 EM tomography of VAPBP56S – positive aggregate in HeLa cells Tomogram JEOL 200 KV STEM on 500 nm thick section
± 60°- 1° tilt

(In collaboration with A.Raimondi and G. Bertone – IIT – Genova)

The same structures viewed in culture of HeLa (FIG.3) and NSC34 (data not shown) cells have been found in spinal cords of transgenic mice carrying the P56S substitution (FIG.5)

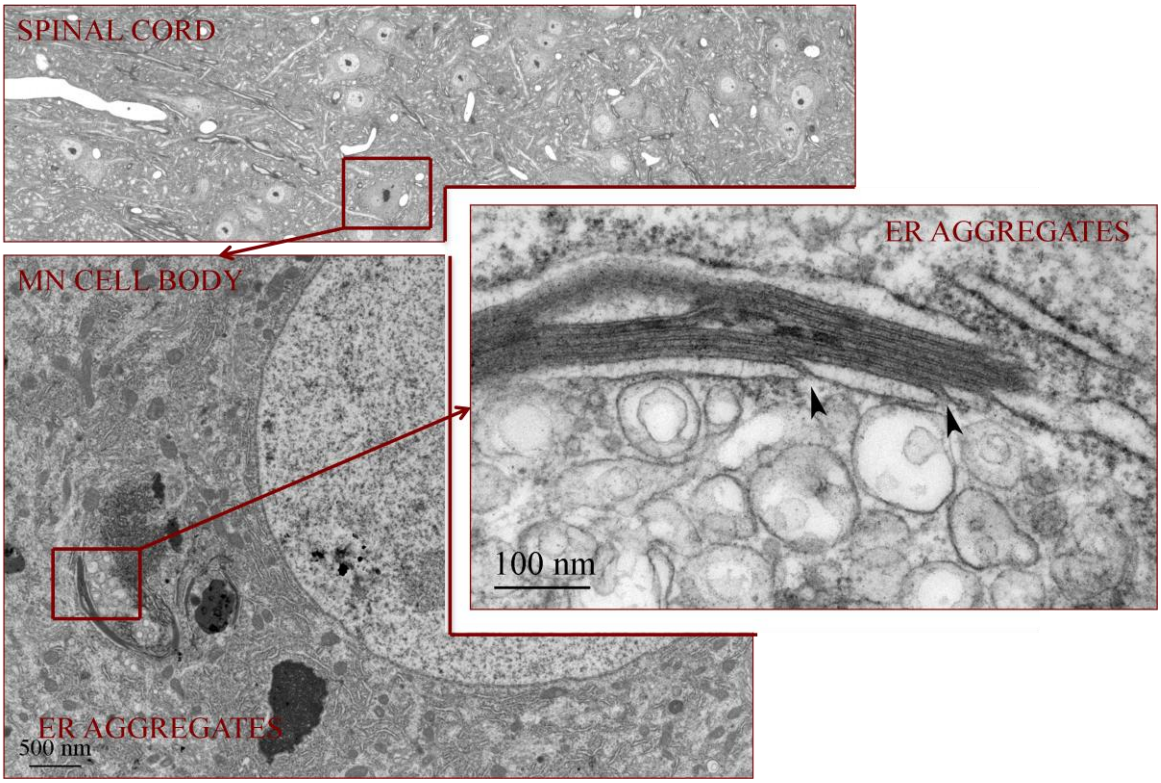


FIG.5 Ultrastructural characterization of VAPB positive aggregates in the spinal cord of transgenic mice. VAPB P56S inclusion were found in semithin section and deeper investigate with conventional EM.

(unpublished data)

Angiogenin (ANG)

Increasing evidence supports the hypothesis that angiogenic factors may be involved in the pathogenesis of ALS. A screening of a large cohort of North European patients reported an association between two haplotypes in the vascular endothelial growth factor gene (*VEGF*) promoter and susceptibility to sALS. The deletion of the hypoxia response element in the gene promoter and the consequent down-regulation of VEGF expression lead to a progressive motoneuron degeneration in mice (Lambrechts et al., 2003).

In 2004, the rs11701 single nucleotide polymorphism (SNP) in the ANG gene, encoding for angiogenin, a downstream effector of VEGF, was shown to be associated to sALS susceptibility in the Irish and Scottish populations (Greenway et al., 2004). Direct sequencing of the coding regions of *ANG* in 1629 ALS patients and 1264 controls identified seven missense mutations in 15 individuals, of which four were fALS and 11 sALS (Greenway et al., 2006).

The association with rs11701, however, could not be replicated. The identification of a large ALS-FTD family in which the K17I mutation segregates with the disease led to the designation of all *ANG*-associated fALS as ALS9 (van Es et al., 2009).

Angiogenin, a member of the pancreatic ribonuclease superfamily, is expressed mainly in hepatocytes and secreted into the serum and the extracellular matrix. After uptaking by still unidentified endothelial receptors, the protein is translocated into the nucleolus where it stimulates tRNA transcription, ribosome biogenesis, protein translation, and cell proliferation (Moroianu et al., 1994; Smith et al., 2006).

The majority of the 15 mutations described so far is clustered in regions encoding for the catalytic site or for the nuclear import signal and are consequently predicted to disrupt angiogenin secretion, ribonucleolytic activity and/or nuclear translocation, ultimately resulting in impairment angiogenesis (Wu et al., 2007).

The loss of angiogenin physiological functions may thus lead to motoneuron degeneration. In fact, wild-type angiogenin has been shown to protect primary motoneurons from hypoxia-induced cell death, while ALS-associated *ANG* mutants do not.

TAR-DNA binding protein (TDP-43)

TDP – 43 is the main component of ubiquitinated cytoplasmic inclusions in ALS (Neumann et al. 2006). In aggregates, TDP-43 is hyperphosphorylated and cleaved to generate abnormal C-terminal fragments.

In unaffected neuron the localization of this protein is nuclear while in mutated cells there is a nucleo-cytoplasmic redistribution of the protein that colocalizes with inclusions.

It is not still establish if the pathogenetic role of mutated TDP-43 is due to the loss of it physiological localization or to a gain of adverse functions that turns aggregates in cytotoxic inclusions (Ticozzi et al., 2010). Mutations in the *TARDBP* gene, encoding for TDP-43, have been consider as the main cause of fALS, because has been identified in several populations of different geographic origin (Kabashi et al., 2008; Kuhnlein et al., 2008; Van Deerlin et al., 2008; Corrado et al., 2009; Del Bo et al., 2009; Ticozzi et al., 2009; Millecamps et al., 2010).

Mutations over TDP gene are responsible for about 5% of familial ALS and it has been find in about 2% sporadic forms. Despite the specific functions of TDP-43 in neuronal cells remain to be completely understood, the protein plays a role in several biological processes, including gene transcription, splicing regulation, transport and stabilization of mRNA molecules (Buratti et al., 2008).

To date, more than 30 different *TARDBP* mutations have been described, all of which are missense substitutions. With a single exception, all of them are clustered in the C-terminal glycine-rich region. Since most *TARDBP* mutations are private, it is difficult to establish clear genotype-phenotype correlation. It has been suggested that A382T, which is the variant most commonly observed, may be associated with a predominantly lower motoneuron disease with an asymmetrical onset in the distal muscles of the limbs, subsequently spreading to proximal muscles, with relative sparing of the bulbar muscles (Corrado et al., 2009).

PI(3,5)P(2)5 – phosphatase (FIG4)

In 2009 ten heterozygous mutations in the *FIG4* gene have been identified in six sALS and three more fALS patients (Chow et al., 2009). The identified variants include missense and nonsense substitutions, mutations at consensus splice sites and frame-shift insertions and deletions. Interestingly, two patients had been diagnosed with primary lateral sclerosis, and the majority of the others had prominent signs of corticospinal tracts degeneration. The

compound heterozygosity of the I41T *FIG4* mutation with a nonsense or frame-shift mutation had been previously been identified as the genetic cause of the Charcot-Marie-Tooth disease type IV, an autosomal recessive neuropathy characterized by an infantile onset and rapid progression (Chow et al., 2007).

*FIG4* encodes for a phosphoinositide phosphatase that regulates the synthesis and turnover of phosphatidylinositol-3,5-bisphosphate, a molecule that is involved in the retrograde transport of endosomal vesicles to the *trans*-Golgi network (Rutherford et al., 2006). Interestingly, null mice for *FIG4* display widespread neuronal degeneration in sensory and autonomic ganglia, motor cortex, striatum, and cerebellum (Chow et al., 2007).

C9ORF72

An intronic expansion in the gene C9ORF72 has been demonstrated to be the underlying cause of a familial form of ALS associated to frontotemporal dementia (Renton et al., 2011; Dejesus-Hernandez et al. 2011).

The linkage between this locus and the risk of development of ALS was already known (Ticozzi et al., 2010 and references therein).

### 2.13 Pharmacological strategies in ALS

At present, there exists neither prophylactic nor curative treatment for ALS and the single prescribed anti-glutamatergic drug Rilutek (riluzole) may have a marginal and unsatisfactory effect in extending life by a few months (Bensimon et al., 1994). All the other therapies are directed against the symptoms.

*Excitotoxicity in ALS and therapeutic strategies*

To date the only therapy accepted by the Food and Drugs Administration (FDA) in the treatment of ALS (both sporadic and familial forms) is the riluzole that inhibits the release of glutamate by inactivating voltage-dependent $Na^+$ channels on glutamatergic nerve terminals, as well as activating a G-protein dependent signal transduction process, thus slowing down disease progression and significantly increasing lifespan of patients by a few months (Doble, 1996). Moreover, riluzole can also block some of the postsynaptic effects of glutamate by non-competitive inhibition at NMDA and AMPA receptors (Albo et al., 2004).

Several studies underlined that also the clearance of glutamate from neuromuscular synapses is diminished in patients with ALS because of the loss of the astroglial glutamate transporter EAAT-2 (excitatory amino acid transporter 2), that is of major importance for synaptic glutamate reuptake (Rothstein et al., 1995).

*Oxidative stress in ALS and therapeutic strategies*

The involvement of oxidative stress in ALS is suggested by the observation that mutations in the SOD1 gene are responsible for approximately 20% fALS forms, mainly inherited with an autosomal dominant trait (Rosen, 1993). Whether oxidative stress is a primary cause of pathogenesis in ALS, or is merely a consequence of the disease, has long been debated. However, extensive evidence shows increased oxidative damage in spinal cord and motor cortex motoneurons (Shaw et al., 1995; Ferrante et al., 1997) in both sporadic and SOD1 familial ALS post mortem tissue (Abe et al., 1995; 1997; Beal et al., 1997).

Mitochondria are implicated in production of oxidative stress, as the major source of ROS, and are also targets of ROS, with decreased mitochondrial efficiency caused by oxidative damage (Beal, 2002; Lenaz et al., 2002; Genova et al., 2004). Although preclinical studies demonstrated a prolonged survival following coenzyme Q10 treatment (Matthews et al., 1998), an antioxidant, essential mitochondrial cofactor facilitating electron transfer in the respiratory chain, the phase II study in ALS (NCT00243932) showed insufficient promise to warrant Phase III testing (Kaufmann et al., 2009).

Several studies with manganoporphyrin, AEOL 10150, an antioxidant molecule that catalytically neutralizes superoxide, hydrogen peroxide and peroxynitrite, and inhibits lipid peroxidation (Patel and Day, 1999) have been performed on ALS patients after positive results obtained in animal models (Crow et al., 2005).

Edaravone is a free-radical scavenger is (3-methyl-1-phenyl-2-pyrazolin-5-one, MCI-186), approved by the Ministry of Health, Labor, and Welfare of Japan in 2001, now widely used for the treatment of acute cerebral infarction (Watanabe et al., 1994) for its neuroprotective effect against oxidative damage (Shichinohe et al., 2004; Uno et al., 2005). Edaravone administered at clinical onset determined a slowing in symptom progression and motor neuron degeneration in the ALS mice model (Ito et al., 2008). More recently the efficacy of edaravone has been investigated even in ALS patients (Yoshino and Kimura, 2006). This study suggested that edaravone is safe and may delay the progression of functional motor disturbances by reducing oxidative stress in ALS patients. However, the

evidence about the effects of edaravone on human ALS patients awaits the publication of the results of a phase III clinical trial of ALS, currently ongoing in Japan.

*Apoptosis in ALS and therapeutic strategies*

Apoptosis mediates the precise and programmed natural death of neurons and is a physiologically important process in neurogenesis during maturation therapeutic strategies in ALS.

However, premature apoptosis and/or an aberration in apoptosis regulation is implicated in the pathogenesis of neurodegeneration, a multifaceted process involved in several neurodegenerative disease, such as Alzheimer, Parkinson, Huntington diseases and ALS (Okouchi et al., 2007).

Valproic acid (VPA) is a histone deacetylase (HDAC) inhibiting drug that promotes gene transcription (Kernochan et al., 2005) and inhibits neuronal cell death by counterbalancing apoptosis, oxidative stress and glutamate toxicity (Hassel et al., 2001; Morland et al., 2004).

Based on the finding that VPA and other HDAC inhibitors increased survival in G93A SOD1mice (Sugai et al., 2004; Leng et al., 2008), it was performed a Randomized, Double-Blind, Placebo-Controlled Sequential Clinical Trial of Sodium Valproate in ALS.

The administration of Minocycline showed very encouraging results in transgenic mice trials (Kriz et al., 2002; Van Den Bosch et al., 2002), while, in a multicentre, randomized placebo-controlled phase III trial, showed negative results that were faster in the minocycline group than in the placebo group (Gordon et al., 2007).

*Neuroinflammation in ALS and therapeutic strategies*

Inflammation in ALS may be a secondary response to neuronal injury by genetic, biochemical, or environmental insults. Inflammatory cells surround degenerating MN (Hirano, 1991), leading to the accumulation of proinflammatory cytokines and free radicals that likely contribute to neurodegeneration. Therefore, modulation of inflammation might reduce cell death.

Pre-clinical studies on SOD1 G93A mice suggested that anti-inflammatory agents may be effective in treating this disease (McGeer and McGeer, 2002). Several reports have demonstrated that pro-inflammatory cytokines have a toxic role in the pathogenesis of ALS (Kiaei et al., 2006; Wu et al., 2006). Inflammatory cascades contribute to motor neuron death

in the spinal cord in the G93A SOD1 transgenic mice, as well as in human ALS patients (Kiaei et al., 2006). Proinflammatory cytokines, such as tumor necrosis factor (TNF), are upregulated in ALS.

Thalidomide shows potent anti-inflammatory properties through the modulation of inflammatory cytokines such as TNF-α and appreciably penetrates the CNS (Franks et al., 2004). In this trial it was demonstrated that thalidomide could cause adverse effects without effectively modulating disease progression (Stommel et al., 2009).

*Neurotrophic factors in ALS and therapeutic strategies*

Neurotrophic factors are involved in the regulation of neuronal survival and differentiation and in maintaining neuronal structural integrity. In SOD1 G93A mice treatment with insulin-like growth factor (IGF)-1 or glial-cell-line-derived neurotrophic factor (GDNF) have beneficial effects on survival and motoneurons morphology, also decreasing gliosis (Kaspar et al., 2003; Dobrowolny et al., 2005).

*Inhibitors of protein aggregation in ALS and therapeutic strategies*

Several neurodegenerative diseases are characterized by the formation of intracellular aggregates, that have been described in neuropathological studies of ALS. Moreover, protein missfolding and aggregation are peculiar features of both neurodegenerative and polyglutamine disease. It has been established that administration of anti-aggregation drugs such as sodium butyrate and HDAC inhibitor ameliorated neurological phenotypes in animal models of spinal and bulbar muscular atrophy (Minamyama et al., 2004).

As for mutant SOD1 (mSOD1) transgenic mice sodium phenylbutyrate promotes survival of animal and regulates the expression of antiapoptotic genes (Ryu et al., 2005). In ALS patients, sodium butyrate is safe and well tolerable, but further clinical trials are required (Cudcowicz et al., 2009).

*Autophagy inducers*

Several targets and signaling pathways regulate autophagy, including the mammalian target of rapamycin, mTOR, as a negative regulator. By inhibiting mTOR, rapamycin is currently used to upregulate autophagy, and has been shown to be beneficial in models of

neurodegenerative diseases (Ravikumar et al., 2004; Berger et al., 2006; Rubinsztein et al., 2007).

Results about the ALS treatment with lithium are still contradictory in terms of its effect on ALS. Lithium targets different molecules, and acts on different pathways, the final effect critically depending on the dose. Defective autophagy has been found in diseased motoneurons (Venkatachalam et al., 2008) and when authopagy is blocked in G93A SOD1 mice, SOD1 accumulates and neuroprotection does not occur (Crippa et al., 2010). Moreover, a 15-month pilot clinical trial in randomized ALS patients showed that lithium and riluzole cotreatment markedly reduced mortality when compared with matched control patients treated with riluzole alone (Fornai et al., 2008). However, inconsistent results have also been reported. In a sibling matched, gender-balanced, investigator-blinded trial, using a standard mouse model of familial ALS chronic lithium treatment showed no benefit (Gill et al., 2009). Another study also found no therapeutic or neuroprotective effects of lithium in female ALS mice (Pizzasegola et al., 2009).

## 2.2 Experimental model of ALS1

Starting from the background knowledge of SOD1 mutations several experimental models of ALS type1 were generated and employed in the study of cellular features, aetiopathogenetic mechanisms, clinical onset and disease progression, involvement of different type of cells as well as in the study of effectiveness of genetic and pharmacologic treatments.

*Cellular models*

Several lines of evidence indicate that, differently of what previously hypothesized, ALS is a non-cell autonomous disease (Ilieva et al., 2009). Thus cultures of isolated MN, or motoneuronal cell lines, are an useful tool to the understanding of sub-cellular compartments of mutant SOD1-mediated toxicity, they are not sufficient to explain the role of other cells/tissues neither in the pathogenesis, nor in the progression.

Despite this consideration cellular models of ALS1 heve been used for example in the investigation of functional and morphological alterations among the mitochondrial pool, highliting that mutant SOD1 expression in neuronal cell lines or in primary culture of

motoneurons induces mitochondrial depolarization, alteration of calcium homeostasis, reduction in ATP production (reviwed in Pasinelli and Brown, 2006).

Finally co-culture of MNs and glial cells are useful in the study of cellular survival: motoneurons are less likely to survive when they are cultured with astrocytes that express mutant SOD1, or exposed to astrocyte-conditioned medium, than on astrocytes that express normal SOD1 (Julien, 2007).

*Transgenic rodent*

The discovery of mutations in SOD1 as a cause of ALS, provided the first opportunity to produce a genetically faithful model of the disease. Transgenic mice that overexpress human SOD1-harboring mutations linked to fALS develop the usual, fatal, progressive neurodegenerative disease seen in human patients.

Mutant human SOD1 (hSOD1) genes that have been introduced into mice include A4V, the most common and severe ALS-associated mutatation, mutatoins that alter the enzymatic function (for example G85R) and mutations that has no effect on its functionality (for example G93A).

The age of clinical onset in mice is higlhly variable, while the duration of illness appears to be characteristic to each mutation, as happen even in human, infact in patients with the L84V mutation, the average life expectancy is less than 18 months after the onset of symptoms, whereas patients harboring the H46R mutation have an average life expectancy of 18 years after the clinical onset. Thus mutations of SOD1 enzymes acquire toxic properties, but, the variations in the duration of illness could be relates with a different degrees of toxicity to the mutant protein. In our project we used trnsgenic mice carring the human mutation, correlated with familial ALS, SOD1 G93A (Gurney et al., 1994).

*Chimeric mice*

The restricted expression of the mutated SOD1 (G93A) gene in skeletal muscle is sufficient to induce , in trangenic mice, the developement of a progressive muscle atrophy, associated with a significant reduction in muscle strength, alterations in the contractile apparatus, and mitochondrial dysfunction (Dobrowolny et al., 2008). On the other hand, higher levels of expression of the same mutant enzyme (G93A and G37R) in skeletal muscle

are shown to induce a distal axonopathy that lead to the degeneration of spinal motorneurons (Wong and Martin, 2010).

The role of glial cells in SOD1–ALS pathogenesis has been examined in chimeric mice that were mixtures of normal cells and mutant SOD1-expressing cells (Clement et al., 2003).

This study indicated that degeneration of motor neurons expressing mutant SOD1 was delayed or prevented when WT non-neuronal cells surrounded them, whereas wild-type motor neurons could develop degenerative changes when surrounded by mutant SOD1-expressing neuronal cells (Clement et al., 2003).

The selective expression of mutant SOD1 in motoneurons (Jaarsma et al., 2008) is sufficient to induce ALS like disease but, maybe due to the lower level of expression, it is not enough to altered the mitochondrial pool nor to induce the formation of SDO1 aggregates both in neurons and glial cells. In particular, it has been demonstrated that, diminishing the SOD1 mutant levels in microglia has little effect on the early disease phase, but markedly slows later disease progression (Boillée et al., 2006). These results suggest that mutant SOD1 in microglia contributes to the propagation of disease at a late stage.

Notably, astrocyte activity normally increases at later stages of ALS disease and is concomitant with motor neuron degeneration, which suggests that astrocytes act as deadly neighbors that exacerbate motor neuron damage.

## 2.3 Motor Units (MU) classification, vulnerability and plasticity

Motor units are made by a lower motoneuron and all the muscular fibers it innervates. Several parameters have been identified to be responsible for a differential susceptibility to the alteration process induced by G93A substitution. These criteria regard both the presynaptic and the postsynaptic elements.

Criteria of classification:

*Contraction type:*

It is generally accepted that muscle fiber types can be divided into two main categories: slow twitch (Type I) muscle fibers and fast twitch (Type II) muscle fibers. Fast

twitch fibers can be further categorized into Type II a (Fast fatigue-resistant (FR)), Type II b (Fast fatigable (FF)) and Type IId/x (Fast fatigue intermediate (FI)) fibers.

These distinctions seem to influence how muscles respond to training and physical activity, and each fiber type is unique in its ability to contract in a certain way. On the other hand, muscles with different contraction capability seem to respond differently to pathology especially those that induce muscular weakness and wasting (Frey et al., 2000; Kanning et al., 2010)

Slow Twitch (S – Myosin heavy chain (MHC) class I)

The slow muscles have an oxidative metabolism for continuous, extended muscle contractions over a long time. They fire more slowly than fast twitch fibers and can go for a long time before they fatigue. Moreover slow fibers are more resistant to the denervation process during pathological progression and more plastic (a denervated neuromuscular junction (NMJ) could be easily reinnervated or a new junction could be formed in the same fiber after the denervation of the old one).

Fast Twitch (F – MHC class II)

Fast fibers have an anaerobic metabolism thus they are much better at generating short bursts of strength or speed than slow muscles. However, they fatigue more quickly. Fast twitch fibers generally produce the same amount of force per contraction as slow muscles, but they get their name because they are able to fire more rapidly. Having more fast twitch fibers can be an asset to a sprinter since she needs to quickly generate a lot of force. The faster metabolism induces a greater level of ROS production in muscles with a predominance of this class of fibers. Moreover those muscles are more sensitive to the denervation and less plastic after this process.

*Synaptogenesis*

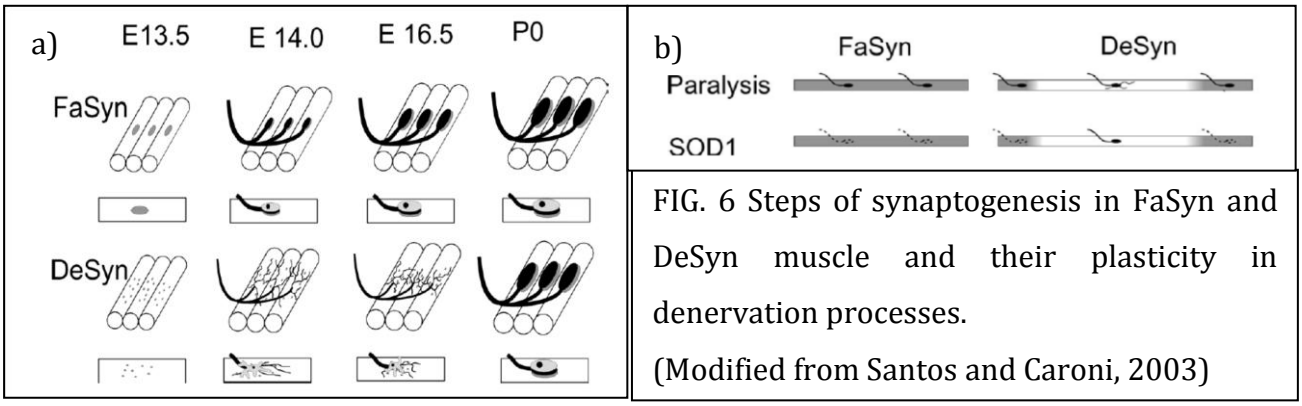


FIG. 6 Steps of synaptogenesis in FaSyn and DeSyn muscle and their plasticity in denervation processes.
(Modified from Santos and Caroni, 2003)

Fast synapsing (FaSyn) muscle

In these muscles the synaptogenetic process requires a shorter time than in other musclesFaSyn muscles assemble focally organized clusters of cholinergic receptors in the absence of nerve, which rapidly become aligned to presynaptic nerve and Schwann cells (FIG.6 a). FaSyn muscles could be considered as non-plastic, in fact in this type of muscles NMJs are lost rapidly in SOD1 mice and plastic processes of reinnervation are not observed (FIG.6 b).

Delayed Synapsing (DeSyn) muscle

In these muscles synaptogenesis requires a longer time because cholinergic receptors exhibit dispersed microclusters of chinergic receptors between E13.5 and E16.5. During this developmental time, nerves and Schwann cells fail to align with AChR microclusters, and extensive sprouting is detected (FIG.6a).
The main evidence of the plasticity response to paralysis or denervation of NMJs in DeSyn muscles is the sprouiting process: the blockade of synaptic activity induces ultraterminal nerve sprouting, followed by disassembly of the original postsynaptic apparatus and extensive collateral sprouting (Santos and Caroni, 2003).

## 2.4 Subcellular targets of motoneuron disease

*Presynaptic terminal*

Mitochondrial pool

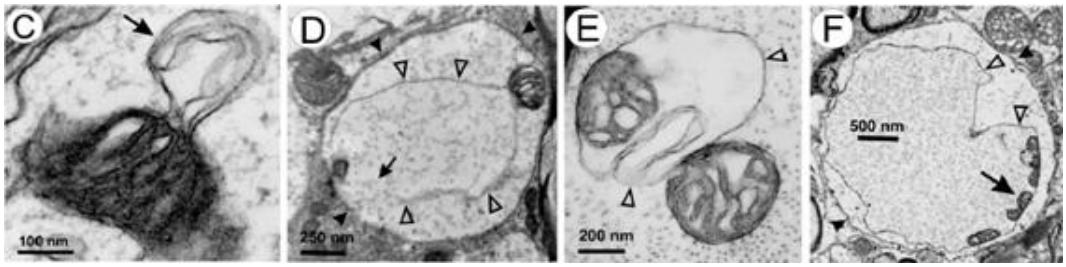


FIG. 7 Patterns of mitochondrial vacuoles: vacuoles are madeby extension of mitochondrial outer membrane and expansion of the intermembrane space (modified from Higgins et al., 2003)

Mitochondrial abnormalities have been found both in cellular and animal model of the pathology as well as in ALS patients (Raimondi et al., 2006; Pasinelli et al., 2006).
Mitochondrial dysfunction in ALS patients includes clusters of abnormal mitochondria and morphological defects identified within mitochondria in skeletal muscles and intramuscular nerves in human sALS cases (Atsumi, 1981; Afifi et al., 1966). In such cases biochemical analyses have delineated defects in the respiratory chain complexes I and IV in muscle (Wiedemann et al., 1998) and elevated levels of mitochondrial calcium (Siklós et al., 1996) in muscle and spinal cord. In ALS mice, the main morphological evidence for mitochondrial pathology is the presence of vacuolated mitochondria (for example, in the G93A and G37R transgenic lines).

In the SOD1 G93A mice, mitochondrial vacuoles derived from a detachment between the inner and the outer membrane (FIG.7; Higgins et al., 2003) are evident early, and drastically increase in both number and volume as the disease progresses (Kong and Xu, 1998; Bendotti et al., 2001; Sasaki et al., 2004).

Synaptic vesicles (SV)

Recent studies in different models of MN disease have emphasized early morphological abnormalities of NMJ synapses including accumulation of neurofilaments (NF) in the presynaptic terminal. Wong and colleagues report that in a spinal muscular atrophy (SMA) model that there is NMJ synaptic dysfunction that precedes axonal degeneration cellular death (Kong et al., 2009).
Moreover was documented a reduction in the total number of SV in the presynaptic terminal of the NMJ in animal models of ALS with an immunofluorescence.

## 2.5 ALS is a non-cell autonomous disease

To date, the attempt to understand the pathogenesis of ALS has not given any results, there are no consensuses about which cells, tissues and pathways are directly affected by mutant SOD1. Several lines of evidence indicate that the causative phenomena inducing MN degeneration is a direct consequence of a dominant paracrine activity that emanates from non-neuronal tissues (Clement et al., 2003).
The obvious loss of motor neurons in the spinal cord initially focused attention on how mutant SOD1 might act within motor neurons to provoke neuronal degeneration and death. However, the mutant proteins are ubiquitously expressed, thus the toxicity might result from the action of mutant SOD1 in non-neuronal cells.

Notably, the restricted expression of mutant SOD1 in postnatal motor neurons fails to produce detectable signs of pathology or motor neuron disease (Lino et al., 2002), while, more recently, has been demonstrated that transgenic mice in which mutant SOD1 was largely restricted to neurons, under the transcriptional control of Thy1.2 promoter, developed disease only at an old age (Jaarsma et al., 2008).

However, the disease progressed slowly without reaching the same degree of paralysis compared to the classical animal model of ALS in which the same mutant SOD1 gene is ubiquitously expressed. Moreover, the analysis of chimeras revealed that the presence of WT non-neuronal cells in adult chimeric mice is sufficient to prolong the lifespan of SOD1 mutant motor neurons. Although mutant SOD1 is also expressed by muscle, it is not clear whether its presence in skeletal muscle directly contributes to any pathological sign of ALS.

This issue has been recently investigated several group and it has been demonstrated that muscle-specific overexpression of mSOD1 induces progressive muscle atrophy

(Dobrowolny et al., 2008) and that alteration in skeletal muscles could exert a neurological effect on lower MN (Wong and Martin, 2010). These works might explain previous findings that have shown how the ubiquitous expression of SOD1 G93A in transgenic mice causes first muscle atrophy, which is later followed by alteration of the NMJ, retrograde axonal degeneration, and lastly, motor neuron death (Dupuis and Loeffler, 2009).

The retrograde mechanism of degeneration suggests the possibility that certain muscle abnormalities indeed precede motor neuron death rather than result from it. These studies are in seem to be in contrast with that reported previously by Miller and colleagues, they found that mutant SOD1 does not cause toxicity by its action within the muscle, which suggests that muscle is not a primary target for non-cell-autonomous toxicity in familial ALS (Miller et al., 2006). But the apparent discrepancy can be explained considering that knocking down of the protein is not complete and so it is not sufficient to delay the progression of the disease in mSOD1 mice: the residual expression of SOD1 G93A mutant gene is able to maintain the pathological phenotype

All the data reported indicate that skeletal muscles play a significant role in the first steps of the pathology and it has not a passive role as had been believed up to now. Moreover skeletal muscle is also a source of signals that influence neuron survival, axonal growth and maintenance of synaptic connections (Funakoshi et al., 1995).

*Postsynapting element*

Cross sectional area (CSA)

The first clinical symptom of ALS in patients and in animal models is the muscular weakness that could be explain through two different mechanisms: 1) the reduction of functional motor units because the denervation of fibers; 2) the reduction of CSA of those fibers that are still innervated and of those that are reinnervated trough the sprouting of new nerve endings (Hegedus et al., 2008; Frey et al., 2000).

## 2.6 Nandrolone decanoate

Anabolic drugs are synthetic analogues of testosterone that exert their action on muscle in a complex fashion, via several diverse mechanisms. These processes include directly binding to androgen receptors, which then undergo conformational changes and translocation into the nucleus to bind to DNA and/or interact with other proteins to regulate transcription (Wiegel and Moore, 2007). Other mechanisms include an anti-catabolic effect due to interference with glucocorticoid receptor expression, and by activating pathways in the CNS, which result in behavioural changes (Kicman, 2008).

Nandrolone has a higher affinity for androgen receptors than does testosterone (Saartok et al., 1984; Bergink et al., 1985). In androgenic tissue, testosterone is converted to a more potent metabolite than is nandrolone (Toth and Zakar, 1982; Sundaram et al., 1995). Consequently, nandrolone has higher anabolic and lower androgenic effects than testosterone (Shahidi, 2001). Nandrolone has been used to prevent muscular weakness and wasting in several pathology, such as chronic obstructive pulmonary disease (COPD), in this case its effect is more pronounced if associated with inspiratory muscle training (IMT) (Schols et al., 1995; Creutzberg et al., 2003), osteoporosis (Flicker et al., 1997; Frisoli et al., 2005), chronic renal failure (Johansen et al., 2006) and acquired immune deficiency syndrome (Dudgeon et al., 2006; Gold et al., 2006). Nandrolone is also the most widespread anabolic steroid used to increase muscle mass by athletes and, especially, bodybuilders (Van Marken Lichtenbelt et al., 2004). Despite its widespread use, however, the effects and mechanisms of action of nandrolone at the cellular level are poorly understood.

Satellite cells are mononuclear stem cells located between plasmalemma and basal lamina of the skeletal muscle fiber (Zammit et al., 2006; Figeac et al., 2007). Satellite cells have the ability to become active, proliferate and differentiate into new myonuclei during the postnatal maintenance, growth, regeneration or repair of muscle fibers (Kuang and Rudnicki, 2008). Satellite cell entry into the cell cycle can be stimulated by a variety of influences including mechanical stressors, such as exercise or stretch, growth factors and hormones (Anderson, 2006; Brack and Rando, 2007). It is thought that satellite cells differentiating into myonuclei will maintain the ratio between cytoplasmic volume and number of myonuclei (Alway and Siu, 2008). The administration of testosterone, the most widely studied anabolic androgenic steroid, has been shown to increase satellite cell numbers in muscle.

Moreover has been demonstrate that nandrolone could increase the level of expression of both mRNA coding for IGF-1 (Gayan Ramirez et al., 2000) and the protein itself (Lewis et

al., 2002) in the diaphragm of rats, and that muscle-specific expression of local IGF-1 stabilizes NMJs in mSOD1 mice (Dobrowolny et al., 2005) delaying disease onset and progression.

In a paper of Bishop and colleagues it has been demonstrate that the effectiveness of nandrolone administration is higher in the diaphragm than in all other skeletal muscles (Bisschop et al., 1997).

# 3. AIM OF THE PROJECT

Amyotrophic lateral sclerosis is a distal axonopathy that begins in the most susceptible and specialized point of a motor unit: the neuromuscular junction. Over the last years was clarified that both the presynaptic terminals (buttons of nerve endings) and the postsynaptic elements (myofibers) are both involved in the degeneration of MU.
What happens later is better described: the nerve terminal retracts in a retrograde manner through a dying back process and at the same time the muscle undergoes atrophy.

The aim of this process is to characterize the anatomical alterations of the components of MUs both at the clinical onset and at the pathological end stage to identified any signs of alteration and how this phenomenon change during the pathological course.

We chose muscle with different characteristics of resistance, strength and plasticity (the soleus, the diaphragm and the gastrocnemius), but we deeper analyzed just diaphragm muscles that showed an intermediate response to the degeneration, moreover the diaphragm plays a key role in the late stage of ALS because patients die to respiratory failure.

The second part of this project is a study of effectiveness of nandrolone administration; we investigated again all the morphological and morphometric parameters to identify, which were rescued at a control level after the treatment with this drug. Nandrolone is already employed in the treatment of pathologies characterized by muscular weakness and wasting and it demonstrated to prevent atrophy and to improve strength and resistance of skeletal muscle.

# 4. MATERIAL AND METHODS

## 4.1 Animals and procedures

The transgenic mice expressing the human SOD1 gene carrying the G93A substitution used in this study belong to the B6SJL-Tg(SOD1*G93A)1Gur/J strain (Gurney et al., 1994) and were initially obtained from Jackson Laboratories (Bar Harbor, ME). The transgenic mice were genotyped by PCR amplification for the human SOD1 gene, as described elsewhere (Kassa et al., 2009). Littermate, non-transgenic B6SJL mice were used as age-matched controls. The appearance of muscular weakness sings was evaluated with standard motor tests (Paw grip endurance test, Rotarod test). The transgenic mice were also monitored for the appearance of tremors and extension reflexes. At P85-P95, first muscular symptoms were detected in transgenic mice, at this time point both transgenic and WT littermate were sacrificed, after deep anesthesia (chloral hydrate, 600 mg/kg i.p.), with trancardiac perfusion with saline solution followed by 4% paraformaldehyde in 0.1M phosphate buffer, pH 7.4 (PB). The mice used in the analysis of the late stage of the pathology were female mice initially obtain from the Jackson Laboratories (Bar Harbor, ME) and belong to the same B6SJL-Tg(SOD1*G93A)1Gur/J strain (Gurney et al., 1994). Animals were sacrified at the end of $20^{th}$ week of age (P140). The muscles soleus, diaphragm and gastrocnemius were dissected and further fixed by 2 h immersion in the same fixative. The analysis of different muscles was aimed, at the comparison of muscles with different fiber composition. The muscles were then extensively washed in PB and stored in 0.01M phosphate-buffered saline, pH 7.4 (PBS: 0.8% NaCl, 0.02% KCl, 0.144% $Na_2HPO_4$, 0.024% $KH_2PO_4$), containing 0.5% sodium azide at 4°C, until further processing. To prevent alteration due to the chemical fixation several samples of soleus and gastrocnemius muscles were dissected and cryo-fixed in liquid nitrogen then stored at T -80°.

Twelve male mSOD1 transgenic mice and wild-type littermates were divided into two groups (n= 6 in each group) and treated with either vehicle (NAN-) or nandrolone (NAN+). Nandrolone (Nandrolon Vetranal®; Sigma-Aldrich, St. Louis, MO; 10 mg/kg, dissolved in peanut oil) was administered once a week by subcutaneous injection, starting at P52 and until symptom onset (as determined by the above tests), when the animals were sacrificed.

## 4.2 Fluorescence and Immunofluorescence Analysis

*Diaphragm*

Small portion of diaphragm close to phrenic nerve were dissected and samples were then blocked in 5% Horse Serum, 1% BSA, 1% Triton X-100 in PBS, and then stained with 1.6% α-Bungarotoxin (BuTX) conjugated with tetramethyl-rhodamine (TRITC) (Molecular Probes – Invitrogen) in the same blocking solution (BS).
After the staining, samples positive for BuTX were collected and incubated with the primary polyclonal antibody, in these sets of experiments were used both a polyclonal antibody directed against Synapsin 1 (a gift from Prof P.De Camilli) (1:400 in BS) or a polyclonal antibody direct against Synaptotagmin 1 (SYSY) (1:400 in BS) were used.
As negative control we used samples in which the step with primary antibody was omitted.
After three steps in washing solution (WS) (0,5% Triton X-100 in PBS), samples and negative controls were incubated with secondary antibody α-rabbit conjugated with Alexa Fluor 488 (1:200 in WS) (Molecular Probes – Invitrogen). Images were collected using a Biorad MRC 1024 confocal laser-scanning microscope and we considered as innervated NMJ in which the staining for the presynaptic compartment was present.

*Soleus and gastrocnemius*

The muscles were embedded in Optimal Cutting Temperature (OCT) and frozen; 20 μm thick cryostat sections of the entire muscle were collected on superfrost ultra plus glass slides (Thermo Scientific) and processed for immunolabelling and BuTX labelling as described above.

*Analysis of acetylcholine receptor clusters*

For the evaluation of the total surface and complexity of AChR clusters on the postsynaptic membrane, z-stacks of confocal images of NMJs were collected and splitted into two classes in relation of their state of innervations. Then the max projection of NMJ (made using the max intensity method) was analyzed with ImageJ software version 1.4. The projection was converted into an 8-bit image, upon which a bitmap mask was generated based

on the fluorescence intensity threshold. The total area of each NMJ was obtained by adding the surface of each fluorescent fragment.

## 4.3 Transmission electron microscopy (TEM)

For transmission electron microscopy (TEM) analysis, bundles of fibers from control and mSOD1 perfused muscles were washed and incubated for 30 min with TRITC-BuTX (15 mg/ml PBS). Regions of the sample enriched in NMJs, identified with BuTX staining, were reduced in size to small segments of 4-5 fibers of 1 mm in length and further fixed with 2% glutaraldehyde in 0.1M cacodylate buffer, pH 7.4, and processed with the conventional embedding protocol as reported in Francolini et al., 2009. Briefly, the samples were post-fixed with osmium tetroxide (2% $OsO_4$ in cacodylate buffer), rinsed, *en bloc* stained with a satured solution of uranyl acetate in absolute ethanol, dehydrated and embedded in epoxy resin (Epon 812, Electron Microscopy Science, Hatfield, PA), that was baked for 48 h at 67°C.

Semithin sections of 0.5 μm were obtained with an ultramicrotome (Reichert Ultracut E, Leica Microsystems, Austria), collected on glass slides and stained with 0.1% methylene blue, 0.1% toluidine blue in PB and observed with an optical microscope with a 60X oil immersion objective (Zeiss, Germany). Images were acquired with a CCD Axiocam HR (Zeiss); both longitudinal and coronal sections of muscle were used for the evaluation of the fiber diameter using the ImageJ software.

Thin sections and collected on EM copper grids (300 mesh), stained with uranyl acetate and lead citrate and examined with a Philips CM10 TEM (FEI, Eindhoven, Holland).

## 4.4 Morphometric analysis at the ultrastructural level

*Synaptic vesicle pools*

Electron micrographs were acquired with an EPSON perfection 4990 Photo scanner (grey scale, 8 bit, 600 ppi, TIF extension) and were used for the evaluation of the total number of synaptic vesicles and of their distribution within the presynaptic terminals.
Each synaptic vesicle has been manually identified with a single pixel point and the presynaptic membrane with a ten pixel-thick continuous line.
Distance between vesicles and active zone were calculated by means of a custom ImageJ macro at pixel resolution.
To automatically find the minimal distance between vesicles and an irregular active zone we started from two binary images. The first reported the position of each vesicle centre (the one-pixel point) whereas the second represented active zones as continuous lines.
The macro causes expansion of active zone in every direction by pixel dilatation according to an octagonal dilatation scheme (Righi et al., 2009).
The distance of each vesicle was collected when the boundary of the growing line superimposed over the vesicle centre. It was then straightforward to build the cumulative curve of vesicles in function of their distance.
Analyzing 3 neuromuscular junctions, we validated the macro, manually and our results were compared to ones obtain by the macro. This comparison showed that errors, due to the octagonal shape of the expansion, instead of circular, and to sub-pixel distances, were lower than 5%.

A particular tool of the macro allowed to classify vesicular pools by their distance from the presynaptic membrane: docked vesicle belonging to readily releasable pool (distance lower than 20 nm), vesicles far from 20 to 200 nm and vesicles more distant than 200 nm as previously described by Kong and colleagues (Kong et al., 2009).

*Mitochondrial pool*

Mitochondria of the presynaptic terminal were divided into two classes in terms of their morphology state (intact or altered) and in NMJ button were evaluated the density of mitochondria, the number of altered profiles and the morphometric parameters of any mitochondrion (area and circularity).

Digital images were gathered using the same parameters of acquisition that was employed for SV micrographs, and analyzed using ImageJ standard tools.

Macro text

```
/*
Macro for classification of synaptic vescicle in zones, according to
distances from a single active zone. Single image version.

Versions.
v. 1.0 10feb2010

*/

macro "Vescicle classification" {vesciclass();}

function vesciclass() {
      requires("1.35b");

// Definition of interface arrays

      Ingrandimenti = newArray("8900x", "11500x", "15500x", "21000x");
      Risoluzione = newArray("300ppi", "600ppi", "1200ppi");
      Rapporto = newArray("1:1");
      up = newArray(0,0,0,0,0,0,0,0,0,0,0,0,0,0,0,0,0,0,0,0,0,0,0,0,0);
      limite = newArray(0,0,0,0,0,0,0,0,0,0,0,0,0,0,0,0,0,0,0,0,0,0,0,0,0,0);
      totves = newArray(0,0,0,0,0,0,0,0,0,0,0,0,0,0,0,0,0,0,0,0,0,0,0,0,0,0);

// User interface for input of image data

      Dialog.create("Settings");
      Dialog.addString("Job title?", "",15);
      Dialog.addMessage("Set magnification and image resolution\n");
      Dialog.addChoice("Photo enlargements", Ingrandimenti,
Ingrandimenti[1]);
      Dialog.addChoice("Scanner resolution", Risoluzione, Risoluzione[1]);
      Dialog.addChoice("Pixel X/Y ratio", Rapporto, Rapporto[0]);
      Dialog.addNumber("Number of zones ", 2,0,3," except the last one");
      Dialog.addMessage("\n");
      Dialog.show();
      Identificativo = Dialog.getString;
      magni = Dialog.getChoice();
      resol = Dialog.getChoice();
      ratio = Dialog.getChoice();
      nclass = Dialog.getNumber();

      if (nclass < 1) {
            exit("You must set at least 1 zone!");
      }
      if (nclass > 25) {
            exit("No more than 25 zones available!");
      }

      Dialog.create("Zone dimensions");
      Dialog.addMessage("Max distance from active zone:");
      Dialog.addMessage("N.B.: each value must be greater then the previous
ones!\n");
      for (i=1; i<nclass+1; i++) {
```

```
            Dialog.addNumber("     Zone "+i+" up to: ", 0, 0, 5,
"nanometers");
      }
      Dialog.addMessage("Final zone for data external to previous zones");
      Dialog.show();
      for (i=0; i<nclass; i++) {
            up[i] = Dialog.getNumber();
      }

// Calculating pixel dimension

      val_magni = parseInt(replace(magni, "x", ""));
      val_res = parseInt(replace(resol, "ppi", ""));

      pxdim = 25400000 / (val_res * val_magni);
      for (i=0; i<nclass; i++) {
            limite[i] = round(2*up[i]/pxdim);
            totves[i] = 0;
      }

// Definitions of variables

      k = 0;
      r = 0;
      Initvesc = 0;
      vestot = 0;
      ves_actual = 0;

// Recording start time

      getDateAndTime(year, month, week, day, hour, min, sec, msec);
      mese = month+1;

      setBatchMode(true);

      dir1 = getDirectory("Where would you save the result file?");

      showMessage("Open input image");
      open();

      a=getTitle();
      altezza = getHeight();
      larghezza = getWidth();
      if ((altezza-larghezza) > 0) {
            totpx = altezza;
      }
      else {
            totpx =larghezza;
      }
      results=File.open(dir1+"V_"+a+".txt");
      firstline = "Job: "+Identificativo+"\n";
      secondline = "Analyzed image: "+a+"\tthe day:
"+day+"."+mese+"."+year+" at: "+hour+":"+min+":"+sec+"\n\n";
      print(results, firstline);
      print(results, secondline);
      print(results, "Parameters:\n");
      print(results, "Magnification: "+magni+"\n");
      print(results, "Resolution: "+resol+"\n");
      print(results, "Pixel dimension: "+pxdim+" nanometri\n");
      for (i=0; i<nclass; i++) {
            print(results, "Pixels for "+up[i]+" nanometers:
"+limite[i]/2+"\t");
```

```
      }
      print(results, "\n");


// Identify vescicle positions

      run("Analyze Particles...", "size=0-1 circularity=0.00-1.00
show=Masks clear");
      rename("V");

// Identify location of the active zone

      selectWindow(a);
      run("Analyze Particles...", "size=2-infinity circularity=0.00-1.00
show=Masks clear");
      rename("S");
      selectWindow(a);
      close();

// Count the number of initial vescicles and write it on file

      selectWindow("V");
      run("Analyze Particles...", "size=0-1 circularity=0.00-1.00
show=Nothing clear record");
      Initvesc = nResults;
      LeftVesc = Initvesc;

      print(results, "Total Initial Vescicles: "+Initvesc+"\n\n");

/*
Defines the coordinates of the active zone and draws circles with diameter
equal to settings centered on every pixel of the active zone. Summing all
the circles we define the area of the zone within x nm from the active
zone. This step is repeated  for every set limit whereas the external area
is calculated by difference.
*/

      selectWindow("S");
      for (i=0; i<nclass; i++) {
            run("Duplicate...", "title="+i);
      }

      selectWindow("S");
      setThreshold(254,255);
      run("Create Selection");

/*
Given that the Create Selection command define the boundaries of the
external rectangle we perform a cycle on the selction to find the first
black pixel. Once found, we select black pixels by magic wand and escape
from cycles changing cycle limits.
*/
      getSelectionCoordinates(c, d);
      for (j=d[0]; j<d[2]; j++) {
            for (i=c[0]; i<c[1]; i++) {
                  if(getPixel(i,j) == 255) {
                        doWand(i,j);
                        i=c[1];
                        j=d[2];
                  }
            }
      }
```

```
// The macro gets coordinates of every single pixels of the active zone

      getSelectionCoordinates(xx, yy);
// Then for every set zone...

      for (t=0; t<nclass; t++) {
            setForegroundColor(0,0,0);
            setBackgroundColor(255,255,255);
            tit = toString(t);
            selectWindow(tit);

// ...the macro select circles, with the appropriate diameter, centered on
every single pixel of the active zone and fill them, obtaining the area
inside the set  max distance from active zone.

            for (i=0; i<xx.length; i++) {
                  run("Specify...", "width="+limite[t]+"
height="+limite[t]+" x="+xx[i]+" y="+yy[i]+" oval centered");
                  fill();
                  showProgress(i/xx.length);
            }
            setThreshold(1, 255);
            run("Convert to Mask");

// the macro sums images of current sampling zone and vescicles in a new
image. Only pixels which mark vescicles outside of the sampling area appear
isolated.

            imageCalculator("Add create", "V",tit);
            rename("G");

// 1. Counts the number of isolated pixels (external vescicles) in the new
image

            run("Analyze Particles...", "size=0-1 circularity=0.00-1.00
show=Nothing clear record");

// 2. Vescicles in the zone under analysis are obtained subtracting
external vescicles from remaining vescicles (at start remaining vescicles =
initial vescicles).

            totves[t] = LeftVesc - nResults;
            finves = nResults;

// 3. Counts all the vescicles so far counted in zones

            sommatotves = 0;
            for (k=0; k<t+1; k++) {
                  sommatotves = sommatotves + totves[k];
            }

// 4. Set remaining vescicles as initial vescicles minus the vescicles so
far counted in zones

            LeftVesc = Initvesc - sommatotves;
            close();
      }


// Write results on file
```

```
      print(results, "Vescicles between 0 e "+up[0]+" nanometers from the
active zone: "+totves[0]+"\n");
      for (t=0; t<nclass-1; t++) {
            print(results, "Vescicles between "+up[t]+" and "+up[t+1]+"
nanometers from the active zone: "+totves[t+1]+"\n");
      }
      if (nclass > 0) {
            print(results, "Total vescicles beyond "+up[t]+" nanometers
from the active zone: "+finves+"\n");
      }
      else {
            print(results, "Total vescicles external to the active zone:
"+finves+"\n");
      }

// Closing result file and working images. End of the macro

      File.close(results);

      selectWindow("S");
      close();
      selectWindow("V");
      close();
      for (i=0; i<nclass; i++) {
            selectWindow(i);
            close();
      }

      setBatchMode(false);

      showMessage("End of Analysis");
}
```

## 4.5 Statistical analyses

All the data collected were finally analyzed with the statistical software Prism 4.0 and refers to six animals for each experimental point the total number of observation is reported in the text.

Differences in the onset of pathological symptoms between groups of animals were evaluated with the Kaplan-Meier analysis.

Intergroup comparison of any morphometric parameter were evaluated using the two tailed unpaired Student's t test. Data are expressed as mean ± standard deviation; intergroup comparison was also pursued with one-way analysis of variance followed by the Bonferroni *post-hoc* test and gave the same results. Significance threshold was set at $p<0.05$.

# 5. RESULTS

## 5.1 Innervations of skeletal muscle fibers

Neuromuscular junctions are chemical synapses formed by a presynaptic terminal (MN) and by a postsynaptic element, the muscle fiber. We have characterized the innervations of NMJs using an immunofluorescence approach, to obtain these results we have taken small bundles of muscle fibers (diaphragm) or cryostat sections of the muscle (soleus and gastrocnemius). The samples were then stained with TRITC-conjugated α-bungarotoxin, in this way all the Achetylcholine receptor clusters on the postsynaptic membrane were labelled (Fig.1A and C BuTX). Innervation was determined using antibodies direct against presynaptic markers such as synaptotagmin1 or synapsin1. An innervated NMJ shows a labelling for presynaptic proteins (Fig.1A α-syn) that perfectly colocalizes with the postsynaptic staining (Fig.1A merge), while, in a denervated NMJ the staining for the presynaptic compartment is lost as reported in Fig.1C α-syn. The BuTX labeling revealed in both the innervations states that clusters of AChRs had the typical pretzel-like shape.

At the ultrastructural level innervated and denervated NMJ are easily distinguishable: in innervated NMJ (Fig.1B) the presynaptic terminal, containing synaptic vesicles and cytoplasmatic organelles, lie in shallow primary folds on the membranes of muscle fibers and the entire synapse is isolated by processes of Schwann cells that play a structural and functional role in the manteinence of neurotransmission.

In denervated NMJ (Fig.1D) the presynaptic button is lost, the primary fold is flattened while the secondary folds are preserved, processes of Schwann cells and collagene fibers cover the empty space over the cluster of receptors.

We used these approaches to evaluated the percentage of innervations in skeletal muscles both at early stage of the pathology (the clinical onset – P85-P90) and at the end stage (P140). Our results indicated that the denervation process affect differently the muscles that we have analyzed muscles infact, the soleus muscle is completely innervated at the early stage of the disease (Fig.2 B), while just a small amount of fibers are denervated at the end stage (20% - Fig.2B), over a majority of fibers that didn't show any phenotype (Fig.2A).

In our experimental model the diaphragm is more affected than the soleus and the gastrocnemius at P85-95, infact we observed that about 30% of fibers were denervated in transgenic mice compared to control ones, the percentage of innervations is further reduced at the end stage to the value of 46.5%. whereas gastrocnemius that is more resistant at the clinical onset (81% of fibers are innervated) is drastically denervated at the end stage (12% of innervations) (Fig.2C).

The intermediate response to the degeneration observed in diaphragm muscle that could reflect its mixed fibers composition is the reason because we chose to further investigate the ultrastructure of this muscle.

### 5.11 Characterization of the presynaptic terminal

*Mitochondrial pool*

Mitochondrial pool represent one of the primary target of ALS-induced damage in the presynaptic terminal of motor neuron, features of alteration such as vacuolization, swelling and disorganization of cristae, appear early before the beginning of the denervation process. (Duffy et al., 2011).

Alteration in those organelles are deeply characterized both in cellular cultures and in spinal cords of rodents l (Raimondi et al., 2006; Jaarsma et al., 2001), but to date only few papers were published reporting their ultrastructural characterization in the neuromuscular junctions (Dupuis et al., 2009).

Here we performed a morphological and morphometric analysis of the mitochondrial pool both in WT and mSOD1 to clarify mitochondrial involvement in the early stage of degeneration of motor neuron associated with ALS.

In diaphragm NMJs of WT mice each presynaptic button contains one to five mitochondria/$\mu m^2$ as reported in Fig. 3B and the total area of mitochondrial pool occupied about 23% of the presynaptic terminal area (Fig. 3E), mitochondria were round in shape, with continuous inner and outer membranes and slightly electron dense matrix (Fig.3A and inset), while in mSOD1 mice were present two different populations of mitochondria in diaphragm: intact and altered.

The number of mitochondria and their density within the synaptic button did not change significantly between CTRL and mSOD1 mice (Fig. 3 B and E).

In the diaphragm of mSOD1 mice about the 60% of presynaptic buttons contained mitochondria, which had an aspect comparable with the one of mitochondria in CTRL mice (Fig. 3C and inset; Fig. 3F), while in the remaining 40% of NMJ mitochondria showed discontinuity of both the inner and the outer membranes and a pale matrix (Fig. 3D and inset; Fig. 3F).

Altered mitochondria were swollen and in some cases vacuolization phenomena were present, these alteration induce an increase of the average area of mitochondria (0.18 $\mu m^2 \pm$

0.10) compare to intact (0.13 $\mu m^2$ ± 0.05 p = 0.016) and to control (0.11 $\mu m^2$ ± 0.04 p < 0.0001) ones (Fig. 3G). Despite these results we did not observe alteration of other parameters such as circularity index (value of ratio between area and perimeter of mitochondria as reported in Akao et al., 2003) (CTRL 0.89 ± 0.05; n = 76; mSOD1 intact 0.86 ± 0.13; n = 37; mSOD1 altered 0.85 ± 0.11; n = 33. Fig. 3H).

At the pathological end stage mitochondrial pool was even more affected, at the ultrastructural level both inner and outer membranes were completely disorganized (Fig. 4A and inset). Moreover we observed a reduction in the number of mitochondria (between 0.2 and 2.3 mitochondria/$\mu m^2$; n = 11) compare with what observed in NMJ of mice sacrificed at the clinical onset. This phenomenon was accompanied by the reduction of the total size of mitochondrial pool (12% of the presynaptic area; n = 11; Fig. 4C). The percentage of neuromuscular junctions which showed altered mitochondria was increased in these mice compared to the younger ones (72.7%; n = 11; Fig. 4D).

Moreover the mitochondrial area in mSOD1 mice at the end stage is also broader (0.34 $\mu m^2$ ± 0.29) than what observed in mSOD1 mice at the clinical onset of the disease.

*Synaptic vesicles pool*

It has been proposed that alteration in synaptic vesicles pool could be an early contributor to muscle weakness in motor neuron diseases (Kong et al., 2009), so we focused our attention in the analysis of synaptic vesicles density within the nerve ending of MNs using the Imagej tool as reported in Material and Method chapter.

In Fig. 5 is reported a representative micrograph of nerve ending button analized with this approach (Fig.5A) and the mask that the software generated in which each synaptic vesicle is pointed in its centre and the presynaptic membrane is labelled with a 10 pixels-thick line (Fig. 5B).

Panel C in the same figure indicates how the software works: starting from magnification and resolution of each image, the mask was analyzed and data related to the number and the distribution of synaptic vesicles was extrapolated.

In NMJ of mSOD1 mice we observe a significant reduction in the total amount of SV (125.4/$\mu m^2$ ± 80.1) compared to CTRL group (220.3/$\mu m^2$ ± 112.6 p= 0.0035) (Fig. 5D). Although in mSOD1 presynaptic terminals the morphology of synaptic vesicles did not differ from those observed in CTRL samples and the reduction did not correlate with number or the state of mitochondria within the same button.

We next examined the distribution of synaptic vesicles according to their distance from presynaptic plasma membrane, to this aim we classified vesicles as: docked vesicles (0-20 nm from the plasma membrane), vesicles located within 200 nm and vesicles located beyond 200 nm from the plasma membrane.

We did not find any significant difference in SV distribution comparing WT NMJs (10.4//$\mu m^2$ ± 7; 75.7/$\mu m^2$ ± 50.6; 134.2/$\mu m^2$ ± 63.4) with mSOD1 (8.2/$\mu m^2$ ± 6.3; 63.6/$\mu m^2$ ± 40.3; 90.1/$\mu m^2$ ± 55.9) ones (Fig. 5E), nor difference in the synaptic vesicle pool organization between mSOD1 terminals containing intact or altered mitochondria. For the evaluation of SV distribution 12 buttons were analyzed for each experimental point.

### 5.12 Characterization of the postsynaptic element

*Skeletal muscle fibers*

For the evaluation of fibers diameter we used both coronal and longitudinal sections of skeletal muscle inclusions (Fig. 6 A e B), of WT and mSOD1 mice at the clinical onset of the disease.

Muscles analyzed, the soleus, the diaphragm and the gastrocnemius, showed different response to the pathological condition:

| | CTRL | | | mSOD1 | | |
|---|---|---|---|---|---|---|
| | **Mean** | **SD** | **N** | **Mean** | **SD** | **N** |
| **Soleus** | 32.85 | 10.33 | 277 | 41.11 | 14.22 | 277 |
| **Diaph** | 35.75 | 6.47 | 216 | 29.66 | 6.57 | 277 |
| **Gastro** | 35.68 | 11.70 | 178 | 35.79 | 10.90 | 100 |

For the further understanding of these differences we divided fibers in size classes thin fibers (diameter < 20 μm), medium fibers (20 μm < diameter < 30 μm) and thick fibers (diameter > 30 μm).

| | CTRL | | | mSOD1 | | |
|---|---|---|---|---|---|---|
| | x<20 | 20<x<30 | x>30 | x<20 | 20<x<30 | x>30 |
| **Soleus** | 6.86 | 38.27 | 54.87 | 2.17 | 24.55 | 73.29 |
| **Diaph** | 0.00 | 22.22 | 77.78 | 3.97 | 54.51 | 41.52 |
| **Gastro** | 5.62 | 28.09 | 66.29 | 11.00 | 19.00 | 70.00 |

*Clusters of ACh receptors*

Then we then focused our attention on the evaluation of the size and the architecture of the clusters of acetylcholine receptors (AChR) in the postsynaptic membrane.

In IF experiments (see the chapter of Material and Method, paragraph of 'Fluorescence and Immunofluorescence Analysis') we collected z-series of images of AChR clusters, labelled with TRITC-conjugated BuTX (Fig. 7 A and C) and the measure of the total area of the cluster was performed on maximun projection after the application of an intensity threshold (Fig. 7 B and D).

In the diaphragm of CTRL animals, the mean area of AChR cluster is 360.75 $\mu m^2$ ± 126.97 (n = 92; Fig. 7E) compared to 429.53 $\mu m^2$ ± 119.38 (n = 62) of mSOD1 mice, the same increased was observed in the gastrocnemius were the clusters size increased from 297.8 $\mu m^2$ ±120.1 (n = 10) of CTRL muscles up to 352.6 $\mu m^2$ ± 96.16 (n = 10) of mSOD1 ones.

Moreover we evaluated if the innervations state of NMJ had any relevance in this increase so we divided innervated junctions from the denervated ones.

The denervated junctions of mSOD1 diaphragm shown a broader BuTX-positive area (452.2 $\mu m^2$ ± 113.3; n = 21) compared to innervated junctions of transgenic mice (418.2 $\mu m^2$ ± 107.6; n = 34) and also compared to NMJs of control muscle (Fig. 7E).

We also evaluate the size of clusters in the gastrocnemius in samples stained just with BuTX and our results indicated that the mean BuTX-positive surface is broader in mSOD1 mice compared with CTRL ones (CTRL 297.8 $\mu m^2$ ±120.1; n =10; mSOD1 352.6 $\mu m^2$ ±96.16; n = 10; p = n.s.).

## 5.2 Nandrolone administration

In the second part of this project we performed a study of effectiveness of a pharmacological treatment with the steroid nandrolone decanoate.

This drug is employed in the treatment of those pathologies that induce wasting of skeletal muscles (Sardar et al., 2010).

In rodents it has been demonstrated that nandrolone is able improve respiratory functions in rodents, improving the force and the strength of respiratory muscles (including diaphragm) more efficiently than with inspiratory muscle training (Gayan-Ramirez et al., 2000).

### 5.21 Characterization of the presynaptic terminal in treated mice

*Mitochondrial pool*

We then analyzed, using the same morphological and morphometric parameters, the characteristics of the mitochondrial pool in the presynaptic terminal of innervated neuromuscular junctions of treated mice and we compared these results with those obtained in the previous analysis.

The architecture of mitochondria in the presynaptic terminal was rescued in treated mSOD1 mice compared with untreated and the percentage of altered mitochondria (9%) gained levels comparable with CTRL animals (Fig. 8A).

Our observations indicated that altered mitochondria in NMJ of treated mice had a broader area (0.203 $\mu m^2 \pm 0.13$; n = 23), compared with intact mitochondria belonging to the same class (0.113 $\mu m^2 \pm 0.075$; n = 45; p = 0.0055), while there were not differences neither between area of intact mitochondria belonging to different classes nor to altered ones (Fig. 8B).

Circularity index did not change between treated and untreated mice (treated mSOD1 intact 0.83 ± 0.12; n = 45; altered 0.74 ± 0.15; n = 23; p = n.s.) nor between intact and altered mitochondria belonging to different class of mice (Fig. 8C).

Moreover there was no difference in the density of mitochondria within the presynaptic button comparing treated and untreated mice (mSOD1 NAN – 1.987 n/$\mu m^2 \pm 1.3$; n = 12; mSOD1 NAN + 1.96 n/ $\mu m^2 \pm 0.99$; n= 11) (Fig. 8D).

*Synaptic vesicles pool*

Treatment with nandrolone exerted also an effect in the density of synaptic vesicles, the total number of SV was reduced in treated mice (92.69 n/$\mu m^2$ ± 56.73; n = 18) compared with untreated ones (Fig. 8E), but this reduction is more evident in pools of vesicles closer to the presynaptic membrane (mSOD1 treated mice docked vesicle 2.4 n/$\mu m^2$ ± 3.5; between 20 and 200 nm 33.71 n/$\mu m^2$ ± 22.34; beyond 200 nm 64.74 n/$\mu m^2$ ± 48.02; n = 11) compared to untreated animals (Fig. 8F).

**5.22 Characterization of the postsynaptic element in treated mice**

*Skeletal muscle fibers*

The evaluation of fibers diameter in mSOD1 mice indicated that nandrolone was able to induce an increase of this value both in diaphragm (37.24 μm ± 7.64; n = 304; $p < 0.0001$) and in gastrocnemius (45.75 μm ± 13.87; n = 104; $p < 0.0001$) compared to the respective muscles of untreated mSOD1 mice (Fig. 9A).

As we did for control mice we also divided muscular fibers in classes related to their diameter. (Fig. 9B).

| | untreated | | | treated | | |
|---|---|---|---|---|---|---|
| | x<20 | 20<x<30 | x>30 | x<20 | 20<x<30 | x>30 |
| Diaph | 3.97 | 54.51 | 41.520 | 0.66 | 17.43 | 81.910 |
| Gastro | 11.00 | 19.00 | 70.000 | 7.81 | 12.50 | 79.690 |

*Clusters of ACh receptors*

Next we examined the architecture of cholinergic receptor clusters in treated mice as we did for those of untreated ones. The shape and the complexity of cluster did not change between treated and untreated mice neither in the diaphragm nor in the gastrocnemius. The mean area of clusters in the gastrocnemius of treated mice was broader than what observed in untreated muscle (NAN- 352.6 $\mu m^2$ ± 96.16; n = 10; NAN+ 644.6 $\mu m^2$ ± 92.85; n = 10; p = 0.017). In the diaphragm we deeper investigated this phenomenon in IF samples so we divided innervated and denervated junctions. Our results indicated that nandrolone

administration is sufficient to induce an increase of this value both in innervated (538.2 $\mu m^2$ ± 160.8; n = 27; p = 0.005) and denervated (496.4 junctions. $\mu m^2$ ± 127.5; n = 23; p = n.s.) as well as in CTRL animals (410.56 $\mu m^2$ ± 116.11; n = 93; p = 0.0059; Fig. 9C and table).

| | CTRL | | | INN | | | DEN | | |
|---|---|---|---|---|---|---|---|---|---|
| | **Mean** | **SD** | **N** | **Mean** | **SD** | **N** | **Mean** | **SD** | **N** |
| **untreated** | 360.8 | 127.0 | 92 | 418.2 | 107.0 | 34 | 452.2 | 131.3 | 27 |
| **treated** | 410.6 | 116.1 | 93 | 538.2 | 160.8 | 21 | 496.4 | 127.5 | 23 |

## 5.3 Percentage of innervated fibers and clinical onset of the disease in treated mSOD1 mice

The evaluation of percentage of innervated fibers was made both in diaphragm and in gastrocnemius muscle of treated mice, at the clinical onset of the disease, our data indicated that nandrolone administration induced a slight increase of the number of innervated fibers in diaphragm (76.33%) compared to untreated ones, while the effect is mor pronounced in gastrocnemius muscle where the percentage is completely rescued to control level (100%; Fig. 10A )

In our experimental model the percentage of innervations showed a great variability in the diaphragm (Fig. 10B), moreover the partial rescued of this value in treated mice was not enough neither to delay, nor to prevent the clinical onset of the pathology (Fig. 10C).

# 6. DISCUSSION

The first part of this study is focused on the anatomical characterization of motor units and, particularly, on the morphological alteration induced by the ALS phenotype. In this project we use SOD1 G93A mice (Gurney et al., 1994) as model of a familial form of ALS. This is the first time that NMJs of the murine diaphragm were analyzed at an ultrastructural level in this model of ALS, moreover we investigated both the clinical onset of the disease and the pathological end stage to evaluate sings of disease progression.

Our data indicate that different muscles behave differently, in fact the diaphragm and the gastrocnemius show a slight percentage of denervated fibers at the clinical onset and a more severe condiction at a later stage, while the soleus is completely innervated at the early stage and shows just a small amount of denervated fibers at P140, this phenomenon is due probably to the differential MU composition of these muscles (Frey et al., 2000) In this work we focused our attention on the diaphragm because of its role in the death of ALS patients. Treatment with nandrolone preserved the diaphragm muscle mass and reduced mitochondrial damage in nerve endings, but did not significantly increase the number of innervated diaphragm fibers. In the gastrocnemius, where we did not observe ALS-induced reduction of fibers size, nandrolone administration is sufficient to induce fiber hypertrophy, which is probably due to the proliferation of satellite cells (Allouh and Rosser, 2010).

*Presynaptic terminals innervating the diaphragm exhibit structural alterations in mSOD1 mice at early symptomatic stage*

By analyzing the fine structure of mitochondrial pools in presynaptic terminals of NMJs of mSOD1 mice, we here provide evidence of alterations of mitochondria, which exhibited disorganization of cristae in about 40% of presynaptic profiles, this morphological index of alteration is evenmore pronounced at the pathological end stage indicating that mitochondrlia degeneration, which is an early effect in ALS, proceeds during all the degenerative process. In thin sections, the profiles of these mitochondria were significantly broader than those of intact mitochondria in NMJs of both mSOD1 and wild-type mice. Other parameters, such as circularity and density, did not differ between mitochondria of mSOD1 and wild-type NMJs.

Mitochondria are considered one of the major intracellular targets of mSOD1 toxicity in motoneurons (Kong and Xu, 1998; Liu et al., 2004), and several studies have reported alterations in their functionality (Mattiazzi et al., 2002; Ferri et al., 2006), as well as in their morphology in neurons and muscles of ALS patients (Siklós et al., 1996; Menzies et al.,

2002a and references therein; Chung and Suh, 2002). Similarly, swelling, vacuolation and alteration in the organization of mitochondrial cristae have been reported in cellular (Raimondi et al. 2006; Menzies et al., 2002b) and animal models of this pathology by means of ultrastructural analyses of mitochondria in axons and proximal dendrites (Kong and Xu, 1998; Bendotti et al., 2001) and in motoneuron nerve endings (Gould et al., 2006). The present findings in the NMJs of diaphragm of mSOD1 mice support a role for mitochondrial alterations in ALS pathogenesis and show that they precede muscle denervation. We also found that the synaptic vesicle density was significantly reduced in mSOD1 terminals compared to wild-type ones, with no significant changes in their distribution in the presynaptic terminal. Reduction in the number of synaptic vesicles has been previously observed with immunofluorescence in NMJs of locomotor skeletal muscle of mSOD1 mice, and it has been interpreted as a consequence of impaired vesicle transport in the axons of fast fatiguable motoneurons (Pun et al., 2006).

In the murine model of a different neuromuscular disease, spinal muscular atrophy (SMA), the pool of neurotransmitter-containing vesicles in nerve terminals of motoneurons is affected in both size and distribution, indicating that decreased vesicle availability could account for impaired neurotransmission and NMJs dysfunction in SMA (Kong et al., 2009). Thus, similarly to the SMA model, the present findings indicate that defects in neurotransmission may contribute to NMJs dysfunction and lead to denervation. Interestingly, we did not find a relationship between synaptic vesicle pool size and mitochondrial changes in the presynaptic terminals of mSOD1 NMJs. The independence between these parameters is further supported by the findings, discussed below, that nandrolone treatment exerted an effect on mitochondrial changes but not on the synaptic vesicle pool size.

*Effect of nandrolone treatment*

Treatment of mSOD1 mice with nandrolone during the presymptomatic stage of disease was here found to prevent loss of diaphgram muscle mass. In particular, our data indicate that nandrolone, while having no major effect on the size of diaphragm muscle fibers in wild-type mice, exerted a trophic effect by restoring fiber size to control value in mSOD1 mice.

Concerning the lack of effect in wild-type mice, it should be considered that continuous administration of nandrolone increases the cross-sectional area of fibers in the innervated rat diaphragm (Lewis et al., 1999), but this effect did not occur when the administration of high

doses of the drug was intermittent (Bisschop et al., 1997), as in the present paradigm. As for mSOD1 mice, it is worth recalling that gene expression profiles studies have shown that the effect of nandrolone in preventing denervation-induced atrophy may vary depending on the time of denervation (Zhao et al., 2008; Qin et al., 2010). Interestingly, in our study the reduction in the mean diameter of muscle fibers in untreated mSOD1 mice implicated the appearance of very thin fibers with increase of a subpopulation of fibers thinner than in wild-type mice. In nandrolonetreated mSOD1 mice the distribution of fibers according to their diameter was similar to that documented in wild-type littermates. Therefore, given the denervation of some muscle fibers in mSOD1 mice, it can be hypothesized that nandrolone acts on fibers that underwent denervation by fuelling/supporting their metabolism and thus preventing atrophy, with no detectable effects on innervated fibers.

Treatment with nandrolone equally affected the synaptic vesicle pool density of wild-type and mSOD1 mice, with a significant decrease in the mean number of docked vesicles and vesicles within 200 nm in the latter mice. This reduction in the number of vesicles actively involved in neurotransmitter release could reflect a potentiation of synaptic neurotransmission induced by steroid administration (Blanco et al., 2001), an effect here observed in both wild-type and mSOD1 mice. Such effect could be further strengthened by the parallel increase in the total surface area of AChR clusters in the muscle fiber induced by nandrolone administration in both genotypes. In the rat skeletal muscle, androgen receptors are preferentially accumulated in myo-nuclei located under the NMJ where they may specifically control the expression levels of synapse-related proteins (Monks et al., 2004).

The fine structure of presynaptic terminals in nandrolone-treated mSOD1 muscles revealed that the number of presynaptic profiles containing damaged mitochondria was reduced to control values. This observation suggests that nandrolone may exert a protective effect on NMJs by protecting motoneuron mitochondria. Altogether such findings point to a synaptic effect of nandrolone treatment that involves both the mitochondrial pool and synaptic vesicle dynamics. This raises the possibility that either nandrolone acts directly on motoneuron terminals (which express androgen receptors) or this effect is mediated by other trophic factors produced by the muscle fiber in response to treatment. In fact, it has been demonstrated that nandrolone administration increases the levels of muscle insulin growth factor-1 mRNA (Gayan-Ramirez et al., 2000) and protein (Lewis et al., 2002) in the diaphragm of rats, and that muscle-specific expression of local insulin growth factor-1 stabilizes NMJs in mSOD1 mice (Dobrowolny et al., 2005) delaying disease onset and progression. However, the present findings also show that chronic nandrolone treatment does

not exert significant effects in protecting muscle fibers from denervation. An assessment of the potential effect of nandrolone on survival of mSOD1 mice was behind the scope of the present work also considering the fact that, to date, the majority of the results obtained in therapeutic studies on the SOD1 G93A mouse model based on survival analyses have not been consistently reproducible due to high variability caused by confounding variables (Scott et al., 2008). On the other hand, it cannot be excluded that respiratory muscles could behave differently from locomotor muscles with respect to activity-dependent damages and drug susceptibiliy even though no specific effects on muscle mass have been observed among different muscle types, including diaphragm, upon nadrolone treatment (Bisschop et al., 1997). Taken together the present results suggest that the integrity of the mitochondrial pool in motoneuron nerve terminals, which was preserved by nadrolone treatment, is a necessary but not sufficient condition to prevent denervation of mSOD1 muscles.

# 7. FIGURES AND LEGENDS

**Fig. 1 Anatomical and ultrastructural characterization of innervated and denervated neuromuscular junctions**

A: Representative confocal image of an innervated neuromscular junction (NMJ) in diaphragm muscle of P85-P95 mice.
The BuTX panel shows the cluster of AChR in the postsynaptic membrane obtained with TRITC-conjugated α-Bungarotoxin, the architecture of clusters has the usual pretzel-like shape.
The α-synapsin panel represents the immunostaining for the presynaptic marker synapsin1 made through the staining with a polyclonal antibody against the protein and the successive staining with a secondary antibody α-rabbit conjugated with Alexa-488. (Scale bar: 10 μm)

B: Representative EM micrograph of innervated junction in the diaphragm of P85-P95 mice.
The presynaptic button lies over a shallow primary fold and Schwann cells processes cover it, the nerve terminal is filled with cytoplasmatic organelles (mainly mitochondria) and synaptic vesicles (SV).
Beneath the synaptic cleft the postsynaptic membrane is specialized into secondary folds that show an electron dense basal membrane. (Scale bar: 500 nm)

C: Confocal image of a denervated NMJ in diaphragm muscle of P85-P95 mice.
The IF approach used is the same of the A line, despite there are no alterations neither in the complexity nor in the shape of the AChR cluster in the postsynaptic membrane, the lack of the presynaptic staining reveals the denervation of this junction. (Same magnification of the A line)

D: Electron microscopy image of a denervated NMJ in the diaphragm of P85-P95 mice.
At the ultrastructural level, the presynaptic button is absent in denervated junctions, the primary fold is flattened, Schwann cells processes and collagen fibers cover the postsynaptic element.
There is not any alteration, neither in the length, nor in the ramification of secondary folds. (Same magnification of B line)

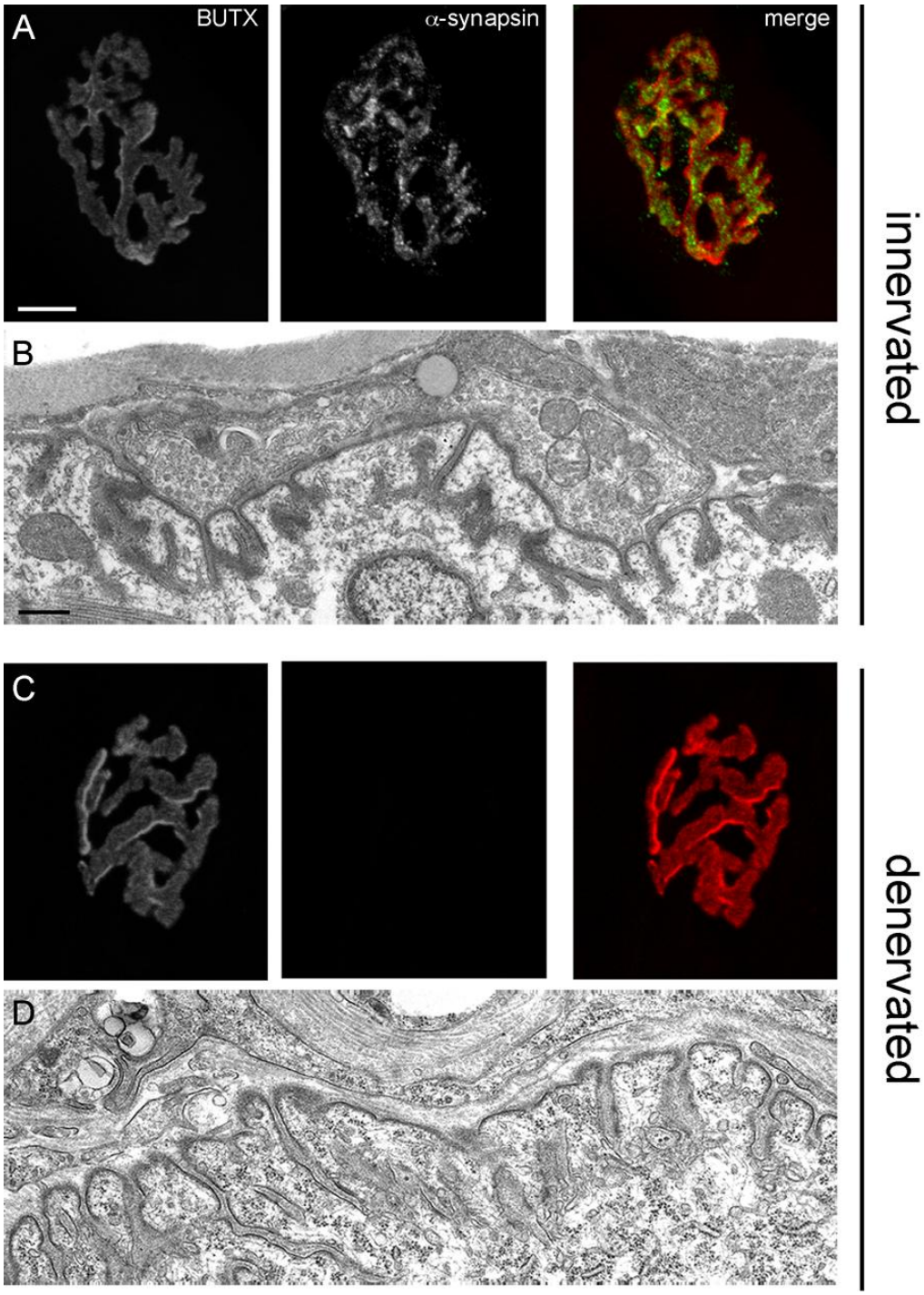
A
BUTX
α-synapsin
merge
B
innervated
C
D
denervated

**Fig. 2 Pathological progression in skeletal muscles**

A: EM micrograph of an innervated NMJ in the soleus of end stage mSOD1 mouse.
Soleus muscle shows a higher plasticity in ALS development, at the end stage (P140) of the disease NMJs are almost completely innervated and there are no sings of ALS-induced alterations in the ultrastructure of presynaptic buttons, mitochondrial pool or synaptic vesicles, primary fold is preserved as well as secondary folds, Schwann cells processes isolate the synapse. (Scale bar: 1μm)

B: Evaluation of percentage of innervated fibres in the soleus, the diaphragm and the gastrocnemius both at the clinical onset (P85-P95) and at the end stage (P140). The graph shows values of innervated fibers evaluated with both IF and EM approaches and normalized for the percentage of innervation of control muscles at the clinical onset of the disease.
At P85-P95 the soleus of mSOD1 mice is entirely innervate while, at the same time point, denervation process starts in the diaphragm (72.53% of innervated fibers) and in the gastrocnemius (81.15% of innervated fibers). At the end stage of the disease the percentage of innervation is further reduced both in soleus muscle (80%), in the diaphragm (46.51%) and in the gastrocnemius that is almost completely denervated (11.99%).

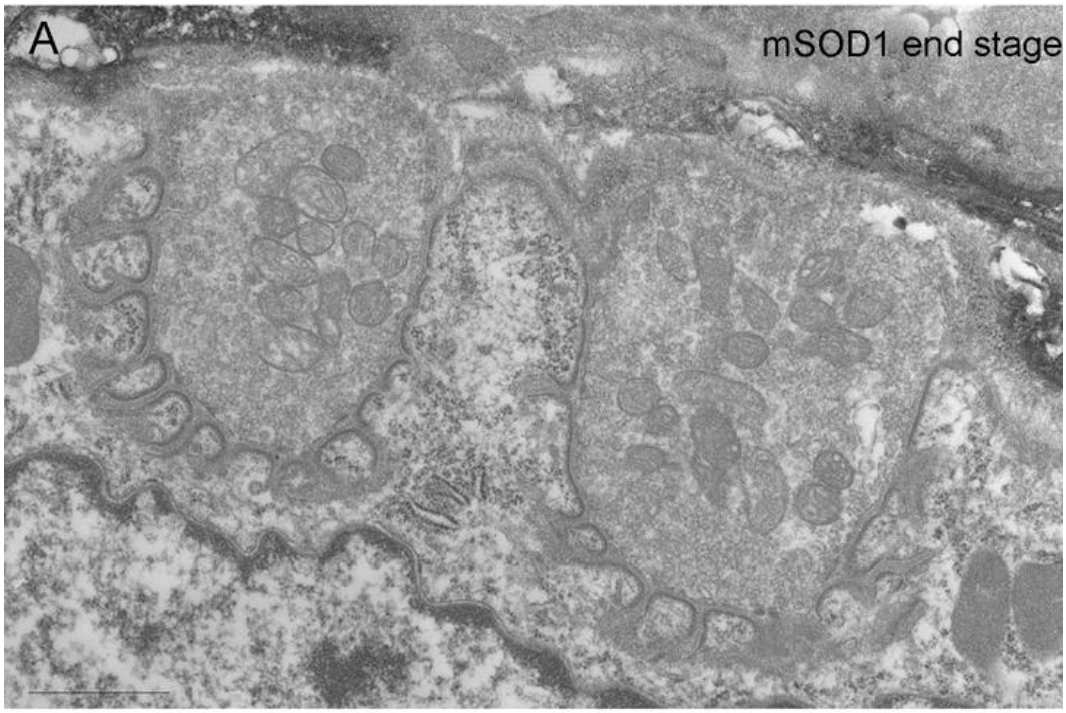


B

Percentage of innervated fibers

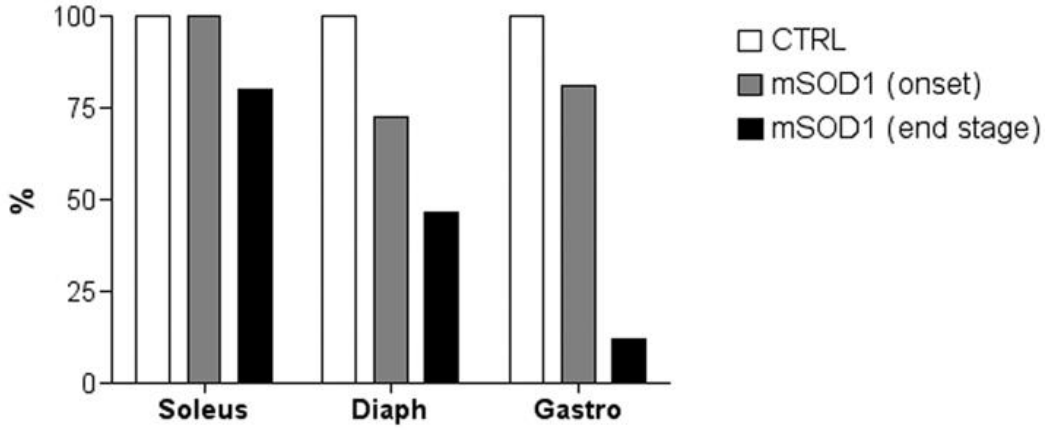


| | CTRL | mSOD1 (onset) | mSOD1 (end stage) |
|---|---|---|---|
| Soleus | 100.00 | 100.00 | 80.00 |
| Diaph | 100.00 | 72.53 | 46.51 |
| Gastro | 100.00 | 81.15 | 11.99 |

**Fig. 3 Morphological and morphometric analysis of mitochondrial pool (P85-P95)**

A: Representative EM micrograph of mitochondrial pool within the presynaptic terminal of an innervated NMJ in the diaphragm of P85-P95 CTRL mice. Each mitochondrion in the buttons of innervated junction has a round profile, continuous inner and outer membranes, a slight electron dense matrix and mitochondrial *cristae* are well organized. In the inset is reported an example of mitochondrial ultrastructure at a higher magnification. (Scale bars: EM 500 nm, inset 200 nm)

B: Number of mitochondria in NMJ. At ALS clinical onset, in diaphragm muscle of mSOD1 mice the total number of mitochondria within the presynaptic terminal does not significantly changes (1.99 ± 1.33 mitochondria/$\mu m^2$; n = 12) compared with whose of CTRL synapses (2.49 ± 1.11 mitochondria/$\mu m^2$; n = 15).

C and D: qualitative analysis of mitochondria into innervated junctions of diaphragm of mSOD1 mouse (P85-P95). In the presynaptic terminal of mSOD1 synapses two population of mitochondria have been observed in C panel the mainly phenotype of mitochondria which have the same aspect of ones observed in CTRL NMJ. In the D panel is reported an example of altered mitochondria that are characterized by fragmented inner and outer membranes, disorganized *cristae* scattered into a pale mitochondrial matrix. Some mitochondria are associated with outer membrane vacuolization phenomena (arrowheads). (Scale bars: EM 500 nm, inset 200 nm)

E: The percentage of the presynaptic area occupied by the mitochondrial pool is slightly reduced in mSOD1 mice (19.48% ± 12.67; n = 12) compared with CTRL ones (23.06% ± 8.30; n = 15). The difference is not statistically significant.

F: Number of NMJ that contain more than 50% of altered mitochondria. This value varies in a significantly manner between CTRL group (0% of alteration) and mSOD1 one (40% of alteration).

G: Average area of mitochondria. Mitochondria of CTRL (0.108 $\mu m^2$ ± 0.04; n = 76) synapses are smaller than what observed in mSOD1 synapses, in both the intact class of mitochondria (0.13 $\mu m^2$ ± 0.05; n = 37; p = 0,0036) and in altered one (0,18 $\mu m^2$ ± 0.1; n = 33; $p < 0.0001$).

H: Evaluation of circularity index. There are no differences between CTRL group and mSOD1 one.

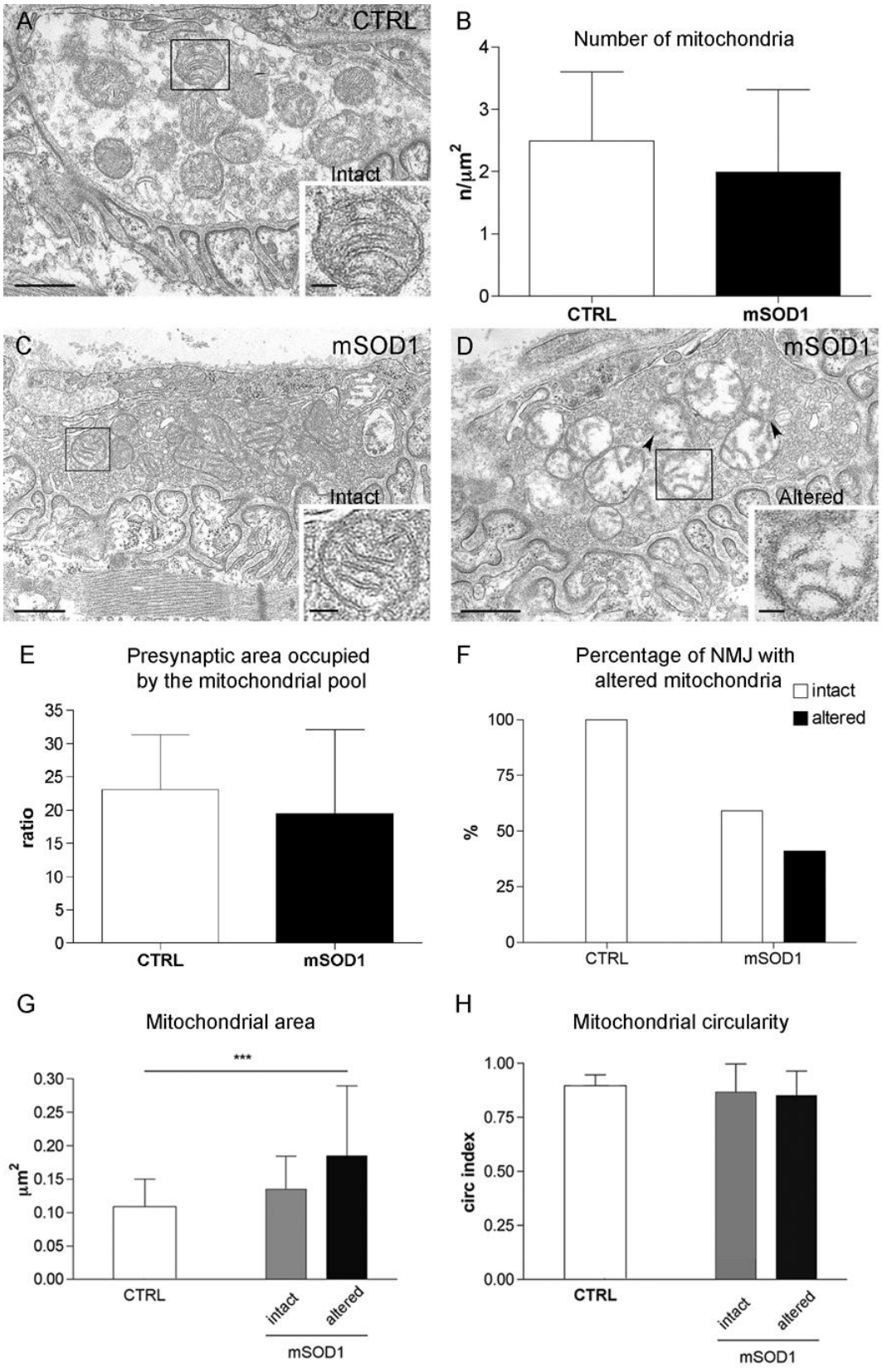
A
CTRL
Intact
B
Number of mitochondria
n/µm2
CTRL
mSOD1
C
mSOD1
Intact
D
mSOD1
Altered
E
Presynaptic area occupied by the mitochondrial pool
ratio
CTRL
mSOD1
F
Percentage of NMJ with altered mitochondria
intact
altered
%
CTRL
mSOD1
G
Mitochondrial area
***
µm2
CTRL
intact
altered
mSOD1
H
Mitochondrial circularity
circ index
CTRL
intact
altered
mSOD1

**Fig. 4 Morphological and morphometric analysis of mitochondrial pool (P140)**

A: Representative image of presynaptic terminal of mSOD1 diaphragm at the pathological end stage (P140). Altered mitochondria show the same phenotype of those observed at the clinical onset of the disease, mitochondrial *cristae* are scattered and the empty mitochondrial matrix is pale (inset), moreover fragmented membranes and vacuolization phenomena (arrowheads) are standard features of the mitochondrial pool in this experimental group compared with CTRL and mSOD1 at the clinical onset. (Scale bars: EM 500 nm, inset 200 nm)

B: The number of mitochondria into synaptic buttons is further reduced in P140 mSOD1 mice (0.734± 0.6 mitochondria/$\mu m^2$; n = 11) compared to the ones sacrificed at the clinical onset.

C: Even the percentage of area occupied by the mitochondrial pool into the nerve ending is reduced at the pathological end stage (12.7% ± 9.2; n = 11), compared with P85-P95 animals.

D: The percentage of NMJs containing more than 50% of altered mitochondria is increased in this animals (72,7%) compared with all the other experimental groups.

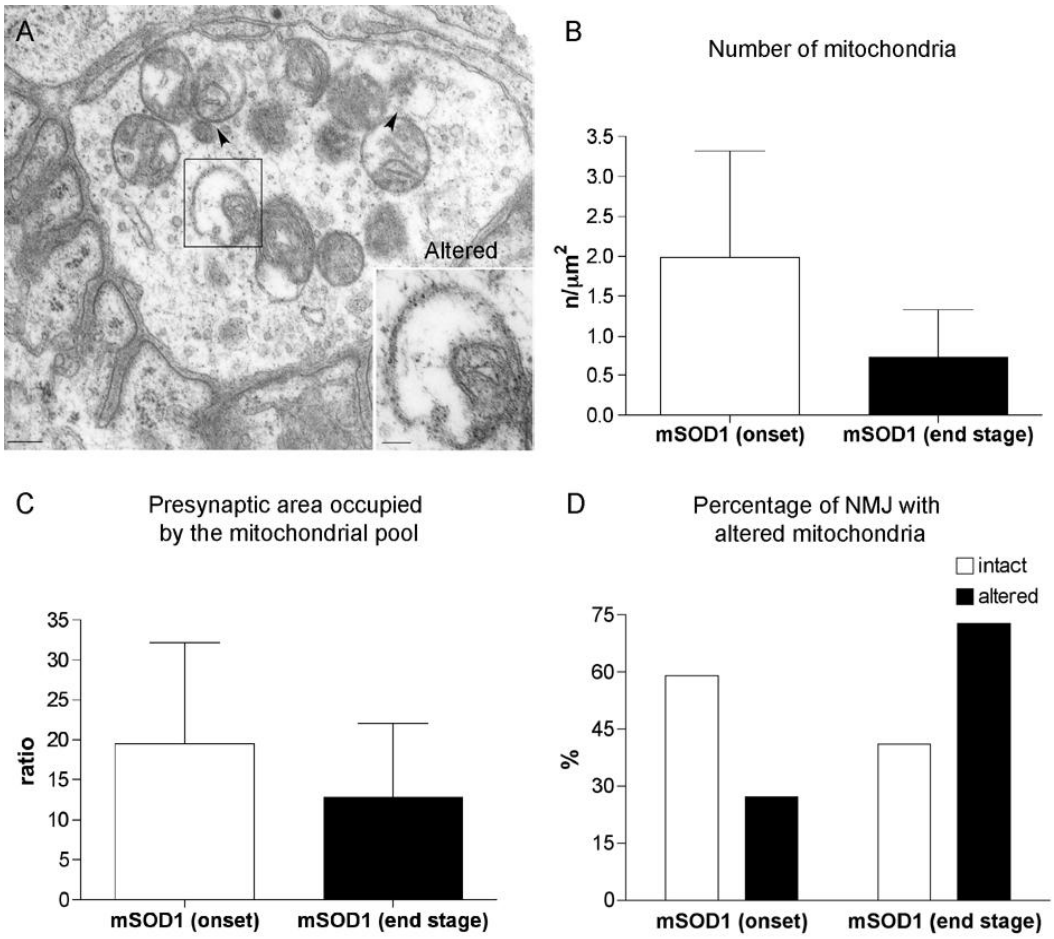
A
Altered
B
Number of mitochondria
n/µm²
3.5
3.0
2.5
2.0
1.5
1.0
0.5
0.0
mSOD1 (onset)
mSOD1 (end stage)
C
Presynaptic area occupied
by the mitochondrial pool
ratio
35
30
25
20
15
10
5
0
mSOD1 (onset)
mSOD1 (end stage)
D
Percentage of NMJ with
altered mitochondria
intact
altered
%
75
60
45
30
15
0
mSOD1 (onset)
mSOD1 (end stage)

**Fig. 5 Density and distribution of synaptic vesicles into the presynaptic terminal**

A and B: Representation of the mask generation. In each EM micrograph (A) analyzed the centre of SVs (arrowheads in A) is labelled with a single pixel point (arrowheads in B), and the presynaptic membrane (arrow in A) is highlighted by a 10-pixels thick line (arrow in B). (Scale bar: 500 nm)

C: Input of the parameter of images acquisition and output of distribution data. The ImageJ macro required information of magnification and resolution of the image and the distance limit for any class of SVs from the presynaptic membrane. The output data indicated the total number of SVs and the number of SVs in the selected classes of distance.

D: Total number of synaptic vesicles in mSOD1 mice (125.4 SVs/$\mu m^2$ ± 80.5; n = 25) is significantly reduced at the onset of the disease compared to data obtain in CTRL mice (220.3 SVs/$\mu m^2$ ± 112.6; n = 15; p = 0.0035).

E: Quantification of vesicle distribution within the presynaptic buttons. There are no significant variations in the number of SVs in the selected classes of distance between CTRL synapses and mSOD1 ones.

| | CTRL | | | mSOD1 | | |
|---|---|---|---|---|---|---|
| | **Mean** | **SD** | **N** | **Mean** | **SD** | **N** |
| **docked** | 10.420 | 7.032 | 15 | 8.221 | 6.303 | 12 |
| **within 200 nm** | 75.700 | 50.630 | 15 | 63.610 | 40.300 | 12 |
| **beyond 200 nm** | 134.200 | 63.370 | 15 | 90.090 | 55.930 | 12 |

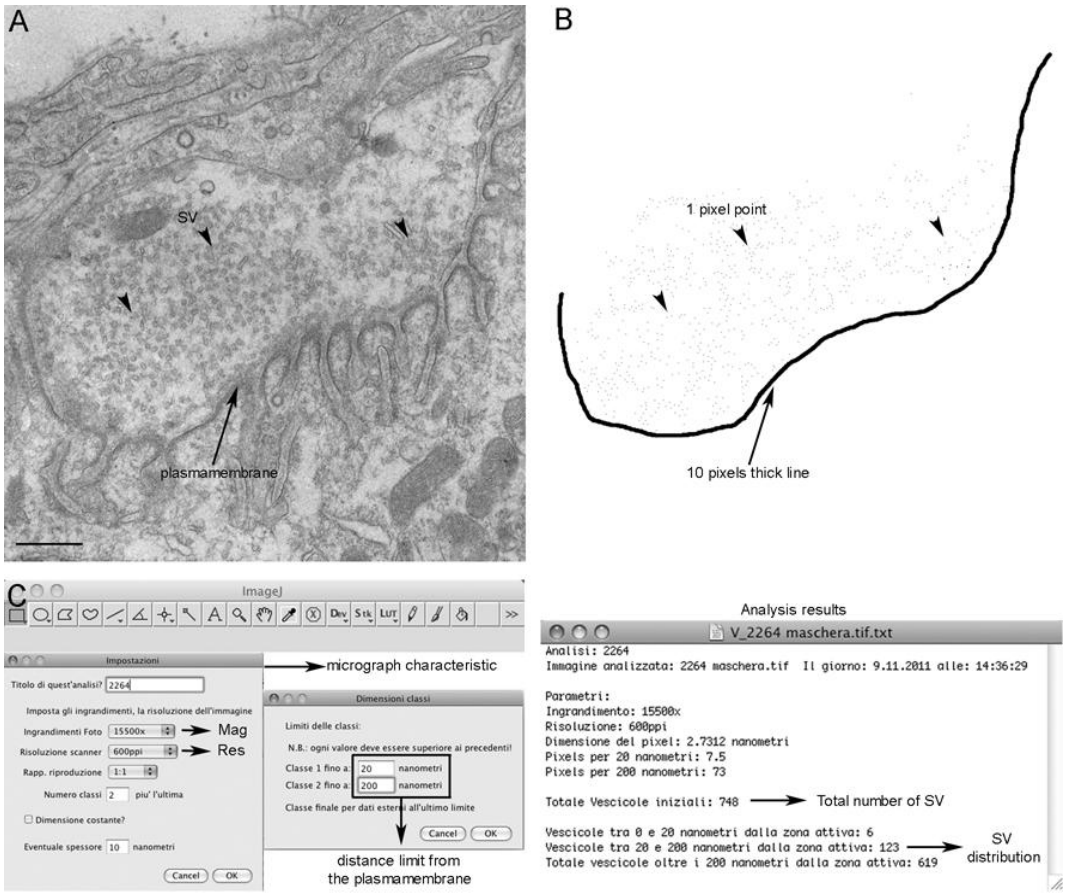
A
SV
plasmamembrane
B
1 pixel point
10 pixels thick line
C
ImageJ
Impostazioni
Titolo di quest'analisi? 2264
Imposta gli ingrandimenti, la risoluzione dell'immagine
Ingrandimenti Foto 15500x
Mag
Risoluzione scanner 600ppi
Res
Rapp. riproduzione 1:1
Numero classi 2 piu' l'ultima
Dimensione costante?
Eventuale spessore 10 nanometri
Cancel
OK
micrograph characteristic
Dimensioni classi
Limiti delle classi:
N.B.: ogni valore deve essere superiore ai precedenti!
Classe 1 fino a: 20 nanometri
Classe 2 fino a: 200 nanometri
Classe finale per dati esterni all'ultimo limite
Cancel
OK
distance limit from
the plasmamembrane
Analysis results
V_2264 maschera.tif.txt
Analisi: 2264
Immagine analizzata: 2264 maschera.tif Il giorno: 9.11.2011 alle: 14:36:29
Parametri:
Ingrandimento: 15500x
Risoluzione: 600ppi
Dimensione del pixel: 2.7312 nanometri
Pixels per 20 nanometri: 7.5
Pixels per 200 nanometri: 73
Totale Vescicole iniziali: 748
Total number of SV
Vescicole tra 0 e 20 nanometri dalla zona attiva: 6
Vescicole tra 20 e 200 nanometri dalla zona attiva: 123
Totale vescicole oltre i 200 nanometri dalla zona attiva: 619
SV
distribution

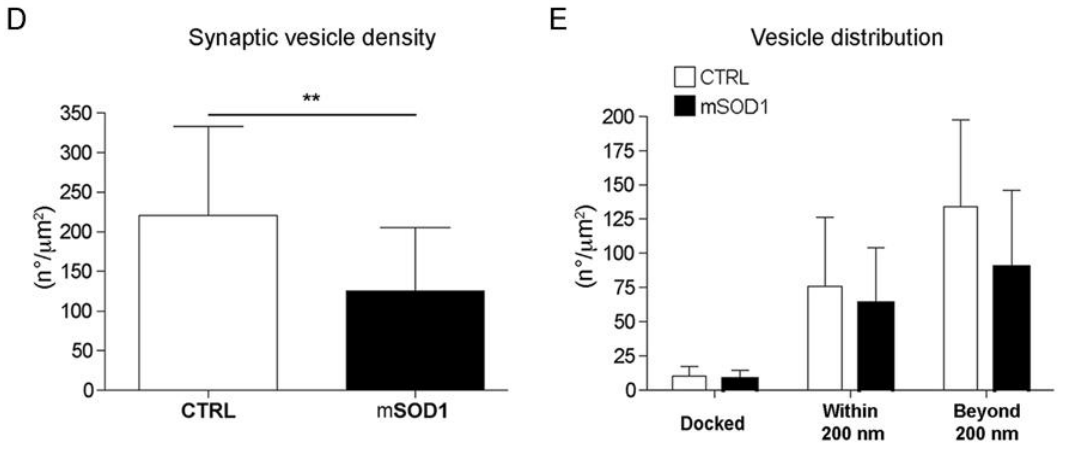
D
Synaptic vesicle density
**
(n°/µm²)
350
300
250
200
150
100
50
0
CTRL
mSOD1
E
Vesicle distribution
CTRL
mSOD1
(n°/µm²)
200
175
150
125
100
75
50
25
0
Docked
Within
200 nm
Beyond
200 nm

**Fig. 6 Diameter of muscular fibers**

A and B: Representative bright field images of longitudinal and coronal sections of skeletal muscle fibers in the diaphragm of CTRL mice. (Scale bars: 10 μm)

C: Mean diameter of fibers in skeletal muscles.

| | CTRL | | | SOD1 G93A | | |
|---|---|---|---|---|---|---|
| | **Mean** | **SD** | **N** | **Mean** | **SD** | **N** |
| **Soleus** | 32.85 | 10.33 | 277 | 41.11 | 14.22 | 277 |
| **Diaph** | 35.75 | 6.47 | 216 | 29.66 | 6.57 | 277 |
| **Gastro** | 35.68 | 11.70 | 178 | 35.79 | 10.90 | 100 |

D, E and F: Subdivision of fibers related to their diameters value.

| | CTRL | | | mSOD1 | | |
|---|---|---|---|---|---|---|
| | x<20 | 20<x<30 | x>30 | x<20 | 20<x<30 | x>30 |
| **Soleus** | 6.86 | 38.27 | 54.87 | 2.17 | 24.55 | 73.29 |
| **Diaph** | 0.00 | 22.22 | 77.78 | 3.97 | 54.51 | 41.52 |
| **Gastro** | 5.62 | 28.09 | 66.29 | 11.00 | 19.00 | 70.00 |

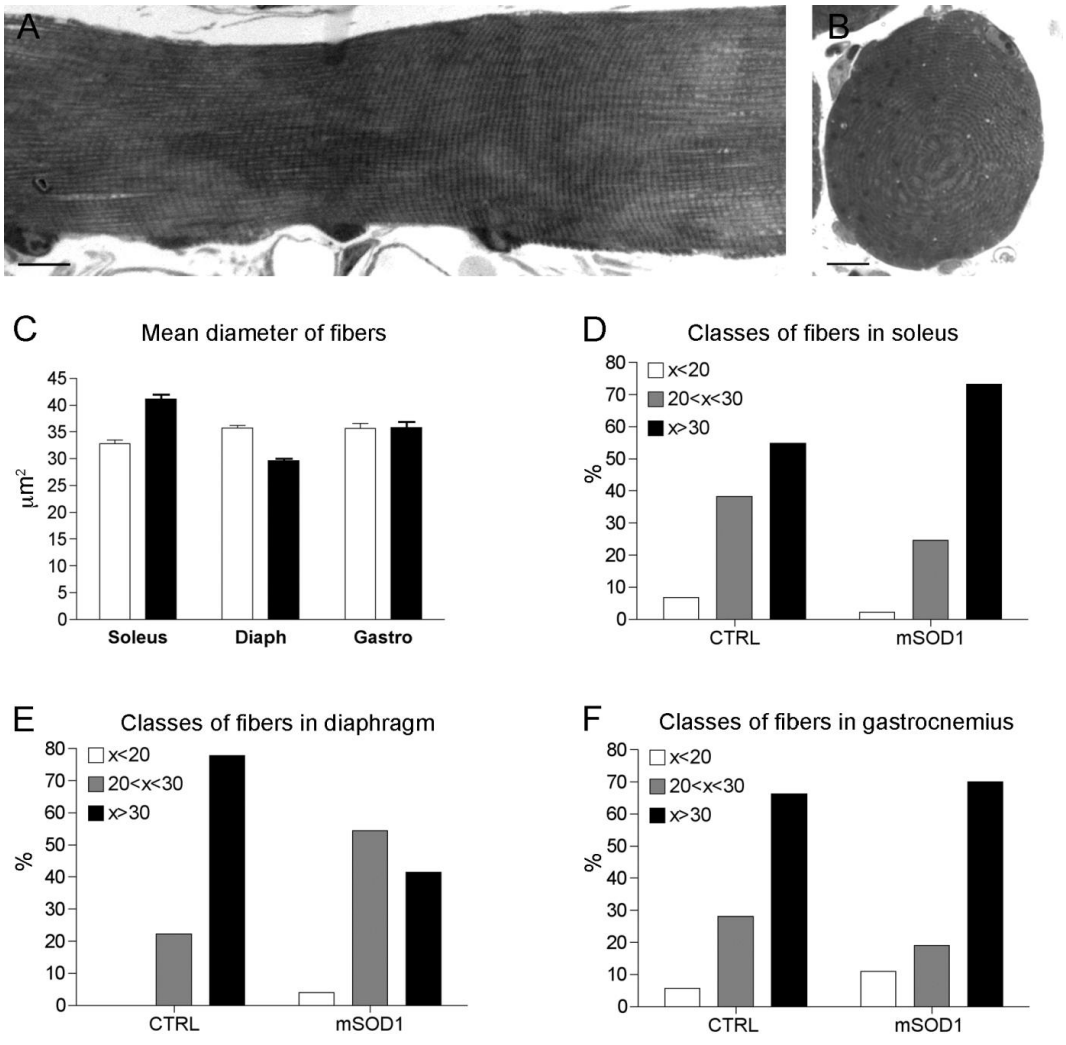
A
B
C
Mean diameter of fibers
µm²
Soleus
Diaph
Gastro
D
Classes of fibers in soleus
x<20
20<x<30
x>30
%
CTRL
mSOD1
E
Classes of fibers in diaphragm
F
Classes of fibers in gastrocnemius

**Fig. 7 Analysis o Acetyl Choline Receptor (AChR) clusters.**

A and C: Representative confocal images of the AChR clusters in an innervated NMJ of diaphragm of CTRL animals (A) and of mSOD1 mice (C). Those images are related with IF experiments reported in Fig. 1A and C (Scale bar 10 μm).

B and D: Bitmap masks of the same cluster reported in panels A and C

E: Statistical analysis of obtained values indicated that CTRL synapses have a smaller BuTX-positive area (360.75 $\mu m^2$ ± 126.97; n = 92) compared with mSOD1 ones both the innervated (418.2 $\mu m^2$ ± 10.6; n = 34; p = 0.02) and denervated ones (452.2 $\mu m^2$ ± 131.3; n = 21; p = 0.0014).

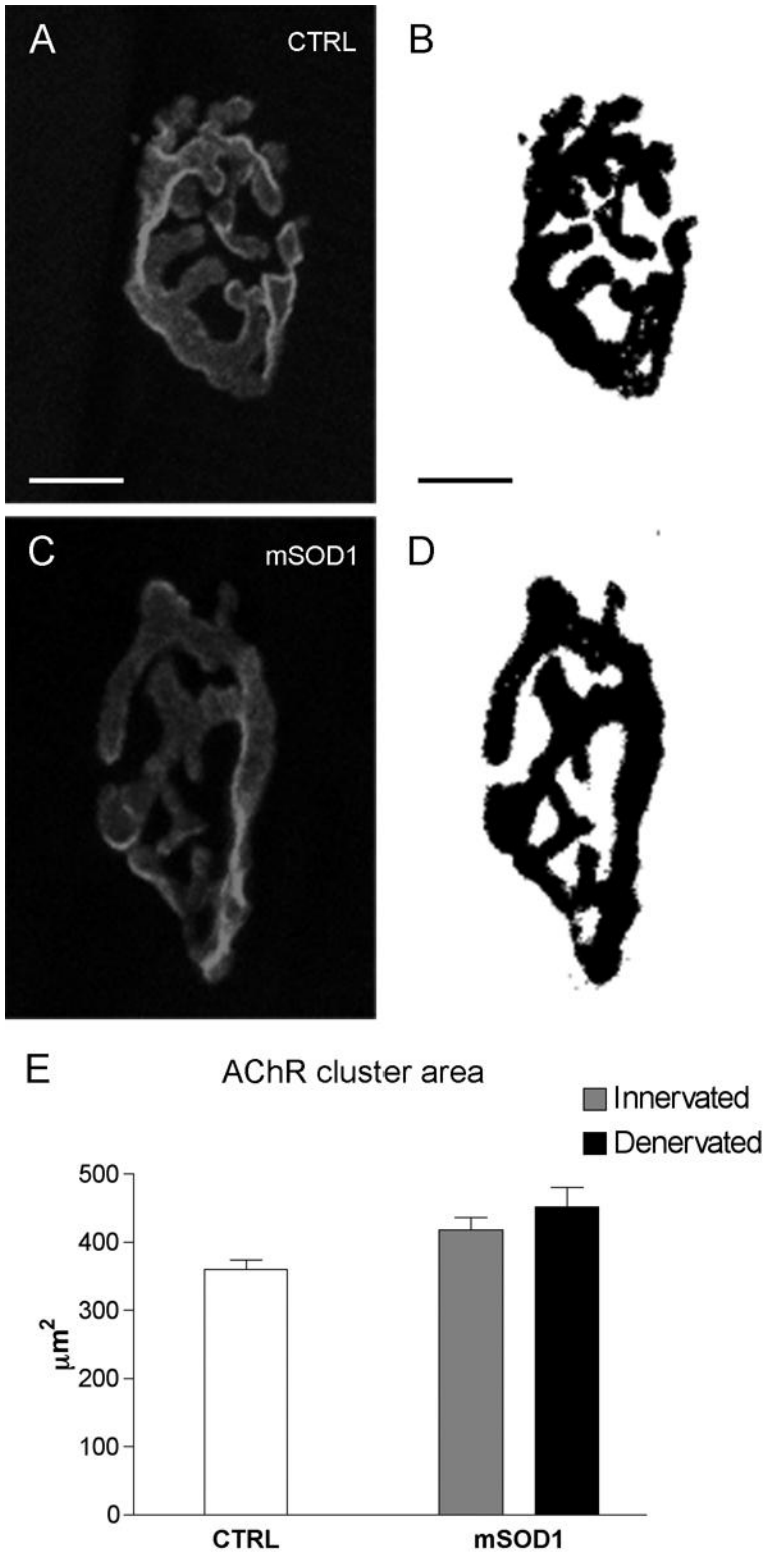
A
CTRL
B
C
mSOD1
D
E
AChR cluster area
Innervated
Denervated
500
400
300
200
100
0
µm2
CTRL
mSOD1

**Fig. 8 Nandrolone-mediated effects in presynaptic terminal**

A: Number of NMJ that contain more than 50% of altered mitochondria. The value of NMJ containing intact mitochondria is rescued in treated mSOD1 mice (91% of NMJ with intact mitochondria) at the same level than what observed in CTRL mice.

B: The mean area of intact mitochondria in innervated NMJ of treated animals is slight reduced compared to untreated mice (0.113 $\mu m^2 \pm 0.075$; n = 45; p = n.s.) while is increased in altered ones (0.203 $\mu m^2 \pm 0.134$; n = 23; p = n.s.). Both intact and altered mitochondria of treated muscles show a broader area compared to untreated ones of the same class (untreated intact/untreated altered p = 0.016; treated intact/treated altered p = 0.0055).

C: Even in this case there are no variations in the value of circularity index.

D: The total number of mitochondria reported to the area of presynaptic terminal does not change between untreated and treated mSOD1 (untreated 1.99/$\mu m^2$; treated 1.97/ $\mu m^2$).

E: Total number of synaptic vesicle in the presynaptic terminal. This value does not change significantly between untreated and treated mice (92,69/$\mu m^2 \pm 56.73$; n = 18; p = n.s.).

F: The distribution of SV indicates a reduction in number of SV in the docked pool of treated mice (2.34/$\mu m^2 \pm 3.51$; n = 11; p = 0.0132) compared to untreated ones. Moreover even in the number of SV distributed within 200 nm from the plasmamembrane the reduction is statistically significant between untreated and treated (33.71/$\mu m^2 \pm 22.34$; n = 11; p = 0.04) NMJ. While no significant variation in the distribution of SV beyond 200 nm is observed between untreated and treated mice.

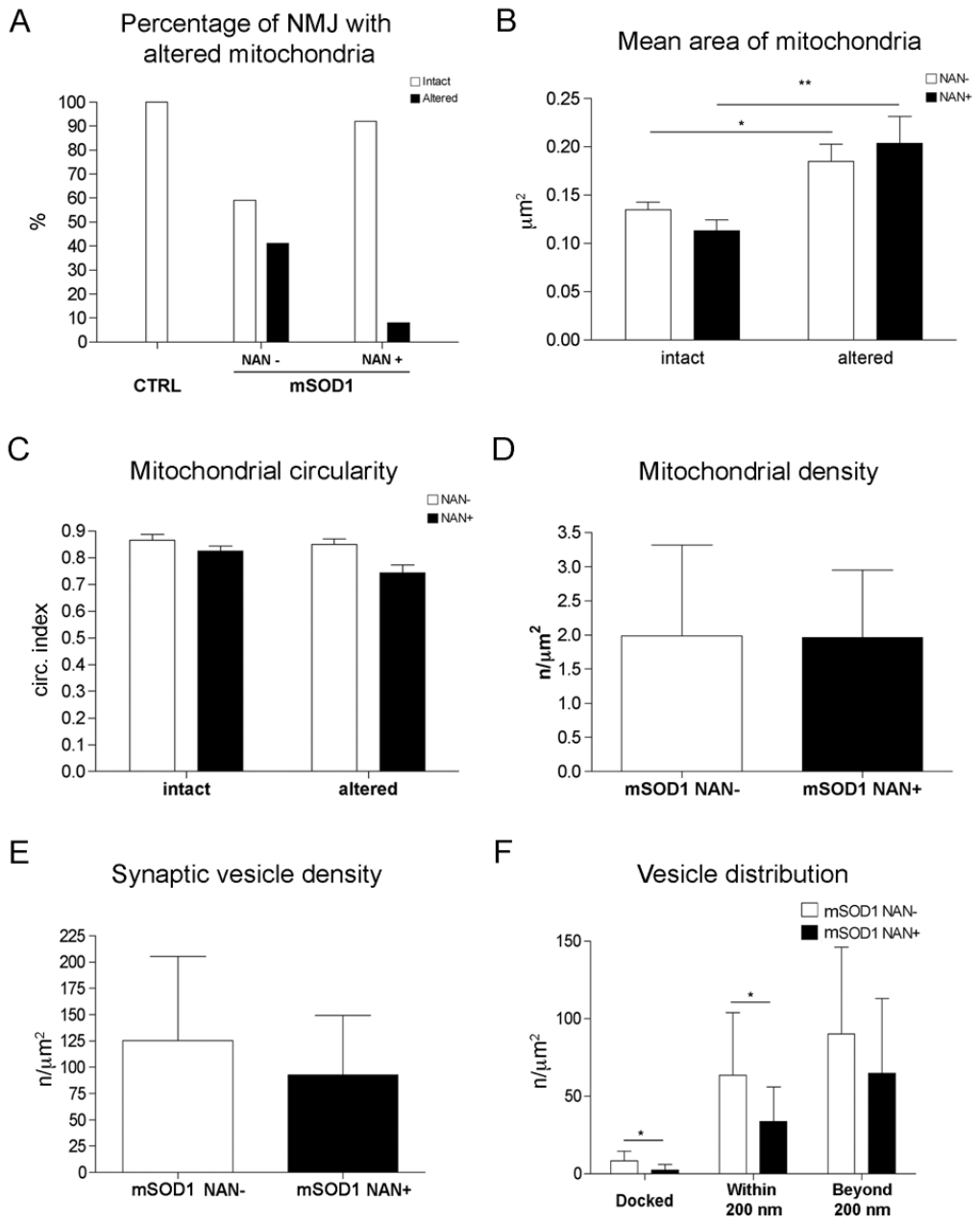
A
Percentage of NMJ with altered mitochondria
Intact
Altered
%
CTRL
NAN -
NAN +
mSOD1
B
Mean area of mitochondria
NAN-
NAN+
μm²
intact
altered
C
Mitochondrial circularity
NAN-
NAN+
circ. index
intact
altered
D
Mitochondrial density
n/μm²
mSOD1 NAN-
mSOD1 NAN+
E
Synaptic vesicle density
n/μm²
mSOD1 NAN-
mSOD1 NAN+
F
Vesicle distribution
mSOD1 NAN-
mSOD1 NAN+
n/μm²
Docked
Within 200 nm
Beyond 200 nm

**Fig. 9 Nandrolone-mediated effects in postsynaptic elements**

A: Fibers diameter evaluation in skeletal muscles of treated mice.

| X Labels | untreated | | | treated | | |
|---|---|---|---|---|---|---|
| X | Mean | SD | N | Mean | SD | N |
| Diaph | 29.66 | 6.58 | 277 | 37.24 | 7.64 | 304 |
| Gastro | 35.79 | 10.90 | 100 | 45.75 | 13.87 | 104 |

B: Subdivision of fibers related to their diameters value.

| | untreated | | | treated | | |
|---|---|---|---|---|---|---|
| | x<20 | 20<x<30 | x>30 | x<20 | 20<x<30 | x>30 |
| Diaph | 3.97 | 54.51 | 41.520 | 0.66 | 17.43 | 81.910 |
| Gastro | 11.00 | 19.00 | 70.000 | 7.81 | 12.50 | 79.690 |

C: Quantification of AChR clusters in the diaphragm of treated mice.

Nandrolone administration induced an increase of the size of AChR clusters in each experimental group:

| | CTRL | | | INN | | | DEN | | |
|---|---|---|---|---|---|---|---|---|---|
| | Mean | SD | N | Mean | SD | N | Mean | SD | N |
| untreated | 360.8 | 127.0 | 92 | 418.2 | 107.0 | 34 | 452.2 | 131.3 | 27 |
| treated | 410.6 | 116.1 | 93 | 538.2 | 160.8 | 21 | 496.4 | 127.5 | 23 |

In CTRL group the difference between treated and untreated mice is statistically significant ($p = 0.0059$), the average BuTX positive area is broader in treated innervated NMJ compared to untreated ones ($p = 0.005$) in a statistically significant manner, even in denervated junction treated with nandrolone there is an increaser of clusters area while this difference is not significant.

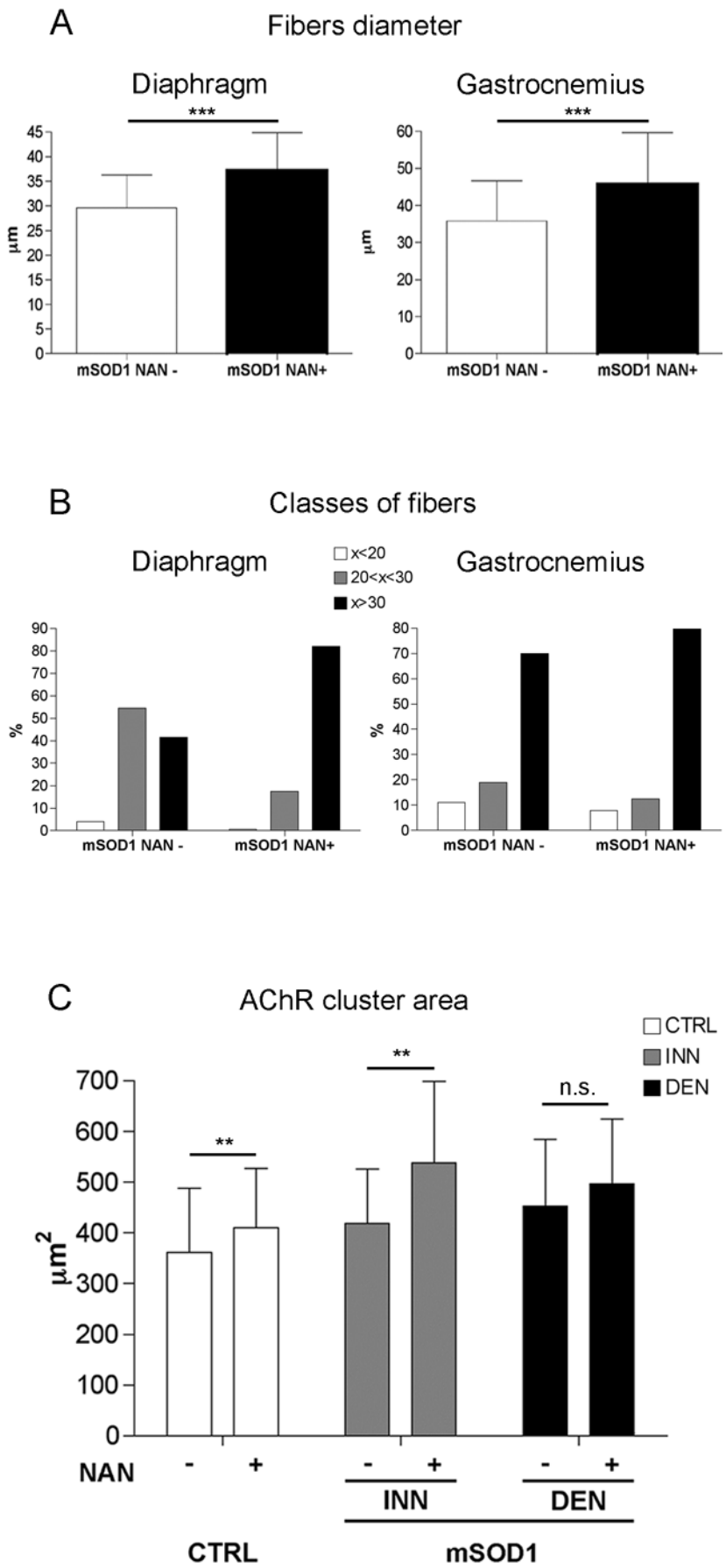
A
Fibers diameter
Diaphragm
Gastrocnemius
***
***
µm
mSOD1 NAN -
mSOD1 NAN+
B
Classes of fibers
Diaphragm
Gastrocnemius
x<20
20<x<30
x>30
%
mSOD1 NAN -
mSOD1 NAN+
C
AChR cluster area
CTRL
INN
DEN
**
**
n.s.
µm2
NAN
-
+
INN
DEN
CTRL
mSOD1

**Fig. 10 Percentage of innervated fibers and disease clinical onset in treated mice**

A: The mean value of innervation is evaluated in both the diaphragm and the gastrocnemius at the clinical onset of the disease. There is a slight increase of the percentage of innervated fibers in treated mSOD1 diaphragm (76.3%) compared to untreated one (71.8%), in gastrocnemius muscle the effect of nandrolone administration rescues completely the value at the CTRL level (100%).

B: The percentage of innervation is evaluated in each mouse and we observe a great variability between animals especially in mSOD1 mice both treated and untreated ones.

C: The Kaplan-Meier analysis reveals that there are no significant variation in the age of onset of the disease between treated and untreated mice.

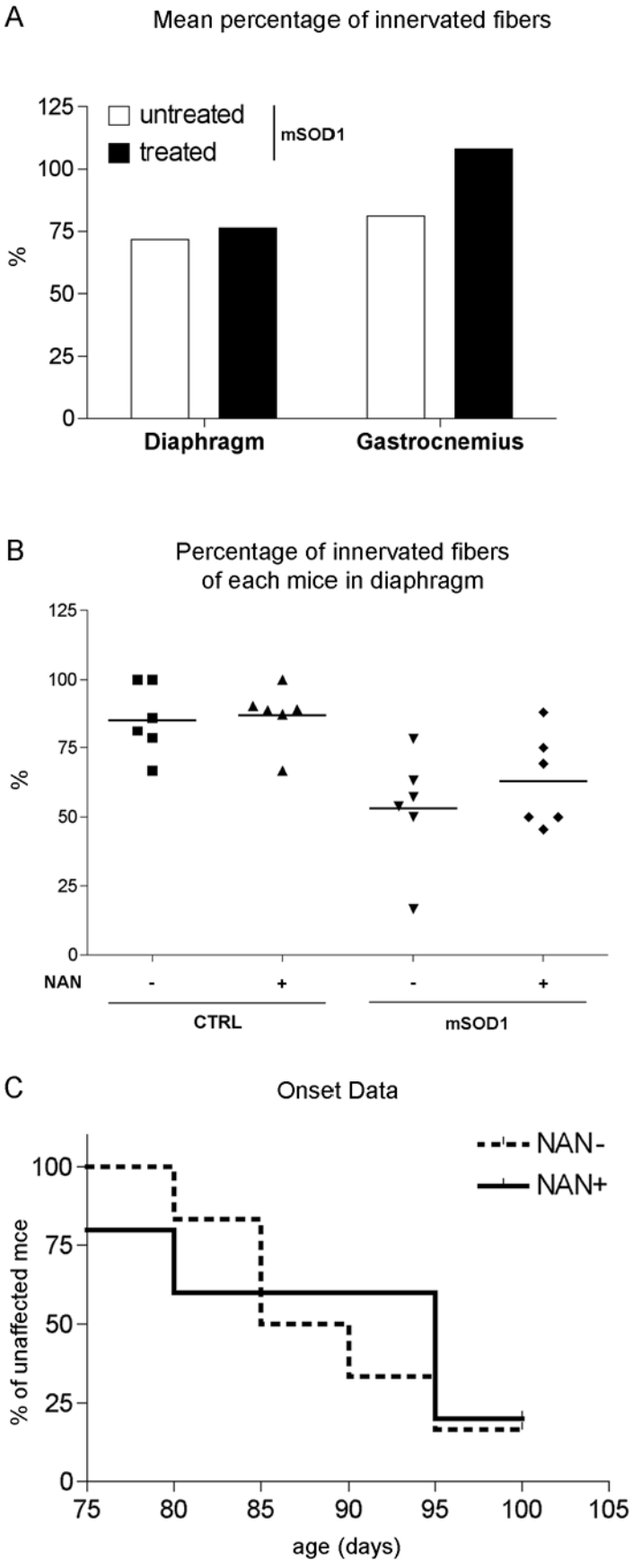
A
Mean percentage of innervated fibers
untreated
treated
mSOD1
125
100
75
50
25
0
%
Diaphragm
Gastrocnemius
B
Percentage of innervated fibers
of each mice in diaphragm
125
100
75
50
25
0
%
NAN
-
+
-
+
CTRL
mSOD1
C
Onset Data
NAN-
NAN+
100
75
50
25
0
% of unaffected mce
75
80
85
90
95
100
105
age (days)

## Abbreviations

- ACh Acetylcholine
- AChR Acetylcholine Receptor
- ALS Amyotrophic Lateral Sclerosis
- ALS2 Alsin2
- AMPA 2-amino-3-(5-methyl-3-oxo-1,2-oxazol-4-yl)propanoic acid
- ANG ANGiogenin
- ATP/GTP Adenosine/Guanosin Tri-Phosphate
- BS Blocking Solution
- BuTX α-BungaroToXin
- CNS Central Nervous System
- COPD Chronic Obstructive Pulmonary Disease
- CSA Cross Sectional Area
- CTRL Control
- DeSyn Delayed Synapsing
- DNA DeoxyriboNucleic Acid
- EAAT Excitatory AminoAcid Transporter
- EM Electron Microscopy
- fALS Familial Amyotrophic Lateral sclerosis
- FaSyn Fast Synapsing
- FDA Food and Drugs Administration
    - FF Fast Fatigable
    - FI Fast fatigue Intermediate
    - FR Fast Fatigue-Resistant
    - S Slow
- FIG4 PI(3,5)P(2)5-Phosphatase
- FTD FrontoTemporal Dementia
- FUS FUsed in Sarcoma
- GDNF Glial-cell-line Derived Neurotrophic Factor
- GLT GLial Glutamate Transporter
- HDAC Histone DeACetylase
- HIV Human Immunodeficency Virus
- hSOD Human SuperOxide Dismutase

- IGF Insulin-like Growth Factor
- IMT Inspiratory Muscle Training
- KO Knock Out
- LMN Lower MotoNeuron
- MHC Myosin Heavy Chain
- MN MotoNeuron
- MND MotoNeuron Disease/Disorder
- mRNA Messanger RiboNucleic Acid
- mSOD Mutant SuperOxide Dismutase
- MU Motor Unit:
- NAN NANdrolone decanoate
    - NAN– Untreated
    - NAN+ Treated
- NF NeuroFilament
- NMDA N-Methyl-D-aspartate
- NMJ NeuroMuscular Junction
- OCT Optimal Cutting Temperature
- PBS Phosphate Buffer Saline
- PDC Parkinson-Dementia Complex
- PLS Primary Lateral Sclerosis
- PMA Progressive Muscular Atrophy
- RNA RiboNucleic Acid
- ROS Reactive Oxygen Species
- sALS Sporadic Amyotrophic Lateral Sclerosis
- SETX SEnTaXin
- SMA Spinal Muscular Atrophy
- SNP Single Nucleotide Polymorphism
- SOD SuperOxide Dismutase
- SPG11 Spatacsin
- SV Synaptic Vesicle
- TARDBP TAR DNA Binding Protein
- TDP TAR DNA binding Protein
- TEM Transmission Electrom Microscopy

- TNF Tumor Necrosis Factor
- TRITC Tetamethyl-Rhodamine
- UMN Upper MotoNeuron
- UPR Unfolded Protein Response
- VAMP Vesicle-Associated Membrane Protein
- VAPB/C Vesicle-associated membrane protein-Associated Protein B/C
- VEGF Vascular Endothelial Growth Factor
- VPA ValProic Acid
- WS Washing Solution
- WT Wild Type

## References


1. Abe K, Pan LH, Watanabe M, Kato T, Itoyama Y. Induction of nitrotyrosine-like immunoreactivity in the lower motor neuron of amyotrophic lateral sclerosis. Neurosci. Lett. 1995; 199: 152-154
2. Afifi AK, Aleu FP, Goodgold J, MacKay B. Ultrastructure of atrophic muscle in amyotrophic lateral sclerosis. Neurology. 1966; 16 (5): 475-481
3. Albo F, Pieri M, Zona C. Modulation of AMPA receptors in spinal motor neurons by the neuroprotective agent riluzole. J. Neurosci. Res. 2004; 78: 200-207
4. Alway SE, Siu PM. Nuclear apoptosis contributes to sarcopenia. Exerc. Sport Sci. Rev. 2008; 36: 51-57
5. Allouh MZ, Rosser BW. Nandrolone decanoate increases satellite cells number in the chicken pectoralis muscle. Histol Histopathol. 2010; 25 (2): 133-140
6. Anderson JE. The satellite cell as a companion in skeletal muscle plasticity: currency, conveyance, clue, connector and colander. J. Exp. Biol. 2006; 209: 2276-2292
7. Atsumi T. The ultrastructure of intramuscular nerves in amyotrophic lateral sclerosis. Acta Neuropathol. 1981; 55 (3): 193-198
8. Beal MF. Oxidatively modified proteins in aging and disease. Free Radical Biol. Med. 2002; 32: 797-803
9. Beal MF, Ferrante RJ, Browne SE, Matthews RT, Kowall NW, Brown Jr, RH. Increased 3-nitrotyrosine in both sporadic and familial amyotrophic lateral sclerosis. Ann. Neurol. 1997; 42: 644-654
10. Belli S, Vanacore N. Proportionate mortality of Italian soccer players: is amyotrophic lateral sclerosis an occupational disease? Eur J Epidemiol. 2005; 20 (3): 237- 242.
11. Bendotti C, Calvaresi N, Chiveri L, Prelle A, Moggio M, Braga M, Silani V, De Biasi S. Early vacuolization and mitochondrial damage in motor neurons of FALS mice are not associated with apoptosis or with changes in cytochrome oxidase histochemical reactivity. J Neurol Sci. 2001; 191 (1-2): 25-33
12. Bensimon G, Lacomblez L, Meininger V. A controlled trial of riluzole in amyotrophic lateral sclerosis. ALS/Riluzole Study Group. N. Engl. J. Med.1994; 330: 585-591

13. Berger JR, Espinosa PS, Kissel J. Brachial amyotrophic diplegia in a patient with human immunodeficiency virus infection: widening the spectrum of motor neuron diseases occurring with the human immunodeficiency virus. Arch Neurol 2005; 62:817–23.
14. Berger Z, Ravikumar B, Menzies FM, Oroz LG, Underwood BR, Pangalos MN, Schmitt I, Wullner U, Evert BO, O'Kane CJ, Rubinsztein DC. Rapamycin alleviates toxicity of different aggregate-prone proteins. Hum. Mol. Genet. 2006; 15: 433-442
15. Bergink EW, Janssen PSL, Turpijn EW, Vander Vies J. Comparison of the receptor-binding properties of nandrolone and testosterone under in vitro and in vivo conditions. J. Steroid Biochem. Mol. Biol. 1985; 22: 831-836
16. Bisschop A, Gayan-Ramirez G, Rollier H, Dekhuijzen PNR, Dom R, de Bock V, Decramer M. Effects of nandrolone decanoate on respiratory and peripheral muscles in male and female rats. J Appl Physiol. 1997; 82 (4): 1112-1118
17. Blanco CE, Zhan WZ, Fang YH, Sieck GC. Exogenous testosterone treatment decreases diaphragm neuromuscular transmission failure in male rats. J. Appl. Physio. 2001; 90: 850-856.
18. Boillée S, Yamanaka K, Lobsiger CS, Copeland NG, Jenkins NA, Kassiotis G, Kollias G, Cleveland DW. Onset and progression in inherited ALS determined by motor neurons and microglia. Science 2006; 312: 1389-1392
19. Brack AS, Rando TA. Intrinsic changes and extrinsic influences of myogenic stem cell function during aging. Stem Cell Rev. 2007; 3: 226-237
20. Bruijn LI, Becher MW, Lee MK, Anderson KL, Jenkins NA, Copeland NG, Sisodia SS, Rothstein JD, Borchelt DR, Price DL, Cleveland DW. ALS-linked SOD1 mutant G85R mediates damage to astrocytes and promotes rapidly progressive disease with SOD1-containing inclusions. Neuron. 1997; 18(2):327-38.
21. Bruijn LI, Houseweart MK, Kato S, Anderson KL, Anderson SD, Ohama E, Reaume AG, Scott RW, Cleveland DW. Aggregation and motor neuron toxicity of an ALS-linked SOD1 mutant independent from wild-type SOD1. Science 1998; 281(5384):1851-1854
22. Buratti E, Baralle FE. Multiple roles of TDP-43 in gene expression, splicing regulation, and human disease. Front. Biosci. 2008; 13: 867-878
23. Cai H, Lin X, Xie C, Laird FM, Lai C, Wen H, Chiang HC, Shim H, Farah MH, Hoke A, Price DL, Wong PC.Loss of ALS2 function is insufficient to trigger motor

neuron degeneration in knock-out mice but predisposes neurons to oxidative stress. J Neurosci. 2005; 25 (33): 7567-7574

24. Chai A, Withers J, Koh YH, Parry K, Bao H, Zhang B, Budnik V, Pennetta G. hVAPB, the causative gene of a heterogeneous group of motor neuron diseases in humans, is functionally interchangeable with its Drosophila homologue DVAP-33A at the neuromuscular junction. Hum. Mol. Genet. 2008 17: 266-280
25. Chance PF, Rabin BA, Ryan SG, Ding Y, Scavina M, Crain B, Griffin JW, Cornblath DR. Linkage of the gene for an autosomal dominant form of juvenile amyotrophic lateral sclerosis to chromosome 9q34. Am J Hum Genet. 1998; 62 (3): 633-640.
26. Chen H, Richard M, Sandler DP, Umbach DM, Kamel F. Head injury and amyotrophic lateral sclerosis. Am J Epidemiol. 2007; 166 (7): 810-816
27. Chen YZ, Bennett CL, Huynh HM, Blair IP, Puls I, Irobi J, Dierick I, Abel A, Kennerson ML, Rabin BA, Nicholson GA, Auer-Grumbach M, Wagner K, De Jonghe P, Griffin JW, Fischbeck KH, Timmerman V, Cornblath DR, Chance PF. DNA/RNA helicase gene mutations in a form of juvenile amyotrophic lateral sclerosis (ALS4). Am J Hum Genet. 2004; 74 (6):1128-1135
28. Chow CY, Zhang Y, Dowling JJ, Jin N, Adamska M, Shiga K, Szigeti K, Shy ME, Li J, Zhang X, Lupski JR, Weisman LS, Meisler MH. Mutation of FIG4 causes neurodegeneration in the pale tremor mouse and patients with CMT4J. Nature 2007; 448: 68-72
29. Chow CY, Landers JE, Bergren SK, Sapp PC, Grant AE, Jones JM, Everett L, Lenk GM, McKenna-Yasek DM, Weisman LS, Figlewicz D, Brown RH, Meisler MH. Deleterious variants of FIG4, a phosphoinositide phosphatase, in patients with ALS. Am. J. Hum. Genet. 2009; 84: 85-88
30. Chung MJ, Suh YL. Ultrastructural changes of mitochondria in the skeletal muscle of patients with amyotrophic lateral sclerosis. Ultrastruct Pathol 2002; 26 (1): 3-7
31. Clement AM, Nguyen MD, Roberts EA, Garcia ML, Boillée S, Rule M, McMahon AP, Doucette W, Siwek D, Ferrante RJ, Brown RH Jr, Julien JP, Goldstein LS, Cleveland DW. Wildtype nonneuronal cells extend survival of SOD1 mutant motor neurons in ALS mice. Science 2003; 302: 113-117
32. Corrado L, Ratti A, Gellera C, Buratti E, Castellotti B, Carlomagno Y, Ticozzi N, Mazzini L, Testa L, Taroni F, Baralle FE, Silani V, D'Alfonso S. High frequency of

TARDBP gene mutations in Italian patients with amyotrophic lateral sclerosis. Hum. Mutat. 2009; 30: 688-694

33. Creutzberg EC, Wouters EFM, Mostert R, Pluymers RJ, Schols AMWJ. A role for anabolic steroids in the rehabilitation of patients with COPD? Chest 2003; 124: 1733-1742

34. Crippa V, Sau D, Rusmini P, Boncoraglio A, Onesto E, Bolzoni E, Galbiati M, Fontana E,Marino M, Carra S, Bendotti C, De Biasi S, Poletti A. The small heat shock protein B8 (HspB8) promotes autophagic removal of misfolded proteins involved in amyotrophic lateral sclerosis (ALS). Hum. Mol. Genet. 2010; 19: 3440-3456

35. Crow JP, Calingasan NY, Chen J, Hill JL, Beal MF. Manganese porphyrin given at symptom onset markedly extends survival of ALS mice. Ann. Neurol. 2005; 58: 258-265

36. Cudkowicz ME, Andres PL, Macdonald SA, Bedlack RS, Choudry R, Brown RH Jr, Zhang H, Shoenfeld DA, Shefner J, Matson S, Matson WR, Ferrante RJ, Northeast ALS and National VA ALS Research Consortiums. Phase 2 study of sodium phenylbutyrate in ALS. Amyotroph Lateral Scler. 2009; 10 (2): 99-106

37. DeJesus-Hernandez M, Mackenzie IR, Boeve BF, Boxer AL, Baker M, Rutherford NJ, Nicholson AM, Finch NA, Flynn H, Adamson J, Kouri N, Wojtas A, Sengdy P, Hsiung GY, Karydas A, Seeley WW, Josephs KA, Coppola G, Geschwind DH, Wszolek ZK, Feldman H, Knopman DS, Petersen RC, Miller BL, Dickson DW, Boylan KB, Graff-Radford NR, Rademakers R. Expanded GGGGCC hexanucleotide repeat in noncoding region of C9ORF72 causes chromosome 9p-linked FTD and ALS. Neuron. 2011; 72 (2): 245-256.

38. Del Bo R, Ghezzi S, Corti S, Pandolfo M, Ranieri M., Santoro D, Ghione I, Prelle A, Orsetti V, Mancuso M, Soraru G, Briani C, Angelini C, Siciliano G, Bresolin N, Comi GP. TARDBP (TDP-43) sequence analysis in patients with familial and sporadic ALS: identification of two novel mutations. Eur. J. Neurol. 2009; 16: 727-732

39. Doble A. The pharmacology and mechanism of action of riluzole. Neurology 1996; 47: S233-241

40. Dobrowolny G, Giacinti C, Pelosi L, Nicoletti C, Winn N, Barberi L, Molinaro M, Rosenthal N, Musarò A. Muscle expression of a local Igf-1 isoform protects motor neurons in an ALS mouse model. J Cell Biol 2005; 168: 193-199

41. Dobrowolny G, Aucello M, Rizzuto E, Beccafico S, Mammucari C, Boncompagni S, Belia S, Wannenes F, Nicoletti C, Del Prete Z, Rosenthal N, Molinaro M, Protasi F, Fanò G, Sandri M, Musarò A. Skeletal muscle is a primary target of SOD1G93A-mediated toxicity. Cell Metab 2008; 8: 425-436

42. Doi H, Kikuchi H, Murai H, Kawano Y, Shigeto H, Ohyagi Y, Kira J. Motor neuron disorder simulating ALS induced by chronic inhalation of pyrethroid insecticides. Neurology. 2006; 67 (10): 1894-1985

43. Dudgeon WD, Phillips KD, Carson JA, Brewer RB, Durstine JL, Hand GA. Counteracting muscle wasting in HIVinfected individuals. HIV Med. 2006; 7: 299-310

44. Dupuis L, Gonzales de aguilar JL, Echaniz-Laguna A, Eschbach J, Rene F, Oudart H, Halter B, Huze C, Schaeffer L, Bouillaud F, Loeffler JP. Muscle mitochondrial uncoupling dismutase neuromuscular junction and triggers distal degeneration of motor neurons. PLoS One. 2009; 4 (4): e5390

45. Dupuis L, Loeffler JP. Neuromuscular junction destruction during amyotrophic lateral sclerosis: insights from transgenic models. Curr Opin Pharmacol. 2009; 9 (3): 341-346

46. Eymard-Pierre E, Yamanaka K, Haeussler M, Kress W, Gauthier-Barichard F, Combes P, Cleveland DW, Boespflug-Tanguy O. Novel missense mutation in ALS2 gene results in infantile ascending hereditary spastic paralysis. Ann Neurol. 2006; 59 (6): 976-980

47. Fasana E, Fossati M, Ruggiano A, Brambillasca S, Hoogenraad CC, Navone F, Francolini M, Borgese N. A VAPB mutant linked to amyotrophic lateral sclerosis generates a novel form of organized smooth

48. Ferrante RJ, Browne SE, Shinobu LA, Bowling AC, Baik MJ, MacGarvey U, Kowall NW, Brown Jr RH, Beal MF. Evidence of increased oxidative damage in both sporadic and familial amyotrophic lateral sclerosis. J. Neurochem. 1997; 69: 2064-2074

49. Ferri A, Cozzolino M, Croscio C, Nencini M, Casciati A, Gralla EB, Rotillo G, Valentine JS, Carrì MT. Familial ALS-superoxide dismutases associate with mitochondria and shift their redox potentials. Proc Natl Acad Sci U S A 2006; 103 (37): 13860-13865

50. Figeac N, Daczewska M, Marcelle C, Jagla K. Muscle stem cells and model systems for their investigation. Dev. Dyn. 2007; 236: 3332-3342

51. Flicker L, Hopper JL, Larkins RG, Lichtenstein M, Buirski M, Wark JD. Nandrolone decanoate and intranasal calcitonin as therapy in established osteoporosis. Osteoporosis Int.1997; 7: 29-35

52. Fornai F, Longone P, Cafaro L, Kastsiuchenka O, Ferrucci M, Manca ML, Lazzeri G, Spalloni A, Bellio N, Lenzi P, Modugno N, Siciliano G, Isidoro C, Murri L, Ruggieri S, Paparelli A. Lithium delays progression of amyotrophic lateral sclerosis. Proc. Natl. Acad. Sci. U.S.A. 2008; 105: 2052- 2057

53. Forsberg K, Jonsson PA, Andersen PM, Bergemalm D, Graffmo KS, Hultdin M, Jacobsson J, Rosquist R, Marklund SL, Brännström T. Novel antibodies reveal inclusions containing non-native SOD1 in sporadic ALS patients. PLoS One. 2010; 5 (7): e11552

54. Franks ME, Macpherson GR, Figg WD. Thalidomide. Lancet 2004; 363, 1802-1811

55. Frey D, Schneider C, Xu L, Borg J, Spooren W, Caroni P. Early and selective loss of neuromuscular synapse subtypes with low sprouting competence in motoneuron diseases. J Neurosci 2000; 20 (7): 2534-2542

56. Frisoli A, Chaves PHM, Pinheiro MM, Szejnfeld VL. The effect of nandrolone decanoate on bone mineral density, muscle mass, and hemoglobin levels in elderly women with osteoporosis: a double-blind, randomized, placebo-controlled clinical trial. J. Gerontol., Series A, Biological Sciences and Medical Sciences 2005; 60: 648-653

57. Fujii R, Okabe S, Urushido T, Inoue K, Yoshimura A, Tachibana T, Nishikawa T, Hicks GG, Takumi T. The RNA binding protein TLS is translocated to dendritic spines by mGluR5 activation and regulates spine morphology. Curr. Biol. 2005; 15: 587-593

58. Funakoshi H, Belluardo N, Arenas E, Yamamoto Y, Casabona A, Persson H, Ibáñez CF. Muscle-derived neurotrophin-4 as an activity-dependent trophic signal for adult motor neurons. Science 1995; 268: 1495-1499

59. Gayan-Ramirez G, Rollier H, Vanderhoydonc F, Verhoeven G, Gosselink R, Decramer M. Nandrolone decanoate does not enhance training effects but increases IGF-I mRNA in rat diaphragm. J Appl Physiol 2000; 88 (1): 26-34

60. Genova ML, Pich MM, Bernacchia A, Bianchi C, Biondi A, Bovina C, Falasca AI, Formiggini G, Castelli GP, Lenaz G. The mitochondrial production of reactive oxygen species in relation to aging and pathology. Ann. N.Y. Acad. Sci. 2004; 1011: 86-100

61. Gill A, Kidd J, Vieira F, Thompson K, Perrin S. No benefit from chronic lithium dosing in a siblingmatched, gender balanced, investigator-blinded trial using a standard mouse model of familial ALS. PLoS One 2009; 4: e6489

62. Gold J, Batterham MJ, Rekers H, Harms MK, Geurts TBP, Helmyr PME, Silva de Mendonc J, Falleiros Carvalho LH, Panos G, Pinchera A, Aiuti F, Lee C, Horban A, Gatell J, Phanuphak P, Prasithsirikul W, Gazzard B, Bloch M, Danner SA. Effects of nandrolone decanoate compared with placebo or testosterone on HIV-associated wasting. HIV Med. 2006; 7: 146-155

63. Gordon PH, Moore DH, Miller RG, Florence JM, Verheijde JL, Doorish C, Hilton JF, Spitalny GM, MacArthur RB, Mitsumoto H, Neville HE, Boylan K, Mozaffar T, Belsh JM, Ravits J, Bedlack RS, Graves MC, McCluskey LF, Barohn RJ, Tandan R, Western ALS Study Group. Efficacy of minocycline in patients with amyotrophic lateral sclerosis: a phase III randomized trial. Lancet Neurol. 2007; 6: 1045-1053

64. Gould TW, Buss RR, Vinsant S, Prevette D, Sun W, Knudson CM, Milligan CE, Oppenheim RW. Complete dissociation of motor neuron death from motor dysfunction by Bax deletion in a mouse model of ALS. J Neurosci 2006; 26 (34): 2774-8786

65. Greenway MJ, Alexander MD, Ennis S, Traynor BJ, Corr B, Frost E, Green A, Hardiman O. A novel candidate region for ALS on chromosome 14q11.2. Neurology 2004; 63: 1936-1938

66. Greenway MJ, Andersen PM, Russ C, Ennis S, Cashman S, Donaghy C, Patterson V, Swingler R, Kieran D, Prehn J, Morrison KE. Green A., Acharya K.R., Brown R.H. Jr., Hardiman O. ANG mutations segregate with familial and ‘sporadic’ amyotrophic lateral sclerosis. Nat. Genet. 2006; 38: 411-413

67. Gurney ME, Pu H, Chiu AY, Dal Canto MC, Polchow CY, Alexander DD, Caliendo J, Hentati A, Kwon YW, Deng HX. Motor neuron degeneration in mice that express a human Cu,Zn superoxide dismutase mutation. Science 1994; 264: 1772-1775

68. Hassel B, Iversen EG, Gjerstad L, Tauboll E. Up-regulation of hippocampal glutamate transport during chronic treatment with sodium valproate. J. Neurochem. 2001; 77: 1285-1292

69. Hegedus J, Putman CT, Tyreman N, Gordon T. Preferential motor unit loss in the SOD1 G93A transgenic mouse model of amyotrophic lateral sclerosis. J Physiol 2008; 586 (14): 3337-3351

70. Hentati A, Ouahchi K, Pericak-Vance MA, Nijhawan D, Ahmad A, Yang Y, Rimmler J, Hung W, Schlotter B, Ahmed A, Ben Hamida M, Hentati F, Siddique T. Linkage of a commoner form of recessive amyotrophic lateral sclerosis to chromosome 15q15-q22 markers. Neurogenetics. 1998; 2 (1): 55-60.
71. Higgins CM, Jung C, Xu Z. ALS-associated mutant SOD-1G93A causes mitochondrial vacuolation by expansion of the intermembrane space and by involvement of SOD1 aggregation and peroxisomes. BMC Neurosci 2003; 4: 16
72. Hirano A. Cytopathology in amyotrophic lateral sclerosis. Adv. Neurol. 1991; 56: 91-101
73. Horner RD, Kamins KG, Feussner JR, Grambow SC, Hoff-Lindquist J, Harati Y, Mitsumoto H, Pascuzzi R, Spencer PS, Tim R, Howard D, Smith TC, Ryan MA, Coffman CJ, Kasarskis EJ. Occurrence of amyotrophic lateral sclerosis among Gulf War veterans. Neurology. 2003; 61 (6): 742-749
74. Ilieva H, Polymenidou M, Cleveland DW. Non–cell autonomous toxicity in neurodegenerative disorders: ALS and beyond. J. Cell Biol. 2009; 187 (6): 761–772
75. Ito H., Wate R., Zhang J., Ohnishi S., Kaneko S., Ito H., Nakano S., Kusaka H. Treatment with edaravone, initiated at symptom onset, slows motor decline and decreases SOD1 deposition in ALS mice. Exp. Neurol. 2008 213: 448-455
76. Jaarsma D, Rognoni F, van Duijn W, Verspaget HW, Haasdijk ED, Holstege JC. CuZn superoxide dismutase (SOD1) accumulates in vacuolated mitochondria in transgenic mice expressing amyotrofic lateral sclerosis-linked SOD1 Mutations. Acta Neuropathol. 2001; 102 (4): 293-305
77. Jaarsma D, Teuling E, Haasdijk ED, De Zeeuw CI, Hoogenraad CC. Neuron-specific expression of mutant superoxide dismutase is sufficient to induce amyotrophic lateral sclerosis in transgenic mice. J Neurosci 2008; 28: 2075-2088
78. Johansen KL, Painter PL, Sakkas JK, Gordon P, Doyle J, Shubert T. Effects of resistance exercise training and nandrolone decanoate on body composition and muscle function among patients who receive hemodialysis: A randomized, controlled trial. J. Am. Soc. Nephrol. 2006; 17 (8): 2307-2314
79. Johnson BS, Snead D, Lee JJ, McCaffery JM, Shorter J, Gitler AD. TDP-43 is intrinsically aggregation-prone, and amyotrophic lateral sclerosis-linked mutations accelerate aggregation and increase toxicity. J Biol Chem 2009; 284 (30): 20329-20339.

80. Julien JP. ALS: astrocytes move in as deadly neighbors. Nat Neurosci 2007; 10: 535-537

81. Kabashi E, Durham HD. Failure of protein quality control in amyotrophic lateral sclerosis. Biochim Biophys Acta 2006; 1762: 1038-1050

82. Kabashi E, Valdmanis PN, Dion P, Spiegelman D, McConkey BJ, Vande Velde C, Bouchard JP, Lacomblez L, Pochigaeva K, Salachas F, Pradat PF, Camu W, Meininger V., Dupre N, Rouleau GA. TARDBP mutations in individuals with sporadic and familial amyotrophic lateral sclerosis. Nat. Genet. 2008; 40: 572-574

83. Kanekura K, Nishimoto I, Aiso S, Matsuoka M. Characterization of amyotrophic lateral sclerosis linked P56S mutation of vesicle-associated membrane protein-associated protein B (VAPB/ALS8) J. Biol. Chem. 2006; 281: 30223-30233

84. Kanning KC, Kaplan A, Henderson CE. Motor Neuron Diversity in Development and Disease. Annu Rev Neurosci. 2010; 33: 409-440

85. Kaspar BK, Lladó J, Sherkat N, Rothstein JD, Gage FH. Retrograde viral delivery of IGF-1 prolongs survival in a mouse ALS model. Science 2003; 301: 839-842

86. Kassa RM, Mariotti R, Bonaconsa M, Bertini G, Bentivoglio M. Gene, cell, and axon changes in the familial amyotrophic lateral sclerosis mouse sensorimotor cortex. J Neuropathol Exp Neurol 2009; 68 (1): 59-72

87. Kaufmann P, Thompson JL, Levy G, Buchsbaum R, Shefner J, Krivickas LS, Katz J, Rollins Y, Barohn RJ, Jackson CE, Tiryaki E, Lomen-Hoerth C, Armon C, Tandan R, Rudnicki SA, Rezania K, Sufit R, Pestronk A, Novella SP,Heiman-Patterson T, Kasarskis EJ, Pioro EP, Montes J, Arbing R, Vecchio D, Barsdorf A, Mitsumoto H, Levin B, QALS Study Group. Phase II trial of CoQ10 for ALS finds insufficient evidence to justify phase III. Ann. Neurol. 2009; 66: 235-244

88. Kernochan LE, Russo ML, Woodling NS, Huynh TN, Avila AM, Fischbeck KH, Sumner CJ. The role of histone acetylation in SMN gene expression. Hum. Mol. Genet. 2005; 14: 1171-1182

89. Kiaei M, Petri S, Kipiani K, Gardian G, Choi DK, Chen J, Calingasan NY, Schafer P, Muller GW, Stewart C, Hensley K, Beal MF. Thalidomide and lenalidomide extend survival in a transgenic mouse model of amyotrophic lateral sclerosis. J. Neurosci. 2006; 26: 2467-2473

90. Kicman AT. Pharmacology of anabolic steroids. Brit. J. Pharmacol. 2008; 154: 502-521

91. Kim S, Leal SS, Ben Halevy D, Gomes CM, Lev S. Structural requirements for VAPB oligomerization and their implication in amyotrophic lateral sclerosis-associated VAPB(P56S) neurotoxicity. J Biol Chem 2010; 285 (18):13839-13849

92. Kong J, Xu Z. Massive mitochondrial degeneration in motor neurons triggers the onset of amyotrophic lateral sclerosis in mice expressing a mutant SOD1. J Neurosci. 1998; 18 (9): 3241-3250

93. Kong L, Wang X, Choe DW, Polley M, Burnett BG, Bosch-Marcé M, Griffin JW, Rich MM, Sumner CJ. Impaired synaptic vesicle release and immaturity of neuromuscular junctions in spinal muscular atrophy mice. J Neurosci. 2009; 29 (3): 842-851.

94. Kress JA, Kühnlein P, Winter P, Ludolph AC, Kassubek J, Müller U, Sperfeld AD. Novel mutation in the ALS2 gene in juvenile amyotrophic lateral sclerosis.Ann Neurol. 2005; 58 (5):800-803

95. Kriz J, Nguyen M, Julien J. Minocycline slows disease progression in a mouse model of amyotrophic lateral sclerosis. Neurobiol. Dis. 2002; 10: 268-278

96. Kuang S, Rudnicki MA. The emerging biology of satellite cells and their therapeutic potential. Trends Mol. Med. 2008; 14: 82-91

97. Kuhnlein P, Sperfeld AD, Vanmassenhove B,Van Deerlin V, Lee VM, Trojanowski JQ, Kretzschmar HA, Ludolph AC, Neumann M. Two German kindreds with familial amyotrophic lateral sclerosis due to TARDBP mutations. Arch. Neurol. 2008; 65: 1185-1189

98. Kwiatkowski TJ Jr, Bosco DA, Leclerc AL, Tamrazian E, Vanderburg CR, Russ C, Davis A, Gilchrist J, Kasarskis EJ, Munsat T, Valdmanis P, Rouleau GA, Hosler BA, Cortelli P, de Jong PJ, Yoshinaga Y, Haines JL, Pericak-Vance MA, Yan J, Ticozzi N, Siddique T, McKenna-Yasek D, Sapp PC, Horvitz HR, Landers JE, Brown RH Jr. Mutations in the FUS/TLS gene on chromosome 16 cause familial amyotrophic lateral sclerosis. Science. 2009; 323 (5918): 1205-1208

99. Lambrechts D, Storkebaum E, Morimoto M, Del-Favero J, Desmet F, Marklund SL, Wyns S, Thijs V, Andersson J, van Marion I, Al-Chalabi A, Bornes S, Musson R, Hansen V, Beckman L, Adolfsson R, Pall HS, Prats H, Vermeire S, Rutgeerts P, Katayama S, Awata T, Leigh N, Lang-Lazdunski L, Dewerchin M, Shaw C, Moons L, Vlietinck R, Morrison KE, Robberecht W, Van Broeckhoven C, Collen D, Andersen PM, Carmeliet P. VEGF is a modifier of amyotrophic lateral sclerosis in

mice and humans and protects motoneurons against ischemic death. Nat. Genet. 2003; 34: 383-394

100. Law WJ, Cann KL, Hicks GG. TLS, EWS and TAF15: a model for transcriptional integration of gene expression. Brief Funct. Genomic Proteomic 2006; 5: 8-14

101. Lenaz G, Bovina C, D'Aurelio M, Fato R, Formiggini G, Genova ML, Giuliano G, Merlo Pich M, Paolucci U, Parenti Castelli G, Ventura B. Role of mitochondria in oxidative stress and ageing. Ann. N.Y. Acad. Sci. 2002; 959: 199-213

102. Leng Y, Liang MH, Ren M, Marinova Z, Leeds P, Chuang DM. Synergistic neuroprotective effects of lithium and valproic acid or other histone deacetylase inhibitors in neurons: roles of glycogen synthase kinase-3 inhibition. J. Neurosci. 2008; 28: 2576-2588

103. Lewis MI, Fournier M, Yeh AY, Micevych PE, Sieck, GC. Alterations in diaphragm contractility after nandrolone administration: an analysis of potential mechanisms. J. Appl. Physiol. 1999; 86 (3): 985-992.

104. Lewis MI, Horvitz GD, Clemmons DR, Fournier M. Role of IGF-I and IGF-binding proteins within diaphragm muscle in modulating the effects of nandrolone. Am J Physiol Endocrinol Metab 2002; 282 (2): E483-E490

105. Lino MM, Schneider C, Caroni P. Accumulation of SOD1 mutants in postnatal motoneurons does not cause motoneuron pathology or motoneuron disease. J Neurosci 2002; 22: 4825-4832

106. Liu J, Lillo C, Jonsson PA, Vande Velde C, Ward CM, Miller TM, Subramaniam JR, Rothstein JD, Marklund S, Andersen PM, Brännström T, Gredal O, Wong PC, Williams DS, Cleveland DW. Toxicity of familial ALS-linked SOD1 mutants from selective recruitment to spinal mitochondria. Neuron 2004; 43 (1): 5-17

107. Matthews RT, Yang L, Browne S, Baik M, Beal MF. Coenzyme Q10 administration increases brain mitochondrial concentrations and exerts neuroprotective effects. Proc. Natl. Acad. Sci. U.S.A. 1998; 95: 8892-8897

108. Mattiazzi M, D'Aurelio M, Gajewski CD, Martushova K, Kiaei M, Beal MF, Manfredi G. Mutated human SOD1 causes dysfunction of oxidative phosphorylation in mitochondria of transgenic mice. J Biol Chem 2002; 277 (33): 29626-29633

109. McGeer PL, McGeer EG. Inflammatory processes in amyotrophic lateral sclerosis. Muscle and Nerve 2002; 26: 459-470

110. Menzies FM, Ince PG, Shaw PJ. Mitochondrial involvement in amyotrophic lateral sclerosis. Neurochem Int 2002a; 40 (6): 543-551

111. Menzies FM, Cookson MR, Taylor RW, Turnbull DM, Chrzanowska-Lightowlers ZM, Dong L, Figlewicz DA, Shaw PJ. Mitochondrial dysfunction in a cell culture model of familial amyotrophic lateral sclerosis. Brain 2002b; 125 (Pt 7): 1522-1533

112. Millecamps S, Salachas F, Cazeneuve C, Gordon P, Bricka B, Camuzat A, Guillot-Noel L, Russaouen O, Bruneteau G, Pradat PF, Le Forestier N, Vandenberghe N, Danel-Brunaud V, Guy N, Thauvin-Robinet C, Lacomblez L, Couratier P, Hannequin D, Seilhean D, Le Ber I, Corcia P, Camu W, Brice A, Rouleau G, LeGuern E, Meininger V. SOD1, ANG, VAPB, TARDBP, and FUS mutations in familial amyotrophic lateral sclerosis: genotype-phenotype correlations. J. Med. Genet. 2010; 47: 554-560

113. Miller TM, Kim SH, Yamanaka K, Hester M, Umapathi P, Arnson H, Rizo L, Mendell JR, Gage FH, Cleveland DW, Kaspar BK. Gene transfer demonstrates that muscle is not a primary target for non-cell-autonomous toxicity in familial amyotrophic lateral sclerosis. Proc Natl Acad Sci USA 2006; 103: 19546-19551

114. Minamiyama M, Katsuno M, Adachi H, Waza M, Sang C, Kobaiashi Y, Tanaka F, Doyu M Inukai A, Sobue G. Sodium butyrare ameliorates phenotypic expression in a transgenic mouse model of spinal and bulbar muscular atrophy. Hum Mol Genet. 2004; 13 (11): 1183-1192

115. Monks DA, O'Bryant EL, Jordan CL. Androgen receptor immunoreactivity in skeletal muscle: enrichment at the neuromuscular junction. J. Comp. Neurol. 2004; 473 (1): 59-72.

116. Morland C, Boldingh KA, Iversen EG, Hassel B. Valproate is neuroprotective against malonate toxicity in rat striatum: an association with augmentation of high-affinity glutamate uptake. J. Cereb. Blood Flow Metab. 2004; 24: 1226-1234

117. Moroianu J, Riordan JF. Nuclear translocation of angiogenin in proliferating endothelial cells is essential to its angiogenic activity. Proc. Natl. Acad. Sci. U.S.A., 1994; 91: 1677-1681

118. Musarò A. State of the art and the dark side of amiotrophic lateral sclerosis. World J Biol Chem. 2010; 1 (5): 62-68

119. Neary D, Snowden JS, Gustafson L, Passant U, Stuss D, Black S, Freedman M, Kertesz A, Robert PH, Albert M, Boone K, Miller BL, Cummings J, Benson DF. Frontotemporal lobar degeneration: a consensus on clinical diagnostic criteria. Neurology 1998; 51 (6): 1546-1554

120. Neumann M, Sampathu DM, Kwong LK, Truax AC, Micsenyi MC, Chou TT, Bruce J, Schuck T, Grossman M, Clark CM, McCluskey LF, Miller BL, Masliah E, Mackenzie IR, Feldman H, Feiden W, Kretzschmar HA, Trojanowski JQ, Lee VM. Ubiquitinated TDP-43 in frontotemporal lobar degeneration and amyotrophic lateral sclerosis. Science 2006; 314: 130-133

121. Nishimura AL, Mitne-Neto M, Silva HC, Richieri-Costa A, Middleton S, Cascio D, Kok F, Oliveira JR, Gillingwater T, Webb J, Skehel P, Zatz M. A mutation in the vesicle-trafficking protein VAPB causes late-onset spinal muscular atrophy and amyotrophic lateral sclerosis. Am J Hum Genet 2004; 75: 822-831

122. Oh SS, Kim EA, Lee SW, Kim MK, Kang SK. A case of amyotrophic lateral sclerosis in electronic parts manufacturing worker exposed to lead. Neurotoxicology. 2007; 28 (2): 324-327

123. Okouchi M, Ekshyyan O, Maracine M, Aw TY. Neuronal apoptosis in neurodegeneration. Antioxid. Redox Signal. 2007; 9: 1059-1096

124. Orlacchio A, Babalini C, Borreca A, Patrono C, Massa R, Basaran S, Munhoz RP, Rogaeva EA, St George-Hyslop PH, Bernardi G, Kawarai T. SPATACSIN mutations cause autosomal recessive juvenile amyotrophic lateral sclerosis. Brain. 2010; 133 (Pt 2): 591-598

125. Otomo A, Hadano S, Okada T, Mizumura H, Kunita R, Nishijima H, Showguchi-Miyata J, Yanagisawa Y, Kohiki E, Suga E, Yasuda M, Osuga H, Nishimoto T, Narumiya S, Ikeda JE. ALS2, a novel guanine nucleotide exchange factor for the small GTPase Rab5, is implicated in endosomal dynamics. Hum Mol Genet. 2003; 12 (14): 1671-1687

126. Panzeri C, De Palma C, Martinuzzi A, Daga A, De Polo G, Bresolin N, Miller CC, Tudor EL, Clementi E, Bassi MT. The first ALS2 missense mutation associated with JPLS reveals new aspects of alsin biological function. Brain. 2006; 129 (Pt 7): 1710-1719

127. Pardo CA, Xu Z, Borchelt DR, Price DL, Sisodia SS, Cleveland DW. Superoxide dismutase is an abundant component in cell bodies, dendrites, and axons of motor neurons and in a subset of other neurons. Proc Natl Acad Sci U S A. 1995; 92 (4): 954-958

128. Pasinelli P, Brown RH. Molecular biology of amyotrophic lateral sclerosis: insights from genetics. Nat Rev Neurosci. 2006; 7 (9): 710-723

129. Patel M, Day BJ. Metalloporphyrin class of therapeutic catalytic antioxidants. Trends Pharmacol. Sci.1999 20: 359-364

130. Pizzasegola C, Caron I, Daleno C, Ronchi A, Minoia C, Carri MT, Bendotti C. Treatment with lithium carbonate does not improve disease progression in two different strains of SOD1 mutant mice. Amyotroph. Lateral. Scler. 2009; 10: 221-228

131. Prosser DC, Tran D, Gougeon PY, Verly C, Ngsee JK. FFAT rescues VAPA-mediated inhibition of ER-to-Golgi transport and VAPB-mediated ER aggregation. J Cell Sci 2008; 121(Pt 18): 3052- 3061

132. Pun S, Santos AF, Saxena S, Xu L, Caroni P. Selective vulnerability and pruning of phasic motoneuron axons in motoneuron disease alleviated by CNTF. Nat Neurosci 2006; 9 (3): 408-419

133. Qin W, Pan J, Bauman WA, Cardozo CP. Differential alterations in gene expression profiles contribute to time-dependent effects of nandrolone to prevent denervation atrophy. BMC Genomics. 2010; 11: 596-612.

134. Raimondi A, Mangolini A, Rizzardini M, Tartari S, Massari S, Bendotti C, Francolini M, Borgese N, Cantoni L, Pietrini G. Cell culture models to investigate the selective vulnerability of motoneuronal mitochondria to familial ALS-linked G93ASOD1. Eur J Neurosci 2006; 24 (2): 387-399

135. Ravikumar B, Vacher C, Berger Z, Davies JE, Luo S, Oroz LG, Scaravilli F, Easton DF, Duden R, O'Kane CJ, Rubinsztein DC. Inhibition of mTOR induces autophagy and reduces toxicity of polyglutamine expansions in fly and mouse models of Huntington disease. Nat. Genet. 2004; 36: 585-595

136. Reaume AG, Elliott JL, Hoffman EK, Kowall NW, Ferrante RJ, Siwek DF, Wilcox HM, Flood DG, Beal MF, Brown RH Jr, Scott RW, Snider WD. Motor neurons in Cu/Zn superoxide dismutase-deficient mice develop normally but exhibit enhanced cell death after axonal injury. Nat. Genet. 1996; 13: 43-47

137. Renton AE, Majounie E, Waite A, Simón-Sánchez J, Rollinson S, Gibbs JR, Schymick JC, Laaksovirta H, van Swieten JC, Myllykangas L, Kalimo H, Paetau A, Abramzon Y, Remes AM, Kaganovich A, Scholz SW, Duckworth J, Ding J, Harmer DW, Hernandez DG, Johnson JO, Mok K, Ryten M, Trabzuni D, Guerreiro RJ, Orrell RW, Neal J, Murray A, Pearson J, Jansen IE, Sondervan D, Seelaar H, Blake D, Young K, Halliwell N, Callister JB, Toulson G, Richardson A, Gerhard A, Snowden J, Mann D, Neary D, Nalls MA, Peuralinna T, Jansson L, Isoviita VM,

Kaivorinne AL, Hölttä-Vuori M, Ikonen E, Sulkava R, Benatar M, Wuu J, Chiò A, Restagno G, Borghero G, Sabatelli M; ITALSGEN Consortium, Heckerman D, Rogaeva E, Zinman L, Rothstein JD, Sendtner M, Drepper C, Eichler EE, Alkan C, Abdullaev Z, Pack SD, Dutra A, Pak E, Hardy J, Singleton A, Williams NM, Heutink P, Pickering-Brown S, Morris HR, Tienari PJ, Traynor BJ. A hexanucleotide repeat expansion in C9ORF72 is the cause of chromosome 9p21-linked ALS-FTD. Neuron. 2011; 72 (2): 257-268

138. Righi M, Giacomini A, Lavazza C, Sia D, Carlo-Stella C, Gianni AM. A computational approach to compare microvessel distributions in tumors following antiangiogenic treatments. Lab Invest 2009; 89 (9): 1063-1070

139. Robberecht W, Aguirre T, Van den Bosch L, Tilkin P, Cassiman JJ, Matthijs G. D90A heterozygosity in the SOD1 gene is associated with familial and apparently sporadic amyotrophic lateral sclerosis.Neurology. 1996; 47 (5): 1336-1339

140. Rosen DR, Siddique T, Patterson D, Figlewicz DA, Sapp P, Hentati A, Donaldson D, Goto J, O'Regan JP, Deng HX, Rahmani Z, Krizus A, McKenna-Yasek D, Cayabyab A, Gaston SM, Berger R, Tanzi RE, Halperin JJ, Herzfeldt B, Van den Bergh R, Hung WY, Bird T, Deng G, Mulder DW, Smyth C, Laing NG, Soriano E, Pericak–Vance MA, Haines J, Rouleau GA, Gusella JS, Horvitz HR, Brown RH Jr. Mutations in Cu/Zn superoxide dismutase gene are associated with familial amyotrophic lateral sclerosis. Nature. 1993; 362 (6435), 59-62

141. Rothstein J.D., Van Kammen M., Levey A.I., Martin L.J., Kuncl R.W. Selective loss of glial glutamate transporter GLT1 in amyotrophic lateral sclerosis. Ann. Neurol.1995; 38: 73-84

142. Rubinsztein DC, Gestwicki JE, Murphy LO, Klionsky DJ. Potential therapeutic applications of autophagy. Nat. Rev. Drug. Discov. 2007; 6: 304-312

143. Ryu H, Smith K, Camelo SI, Carreras I, Lee J, Iglesias AH, Dangond F, Cornier KA, Cudkowicz ME, Brown RH Jr, Ferrante RJ. Sodium phenylbutyrate prolongs survival and regulates expression of anti-apoptotic genes in transgenic amyotrophic lateral sclerosis mice. J Neurochem 2005; 93 (5): 1087 -98

144. Saartok T, Dahlberg E, Gustafsson JA. Relative binding affinity of anabolic-androgenic steroids-comparison of the binding to the androgen receptors in skeletal muscle and in prostate, as well as to sex hormone-binding globulin. Endocrinology 1984; 114: 2100-2106

145. Salinas S, Proukakis C, Crosby A, Warner TT. Hereditary spastic paraplegia: clinical features and pathogenetic mechanisms.Lancet Neurol. 2008; 7 (12): 1127-1138

146. Santos AF, Caroni P. Assembly, plasticity and selective vulnerability to disease of mouse neuromuscular junctions. J Neurocytol. 2003; 32 (5-8): 849-862

147. Sapp PC, Hosler BA, McKenna-Yasek D, Chin W, Gann A, Genise H, Gorenstein J, Huang M, Sailer W, Scheffler M, Valesky M, Haines JL, Pericak-Vance M, Siddique T, Horvitz HR, Brown RH Jr. Identification of two novel loci for dominantly inherited familial amyotrophic lateral sclerosis. Am J Hum Genet. 2003; 73 (2): 397-403

148. Sasaki S, Warita H, Murakami T, Abe K, Iwata M. Ultrastructural study of mitochondria in the spinal cord of transgenic mice with a G93A mutant SOD1 gene. Acta Neuropathol. 2004; 107 (5): 461-474

149. Schols AMWJ, Soeters PB, Mostert R, Pluymers RJ, Wouters EFM. Physiological-effects of nutritional support and anabolic-steroids in patients with chronic obstructive pulmonarydisease - a placebo controlled randomized trial. Amer. J. Resp. Crit. Care Med. 1995; 152: 1268-1274

150. Schwarz S, Husstedt I, Bertram HP, Kuchelmeister K. Amyotrophic lateral sclerosis after accidental injection of mercury.J Neurol Neurosurg Psychiatry. 1996; 60 (6): 698

151. Scott S, Kranz JE, Cole J, Lincecum JM, Thompson K, Kelly N, Bostrom A, Theodoss J, Al-Nakhala BM, Vieira FG, Ramasubbu J, Heywood JA. Design, power, and interpretation of studies in the standard murine model of ALS. Amyotroph. Lateral. Scler. 2008; 9 (1): 4-15.

152. Shahidi, NT. A review of the chemistry, biological action, and clinical applications of anabolic-androgenic steroids. Clinical Theraputics 2001; 23: 1355-1390

153. Shaw P, Ince P, Falkous G, Mantel D. Oxidative damage to protein in sporadic motor neuron disease spinal cord. Ann. Neurol. 1995; 38: 691-695

154. Shichinohe H, Kuroda S, Yasuda H, Ishikawa T, Iwai M, Horiuchi M, Iwasaki Y. Neuroprotective effects of the free radical scavenger Edaravone (MCI-186) in micepermanent focal brain ischemia. Brain Res. 2004; 1029: 200-206

155. Siddique T. Molecular genetics of familial amyotrophic lateral sclerosis. Adv Neurol. 1991; 56: 227-231

156. Siklós L, Engelhardt J, Harati Y, Smith RG, Joó F, Appel SH. Ultrastructural evidence for altered calcium in motor nerve terminals in amyotropic lateral sclerosis. Ann Neurol. 1996; 39 (2): 203-216

157. Smith B.D. and Raines R.T. Genetic selection for critical residues in ribonucleases. J. Mol. Biol. 2006; 362: 459-478

158. Steele JC, McGeer PL. The ALS/PDC syndrome of Guam and the cycad hypothesis. Neurology. 2008; 70 (21): 1984-1990

159. Stevanin G, Santorelli FM, Azzedine H, Coutinho P, Chomiller J, Denora PS, Martin E, Ouvrard-Hernandez AM, Tessa A, Bouslam N, Lossos A, Charles P, Loureiro JL, Elleuch N, Confavreux C, Cruz VT, Ruberg M, Leguern E, Grid D, Tazir M, Fontaine B, Filla A, Bertini E, Durr A, Brice A. Mutations in SPG11, encoding spatacsin, are a major cause of spastic paraplegia with thin corpus callosum. Nat Genet. 2007; 39 (3) 366-372

160. Stommel EW, Cohen JA, Fadul CE, Cogbill CH, Graber DJ, Kingman L, Mackenzie T, Channon Smith JY, Harris BT. Efficacy of thalidomide for the treatment of amyotrophic lateral sclerosis: A phase II open label clinical trial. Amyotroph. Lateral Scler. 2009; 10: 393-404

161. Sugai F, Yamamoto Y, Miyaguchi K, Zhou Z, Sumi H, Hamasaki T, Goto M, Sakoda S. Benefit of valproic acid in suppressing disease progression of ALS model mice. Eur. J. Neurosci. 2004; 20: 3179-3183

162. Sundaram K, Kumar N, Monder C, Bardin CW. Different patterns of metabolism determine the relative anabolic activity of 19-norandrogens. J. Steroid Biochem. Molec. Biol. 1995; 53: 253-257

163. Suraweera A, Becherel OJ, Chen P, Rundle N, Woods R, Nakamura J, Gatei M, Criscuolo C, Filla A, Chessa L, Fusser M, Epe B, Gueven N, Lavin MF. Senataxin, defective in ataxia oculomotor apraxia type 2, is involved in the defense against oxidative DNA damage. J Cell Biol. 2007; 177(6) : 969-979

164. Suraweera A, Lim Y, Woods R, Birrell GW, Nasim T, Becherel OJ, Lavin MF. Functional role for senataxin, defective in ataxia oculomotor apraxia type 2, in transcriptional regulation. Hum Mol Genet. 2009; 18 (18): 3384-3396

165. Suzuki H, Kanekura K, Levine TP, Kohno K, Olkkonen VM, Aiso S, Matsuoka M. ALSlinked P56S-VAPB, an aggregated loss-of-function mutant of VAPB, predisposes motor neurons to ER stress-related death by inducing aggregation of co-expressed wild-type VAPB. J. Neurochem. 2009; 108: 973-985

166. Ticozzi N, Silani V, LeClerc AL, Keagle P, Gellera C, Ratti A, Taroni F, Kwiatkowski TJ Jr, McKenna-Yasek DM, Sapp PC, Brown RH Jr, Landers JE. Analysis of FUS gene mutation in familial amyotrophic lateral sclerosis within an Italian cohort. Neurology. 2009; 73 (15): 1180-1185

167. Ticozzi N, LeClerc AL, Keagle PJ, Glass JD, Wills AM, van Blitterswijk M, Bosco DA, Rodriguez-Leyva I, Gellera C, Ratti A, Taroni F, McKenna-Yasek D, Sapp PC, Silani V, Furlong CE, Brown RH Jr, Landers JE. Paraoxonase gene mutations in amyotrophic lateral sclerosis. Ann. Neurol. 2010; 68: 102-107

168. Ticozzi N, Tiloca C, Morelli C, Colombrita C, Poletti B, Doretti A, Maderna L, Messina S, Ratti A, Silani V. Genetics of familial Amyotrophic lateral sclerosis. Arch Ital Biol. 2011; 149 (1): 65-82

169. Toth M, Zakar T. Relative binding affinities of testosterone, 19-nortestosterone and their 5-alpha-reduced derivatives to the androgen receptor and to other androgen binding proteins-a suggested role of 5- alpha-reductive steroid-metabolism in the dissociation of myotropic and androgenic activities of 19-nortestosterone. J. Steroid Biochem. Mol. Biol. 1982; 17, 653-660

170. Uno M, Kitazato KT, Suzue A, Matsuzaki K, Harada M, Itabe H, Nagahiro S. Inhibition of brain damage by edaravone, a free radical scavenger, can be monitored by plasma biomarkers that detect oxidative and astrocyte damage in patients with acute cerebral infarction. Free Radic. Biol. Med. 2005; 39: 1109-1116

171. Van Damme P, Dewil M, Robberecht W, Van Den Bosch L. Excitotoxicity and amyotrophic lateral sclerosis. Neurodegener Dis 2005; 2: 147-159

172. Van Deerlin VM, Leverenz JB, Bekris LM, Bird TD, Yuan W, Elman LB, Clay D, Wood EM, Chen-Plotkin AS, Martinez-Lage M, Steinbart E, McCluskey L, Grossman M, Neumann M, Wu IL, Yang WS, Kalb R, Galasko DR, Montine TJ, Trojanowski JQ, Lee VM, Schellenberg GD, Yu CE. TARDBP mutations in amyotrophic lateral sclerosis with TDP-43 neuropathology: a genetic and histopathological analysis. Lancet Neurol. 2008; 7: 409-416

173. Van Den Bosch L., Tillkin P., Lemmens G., Robberecht W. Minocycline delays disease onset and mortality in a transgenic model of ALS. Neuroreport 2002; 13: 1067-1070

174. van Es MA, Diekstra FP, Veldink JH, Baas F, Bourque PR, Schelhaas HJ, Strengman E, Hennekam EA, Lindhout D, Ophoff RA, van den Berg LH. A case of

ALS-FTD in a large FALS pedigree with a K17I ANG mutation. Neurology 2009; 72: 287-288

175. Van Marken Lichtenbelt WD, Hartgens F, Vollaard NBJ, Ebbing S, Kuipers H. Bodybuilders' body composition: effect of nandrolone decanoate. Med. Sci. Sports Exerc. 2004; 36: 484-489

176. Vance C, Rogelj B, Hortobágyi T, De Vos KJ, Nishimura AL, Sreedharan J, Hu X, Smith B, Ruddy D, Wright P, Ganesalingam J, Williams KL, Tripathi V, Al-Saraj S, Al-Chalabi A, Leigh PN, Blair IP, Nicholson G, de Belleroche J, Gallo JM, Miller CC, Shaw CE. Mutations in FUS, an RNA processing protein, cause familial amyotrophic lateral sclerosis type 6. Science. 2009; 323 (5918): 1208-1211

177. Venkatachalam K, Long AA, Elsaesser R, Nikolaeva D, Broadie K, Montell C. Motor deficit in a Drosophila model of mucolipidosis type IV due to defective clearance of apoptotic cells. Cell 2008; 135: 838-851

178. Verma A, Berger JR. ALS syndrome in patients with HIV-1 infection. J Neurol Sci. 2006; 240 (1-2): 59-64.

179. Vinceti M, Bonvicini F, Rothman KJ, Vescovi L, Wang F. The relation between amyotrophic lateral sclerosis and inorganic selenium in drinking water: a population-based case-control study. Environ Health. 2010; 9:77-84

180. Watanabe T, Yuki S, Egawa M, Nishi H. Protective effects of MCI-186 on cerebral ischemia: possible involvement of free radical scavenging and antioxidant actions. J. Pharmacol. Exp. Ther.1994; 268:1597-1604

181. Wiedemann FR, Winkler K, Kuznetsov AV, Bartels C, Vielhaber S, Feistner H, Kunz WS. Impairment of mitochondrial function in skeletal muscle of patients with amyotrophic lateral sclerosis. J Neurol Sci. 1998; 156 (1): 65-72

182. Wong M, Martin LJ. Skeletal muscle-restricted expression of human SOD1 causes motor neuron degeneration in transgenic mice. Hum Mol Genet 2010; 19 (11): 2284-2302

183. Wu D, Yu W, Kishikawa H, Folkerth RD, Iafrate AJ, Shen Y, Xin W, Sims K, Hu GF. Angiogenin loss-of-function mutations in amyotrophic lateral sclerosis. Ann. Neurol. 2007; 62: 609-617

184. Wu DC, Re DB, Nagai M, Ischiropoulos H, Przedborski S. The inflammatory NADPH oxidase enzyme modulates motor neuron degeneration in amyotrophic lateral sclerosis mice. Proc. Natl. Acad. Sci. U. S. A. 2006; 103: 12132-12137

185. Yamamoto-Watanabe Y, Watanabe M, Okamoto K, Fujita Y, Jackson M, Ikeda M, Nakazato Y, Ikeda Y, Matsubara E, Kawarabayashi T, Shoji M. A Japanese ALS6 family with mutation R521C in the FUS/TLS gene: a clinical, pathological and genetic report. J Neurol Sci. 2010; 296 (1-2): 59-63.

186. Yamanaka K, Vande Velde C, Eymard-Pierre E, Bertini E, Boespflug-Tanguy O, Cleveland DW. Unstable mutants in the peripheral endosomal membrane component ALS2 cause early-onset motor neuron disease. Proc Natl Acad Sci U S A. 2003; 100 (26): 16041-16046

187. Yan J, Deng HX, Siddique N, Fecto F, Chen W, Yang Y, Liu E, Donkervoort S, Zheng JG, Shi Y, Ahmeti KB, Brooks B, Engel WK, Siddique T. Frameshift and novel mutations in FUS in familial amyotrophic lateral sclerosis and ALS/dementia. Neurology. 2010; 75 (9): 807-814

188. Yoshino H, Kimura A. Investigation of the therapeutic effects of edaravone, a free radical scavenger, on amyotrophic lateral sclerosis (Phase II study). Amyotroph. Lateral. Scler. 2006; 7: 241-245

189. Zabłocka A, Janusz M. The two faces of reactive oxygen species. Postepy Hig Med Dosw (Online) 2008; 62: 118-24.

190. Zammit PS, Partridge TA, Yablonka-Reuveni Z. The skeletal muscle satellite cell: the stem cell that came in from the cold. J. Histochem. Cytochem. 2006; 54: 1177-1191

191. Zhao J, Zhang Y, Zhao W, Wu Y, Pan J, Bauman WA, Cardozo C. Effects of nandrolone on denervation atrophy depend upon time after nerve transection. Muscle Nerve. 2008; 37 (1): 42-49

192. Zhao ZH, Chen WZ, Wu ZY, Wang N, Zhao GX, Chen WJ, Murong SX. A novel mutation in the senataxin gene identified in a Chinese patient with sporadic amyotrophic lateral sclerosis. Amyotroph Lateral Scler. 2009; 10 (2): 118-122.

193. Zhou J, Yi J, Fu R, Liu E, Siddique T, Ríos E, Deng HX. Hyperactive intracellular calcium signaling associated with localized mitochondrial defects in skeletal muscle of an animal model sclerosis. J Biol Chem 2010; 285: 705-712